NOTE TO USERS

This reproduction is the best copy available.

UMI®

University of Alberta

OPTIMIZING THE DETECTION OF UVC INDUCED DNA PHOTODAMAGE ON MICROARRAY SLIDES WITH FLUORESCENTLY LABELED HAIRPIN PROBES

by

CHRISTINE LORRAINE PINNOCK

©

A thesis submitted to the Faculty of Graduate Studies and Research
in partial fulfillment of the requirements for the degree of

Master of Science

Department of Chemistry

Edmonton, Alberta
Fall 2008

Library and Archives Canada

Published Heritage Branch

395 Wellington Street
Ottawa ON K1A 0N4
Canada

Bibliothèque et Archives Canada

Direction du Patrimoine de l'édition

395, rue Wellington
Ottawa ON K1A 0N4
Canada

Your file Votre référence
ISBN: 978-0-494-47637-6
Our file Notre référence
ISBN: 978-0-494-47637-6

NOTICE:
The author has granted a non-exclusive license allowing Library and Archives Canada to reproduce, publish, archive, preserve, conserve, communicate to the public by telecommunication or on the Internet, loan, distribute and sell theses worldwide, for commercial or non-commercial purposes, in microform, paper, electronic and/or any other formats.

The author retains copyright ownership and moral rights in this thesis. Neither the thesis nor substantial extracts from it may be printed or otherwise reproduced without the author's permission.

AVIS:
L'auteur a accordé une licence non exclusive permettant à la Bibliothèque et Archives Canada de reproduire, publier, archiver, sauvegarder, conserver, transmettre au public par télécommunication ou par l'Internet, prêter, distribuer et vendre des thèses partout dans le monde, à des fins commerciales ou autres, sur support microforme, papier, électronique et/ou autres formats.

L'auteur conserve la propriété du droit d'auteur et des droits moraux qui protège cette thèse. Ni la thèse ni des extraits substantiels de celle-ci ne doivent être imprimés ou autrement reproduits sans son autorisation.

In compliance with the Canadian Privacy Act some supporting forms may have been removed from this thesis.

While these forms may be included in the document page count, their removal does not represent any loss of content from the thesis.

Conformément à la loi canadienne sur la protection de la vie privée, quelques formulaires secondaires ont été enlevés de cette thèse.

Bien que ces formulaires aient inclus dans la pagination, il n'y aura aucun contenu manquant.

Canada

Abstract

The development of microarrays as an innovative tool to study biochemical samples has benefited us with a deeper understanding of DNA, RNA, and protein behaviour. This thesis will discuss the optimization and use of microarrays in order to reduce the large amounts of error inherent to this technique and to measure photochemistry in different DNA sequences. To do this, we introduced the use of a fluorescently-labeled short single stranded DNA (ssDNA) immobilized to a glass slide as an internal standard. Optimization of this technique required the correction of a number of parameters such as environmental conditions (including ambient light exposure and atmospheric ozone) and target / probe concentrations. We determined 35 μM to be the optimal concentration for the fluorescently-labeled probe and 50 μM to be the optimal concentration for the target. From these corrections, we were able to reduce the obtained error by a factor of 2 or more.

In addition, the detection of DNA damage induced by UVC irradiation on microarray slides is also discussed. Three different ssDNA target sequences 5'-/Am/CGT GCA AAA AAA TTA AAA AAA A-3' (ATTA), 5'-/Am/CGT GCA AAA AAG TTG AAA AAA A-3' (GTTG), and 5'-/Am/CGT GCA AAA AAA AAA AAA AAA A-3' (AAAA) were immobilized to glass slides. The irradiation of these target sequences with UVC light produced photochemical damage, which was detected with target-specific fluorescently-labeled hairpin probes. First-order exponential decay curves were fit to the obtained data and quantitative rate constants were determined for DNA photoproduct formation. The rate constants determined were 51.59113 ± 2.14881 min (R^2

= 0.95881) for ATTA, 47.78764 ± 3.5573 min (R^2 = 0.83409) for AAAA, and 53.52365 ± 1.26358 min (R^2 = 0.99976) for GTTG DNA sequence. The AAAA target sequence was designed as a control sequence due to its limited photochemistry. However, here we detected photodamage induced by UVC light.

Finally, the photoluminescent properties of silicon nanoparticles as potential standards for nucleic acid microarrays were examined. The silicon nanoparticles were measured under two conditions, exposed to air and sealed. Both the sealed and exposed nanoparticles emit in two spectral regions, the near IR and the UV. The average quantum yields for the sealed sample were 17% in the UV region and 1.27% in the near IR. The average quantum yields for the exposed samples were determined to be 4.18% in the UV region and 0.48% in the near IR. The stability of these nanoparticles was investigated by measuring the effects of aging on the emission spectrum. We observed only slight decreases in the quantum yields after a period of 14 days.

TABLE OF CONTENTS

1 GENERAL INTRODUCTION	1
1.1 Nucleic Acids	2
1.2 Microarrays	2
1.3 DNA Photochemistry	8
1.4 Molecular Beacons	11
1.5 Summary of Research	18
1.6 References	20
2 REDUCING THE ERROR IN DNA MICROARRAYS	23
2.1 Introduction	24
2.2 Experimental	27
2.3 Results and Discussion	40
2.4 Conclusions	61
2.5 References	62
3 PHOTOCHEMISTRY OF DNA IN A MICROARRAY	73
3.1 Introduction	74
3.2 Experimental	77
3.3 Results and Discussion	82
3.4 Conclusions	101
3.5 References	102
4 SILICON NANOPARTICLES	104
4.1 Introduction	105
4.2 Experimental	108
4.3 Results and Discussion	111

4.4 Conclusions 120

4.5 References 123

5 CONCLUSIONS AND FUTURE WORK 125

5.1 Reducing Error and Detecting DNA Photodamage on Microarray Slides 126

5.2 Silicon Nanoparticle 127

5.3 Future Work 127

6 APPENDIX 129

LIST OF TABLES

Table 2.1 - Amino terminated target sequences 28

Table 2.2 - Complementary Cy5 modified DNA hairpin probe sequences 28

Table 2.3 - Comparison of pivot table and TIGR Spotfinder statistics 60

Table 4.1 – Calculated quantum yields of SiH samples 121

LIST OF FIGURES

Figure 1.1- Structure of DNA and RNA. 4

Figure 1.2 – Schematic of *in situ* light directed oligonucleotide synthesis on a microarray glass slide with the use of a photolithographic mask. 6

Figure 1.3 – Attachment chemistry of DNA onto a derivatized glass slide. 9

Figure 1.4 – Major photoproducts of thymine upon UV irradiation. 12

Figure 1.5 – Schematic of a classic molecular beacon. 14

Figure 1.6 –Phase transitions for molecular beacons. 16

Figure 2.1 - Structure of 6-carboxyfluorescein (FAM). 29

Figure 2.2 - FAM internal standard absorption. 30

Figure 2.3 - Structure of the thiadicarbocyanine (Cy5). 31

Figure 2.4 –Cy5 probe absorption spectrum. 32

Figure 2.5 - Schematic of experimental slide. 35

Figure 2.6 – Image of TIGR Spotfinder analysis of a microarray slide. 38

Figure 2.7 – Image of TIGR Spotfinder analysis of a subarray. 39

Figure 2.8 – Cy5 fluorescence intensities. 45

Figure 2.9 – Cy5/FAM ratio of fluorescence intensities. 46

Figure 2.10 - Comparison of percent error by sub-array number. 47

Figure 2.11 - Median fluorescence intensities and ratios 48

Figure 2.12 – Schematic of the slide, measuring target concentration dependence. 49

Figure 2.13 - Slide image after hybridization with 5 μM concentration AAAA probe at 635 nm excitation. 50

Figure 2.14 – Cy5 Fluorescence intensity of AAAA probe. 51

Figure 2.15 – Cy5 Fluorescence intensities of AAAA probe. 53

Figure 2.16 - Average fluorescence intensity of AAAA probe. 54

Figure 2.17 – Cy5 Fluorescence intensities of AAAA probe concentrations. 55

Figure 2.18 – Average fluorescence intensity of AAAA probe concentrations. 56

Figure 2.19 – Average AAAA probe Cy5 fluorescence intensity as a function of the probe concentration. 58

Figure 3.1 - Schematic of experimental slide.. 79

Figure 3.2 – FAM fluorescence intensities for the photoreactor control slide. 85

Figure 3.3 – FAM fluorescence intensities for the experimental slide. 86

Figure 3.4 - Ratio of FAM fluorescence intensities for the photoreactor control slide. 87

Figure 3.5 – Ratio of FAM fluorescence intensities for the experimental slide. 88

Figure 3.6 - Schematic of DNA microarray slide.. 90

Figure 3.7 - Median Cy5/FAM fluorescence intensities for the experimental slide. 91

Figure 3.8 – Median Cy5/FAM fluorescence intensities for the photoreactor control slide Enhanced controls. 93

Figure 3.9 – Median Cy5/FAM fluorescence intensity. 94

Figure 3.10 – Summary flow chart of the experimental process. 97

Figure 3.11 – Median Cy5/FAM fluorescence intensities for the photoreactor control slide. 98

Figure 3.12 – Median Cy5/FAM fluorescence intensities for the experimental slide. 99

Figure 4.1 – Normalized UV-Vis spectrum of the sealed SiH in toluene. 112

Figure 4.2 – Normalized UV/Vis spectrum for the exposed SiH sample. 113

Figure 4.3 – Fluorescence emission spectra of the sealed SiH. 115

Figure 4.4 – Fluorescence emission spectra for the exposed SiH sample. 116

Figure 4.5 – Normalized fluorescence emission spectrum of the sealed SiH. 119

Figure 6.1 – Median Cy5/FAM fluorescence intensities for the ATTA. 130

Figure 6.2 – Median Cy5/FAM fluorescence intensities for the AAAA. 131

Figure 6.3 – Median Cy5/FAM fluorescence intensities for the GTTG. 132

Figure 6.4 – Median Cy5/FAM fluorescence intensities for the ATTA. 133

Figure 6.5 – Median Cy5/FAM fluorescence intensities for the AAAA. 134

Figure 6.6 - Median Cy5/FAM fluorescence intensities for the GTTG. 135

Figure 6.7 - Median Cy5 fluorescence intensities for the ATTA. 136

Figure 6.8 - Median Cy5 fluorescence intensities for the AAAA. 137

Figure 6.9 - Median Cy5 fluorescence intensities for the GTTG. 138

Figure 6.10 - Median Cy5 fluorescence intensities for the ATTA. 139

Figure 6.11 – Median Cy5 fluorescence intensities for the AAAA. 140

Figure 6.12 – Median Cy5 fluorescence intensities for the GTTG. 141

1 General Introduction

1.1 Nucleic Acids

Nucleic acids are the genetic material of all organisms (Figure 1.1). DNA is composed of purines: guanine and adenine, and pyrimidine: thymine, and cytosine all bound to a sugar-phosphate backbone. RNA and DNA differ in that thymine is present in DNA, while uracil is present instead of thymine in RNA. The nucleoside subunits of DNA consist of the heterocyclic purine and pyrimidine bases attached to the C1' of 2'-deoxyribose sugar (ribose for RNA) through the N9 of the purine bases or the N1 of the pyrimidine bases[13]. Phosphate groups connect the nucleoside subunits through phosphoester bonds between the OH group on the C3' and C5' of each monomer[13]. Both DNA and RNA exist primarily in a double helix conformation held together through weak interactions between the base pairs. The base pairs in the double helix result from the interaction between specific nucleotides on opposite strands of DNA, here adenine forms 2 hydrogen bonds with thymine, while cytosine will form 3 hydrogen bonds with guanine. In RNA uracil will form 2 hydrogen bonds with adenine in the opposite strand.

1.2 Microarrays

The study of DNA and other biological molecules such as RNA and proteins have been furthered by the use of microarray experiments. This technique allows for high-density samples, small sample sizes, and hundreds of multiple biological experiments to be completed simultaneously[1]. The sample density allows a number of different biological samples present on the slide. Each spot or feature on the microarray slide can

be viewed as an individual experiment. Microarrays have been developed throughout the past few decades for a plethora of applications, including the identification of gene copies in a genome, mutation and single nucleotide polymorphism detection, drug discovery and development, and a diagnostic tool for diseases[2,3,4]. As a result of the rapid advances in microarray technologies, numerous techniques have been developed for the immobilization of biomolecules on surfaces. Important requirements must be considered when binding biomolecules to surfaces for analysis. These essential requirements must be met: (1) retained activity, (2) stability of the sample, and (3) negligible loss of sample during reactions and washing steps[5]. Different fabrication techniques have divided microarray deposition into two classifications, *in situ* synthesis, developed initially by Affymetrix Inc. (Santa Clara, CA), and direct spotting, using either contact or non-contact techniques to position premade biological samples on derivatized surfaces by microspotting or inkjet printing methods[5].

Synthesis. Affymetrix Inc. developed a light-directed chemical synthesis process, which uses solid-phase chemistry and photolithography techniques to produce high density DNA arrays[6] (Figure 1.2). It is capable of synthesizing desired oligonucleotide sequences directly on the glass surface. This method has the advantage of reducing the chances of contamination and higher throughput[7]. Separating the substrate and the printing device during the procedure negates the need for frequent washes of the printing device; this is where contamination would most likely occur. This method deposits an array of oligonucleotides in parallel, increasing the throughput potential. In this method, the glass surfaces are hydroxylated and silanized[5] with *N,N*-bis(hydroxyethyl)aminopropyl-triethoxysilane[8]. A protective group and a linker molecule

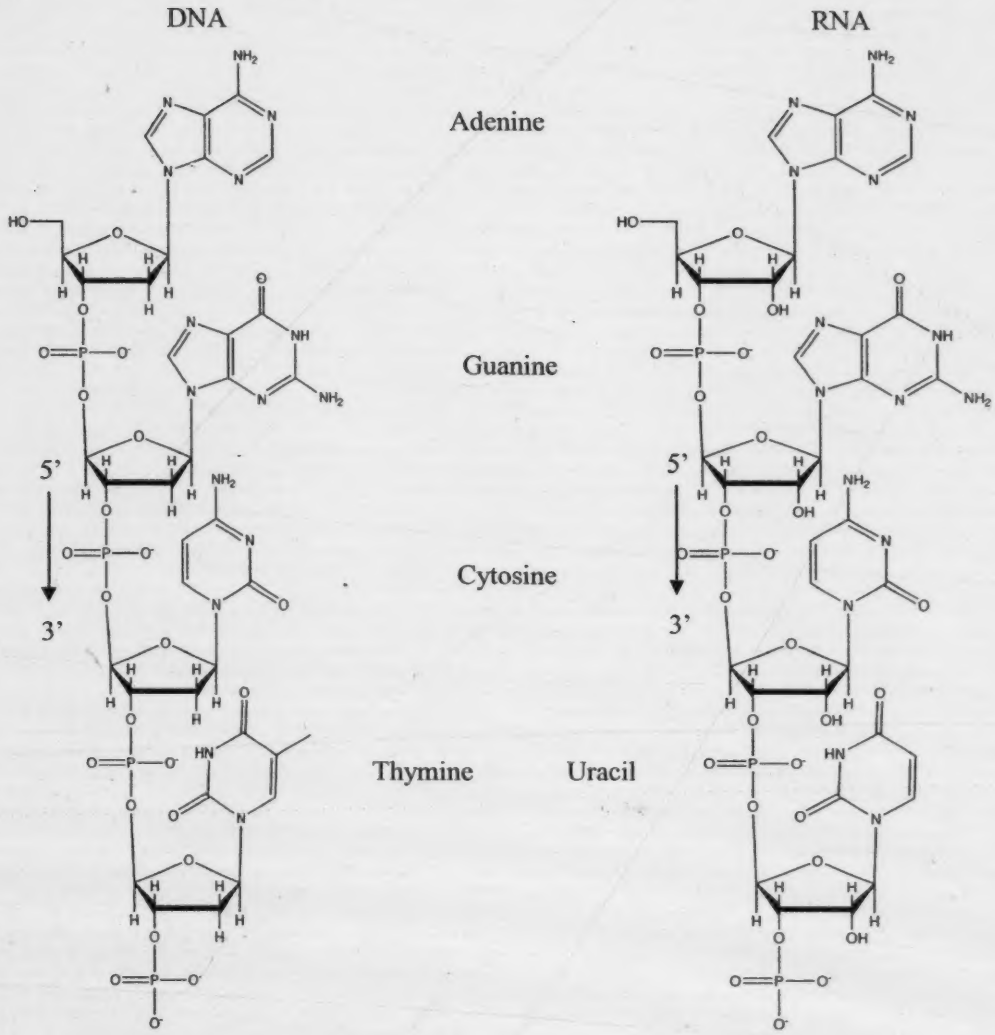

Figure 1.1- Structure of DNA and RNA.

(4,4'-dimethoxytrityl (DMT)-hexaethyleneglycol-(2-cyanoethyl-*N,N*-diisopropyl)phosphoramidite) are then added to the surface. The linker agents bind to the DNA oligonucleotide through the deoxyribose-phosphate. The linker agents are protected with a blocker group that is photosensitive, initially preventing the linker agents from binding to the nucleotides. A grid-like photolithographic mask is prepared and placed over the array such that only the desired positions are exposed. UV exposure on specific positions selectively removes certain blocker groups, and exposes the linker agent, allowing for binding of the nucleotides. The mask is removed and the entire slide is immersed in DNA solution containing only one nucleotide, coupling the nucleotide to the activated groups. The nucleotides are terminated at the 5' end with a photolabile group, *5'*-O-*(*α-methyl-6-nitropiperonyloxycarbonyl)-*N*-acyl-2'-deoxynucleoside. This group was designed with two main factors in mind. First the wavelength at which the photolabile group would be deprotected needed to be longer than 280 nm due to strong π-π^* transitions in that region of the nucleobases, decreasing the possibility of nucleobase photochemistry[9]. Second, the rate of deprotection for the four deoxynucleosides needed to be similar, ensuring light affected all of the UV exposed sites with the same amount of efficiency. Next, a new mask is used to cover the array, exposing different positions on the glass surface to UV light to remove the blocker groups on the deoxynucleosides. The next nucleotide is bound to the slide and the cycle continues, building specific oligonucleotide sequences as light is directed to different regions of the substrate. This method is capable of high throughput production[7], synthesizing a set of 4^n polynucleotides (n = length) in 4 x n chemical steps[2, 6]. This method has been shown to fabricate arrays with densities on the order of 10^6 sequences/cm^2, which corresponds to

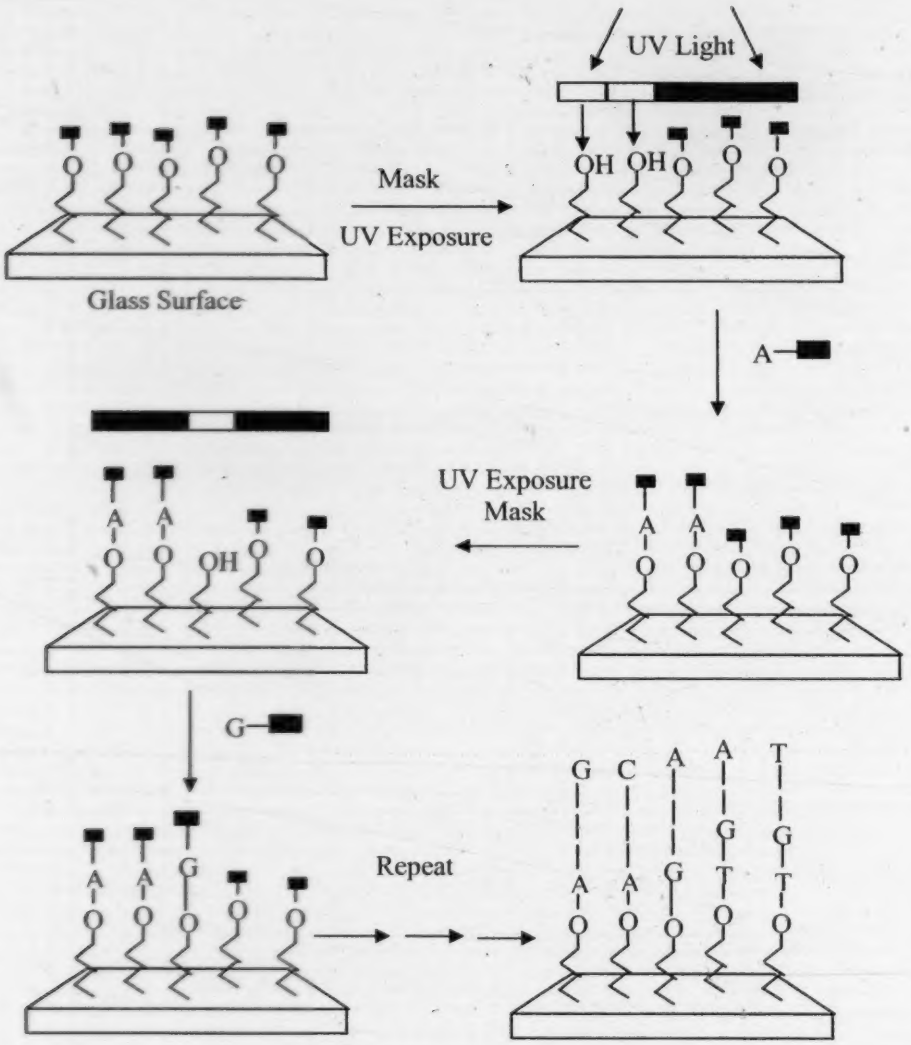

Figure 1.2 – Schematic of *in situ* light directed oligonucleotide synthesis on a microarray glass slide with the use of a photolithographic mask.

an individual feature size of 5-10 μm. The disadvantages of this method include the possibility of denaturation of the biomolecules by the photoresist solvents and the limited miniaturization, which is dependent upon the light and mask resolution. The extent of deprotection in any area of the substrate is linearly related to the amount of light received. A high contrast between illuminated and adjacent masked regions is required to increase the resolution on the slide. In addition, another disadvantage of this method is the cost and time associated with the design of the photolithographic masks[1].

Deposition. Microarrays have also been developed with the use of microspotting techniques, where biomolecules, including DNA are directly spotted onto a derivatized surface. Here small amounts of premade biochemical substances are printed onto the solid surface. This is done by direct contact onto the surface. The delivery mechanism of motion controlled pins or capillaries moved in an XYZ system transfers the samples to the derivatized surface[10,11]. Glass surfaces have been the primary substrate due to their inert chemical properties, ability to be modified through silane chemistry, natural low level of fluorescence, and resistance to high temperatures[1,4]. The deposition of molecules on the glass surface has been prepared with various types of spotters and derivatized substrate surfaces[5]. The use of different substrates determines how biomolecules are immobilized and the types of interactions involved in immobilization, whether van der Waals, ionic, covalent, coordination or affinity[5]. The noncovalent interactions are often manipulated through the presence of phosphate groups on DNA. They provide sites, which can be used for immobilization. The negatively charged phosphate groups bind to positively charged molecules on the surfaces such as amine groups through ionic interactions (Figure 1.3 A). Unfortunately, these interactions are not able to withstand

the high salt or high temperatures inflicted on the surfaces, thus resulting in the removal of the DNA film from the surface[4]. Because of this, covalent binding methods are preferred. Covalent immobilization can occur through the cross-linking of DNA from ultraviolet irradiation, forming covalent bonds between thymidine residues in the DNA and positively charged amino groups on the slide[4,12]. One disadvantage to this method is the variability in binding sites in the DNA strand, limiting the length and sequences of DNA available for hybridization[4]. A different method utilized to covalently bind DNA to the surface is to modify the oligonucleotide at the extremities[4,5]. Carboxylated or phosphorylated DNA can be bound to an aminated support or vice a versa. An amino-modified oligonucleotide could also be bound to an isothiocyanante-activated glass, aldehyde-activated glass, or even to an epoxide-modified glass surface. These amine terminated oligonucleotides can form a covalent bond (Figure 1.3 B), through an S_N2 reaction at slightly basic pH, attaching the DNA to the surface of the slide, and preventing the DNA from being washed off during the rinsing steps of a procedure. This technique is extremely fast and can deposit the spots in an extremely space-efficient manner, printing thousands of spots in a square of about 2 cm.

1.3 DNA Photochemistry

Every living organism contains its entire genetic code within its DNA, hence, protecting our DNA is of great importance[13]. The effect of UV light on DNA induces damage such as single strand breaks, cross-links, and nucleobase damage all of which can affect the structure of DNA in the double helix[14]. Single strand breaks have resulted from

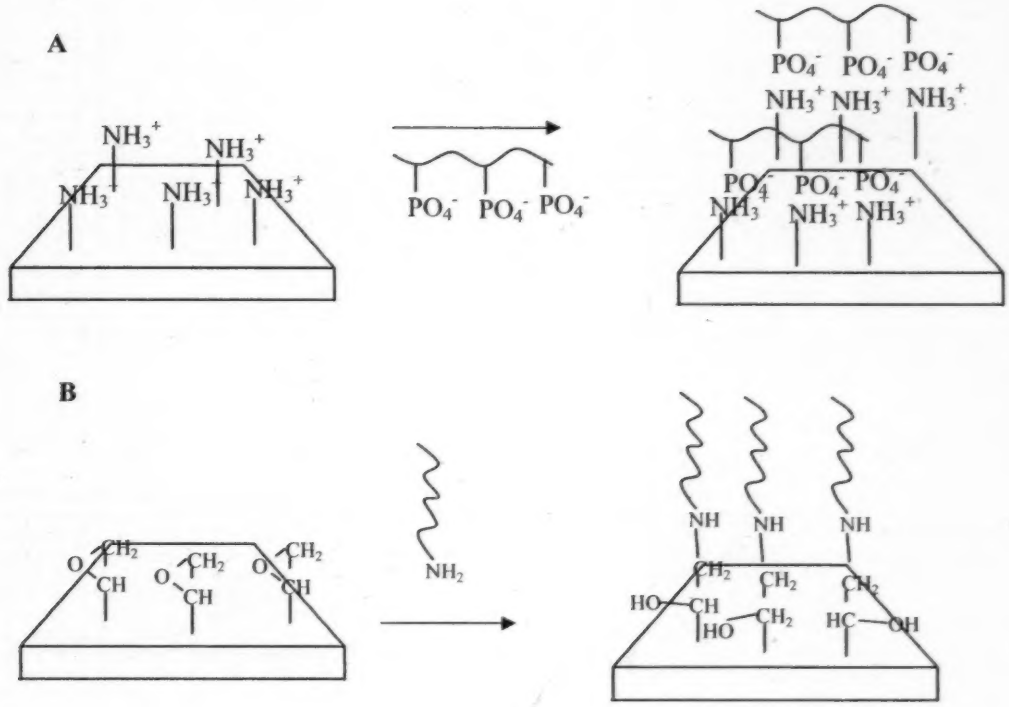

Figure 1.3 – Attachment chemistry of DNA onto a derivatized glass slide. (A) noncovalent interaction between the phosphate groups on DNA and amine groups on the slide surface. (B) covalent binding between amino-terminated oligonucleotide and epoxide derivatized surface.

UV irradiation, however, their frequency is significantly lower than many other photoproducts, especially dimers[14]. Single strand breaks make up <0.1% of the photoproducts resulting from either UVC or UVB irradiation[15]. The work discussed in the following chapters involves damage created only on single strands of DNA. Hence, neither DNA-protein cross-links nor cross-links between two complementary strands of DNA are of great significance to our work. These photoproducts are also of low frequency; cross-links with protein only account for <0.1% of total photoproducts produced by UVC or UVB irradiation[15].

Nucleobase damage, which occurs as a result of UV irradiation, consist of three major photoproducts, cyclobutyl pyrimidine dimers (CPDs), pyrimidine pyrimidinone [6-4]-photoproducts, and photohydrates. The CPDs are the most characterized photoproducts of DNA[15]. This photoproduct is most prevalent between adjacent pyrimidine bases, thymine and cytosine, forming 77 and 78% of the total photoproducts when irradiated with UVC and UVB light, respectively (Figure 1.4). These dimers result from a [2π+2π]-cycloaddition of two double bonds on the adjacent pyrimidines. This reaction can lead to the formation of four isomeric dimers *cis-syn, cis-anti, trans-syn,* and *trans-anti*, where, *cis* and *trans* describe the orientation of the methyl groups on the bases, and *syn* and *anti* describe the orientation between the pyrimidine rings[15]. However, the double helix of DNA only allows the *cis-syn* isomer, due the restricted orientation of the bases. Conversely, ssDNA is capable of forming an additional isomeric dimer, *trans-syn*, due to the added flexibility permitted by a single strand of DNA.[15]

The second most prevalent form of photodamage occurring in DNA is the [6-4]-photoproduct. Similar to the CPD, the [6-4]-photoproduct is also formed through a

[2π+2π]-photocylcoaddition (Figure 1.4). Contrary to the cyclobutyl dimers, this photoproduct takes place at the 3' base of either the C4-O4 carbonyl of thymine or the C4-N4 imino tautomer of cytosine onto the C5-C6 double bond of the adjacent 5' base[15]. The [6-4]-photoproduct also occurs at a much lower frequency compared to CPDs, only producing 20% of the total photoproducts from irradiation with UVC and 10% when irradiated with UVB light[15].

The third photoproduct resulting from UV irradiation is the photohydrate (Figure 1.4). Photohydrates make up approximately 2% of the total photoproducts produced from UVC and UVB radiation. Photohydrates only occur at excited pyrimidine bases and do not involve adjacent bases. This reaction occurs through a nonstereospecific nucleophillic addition of water onto the C6 position across the C5-C6 double bond. It is believed that the reaction occurs through an excited singlet state intermediate which may be in the form of a carbocation resulting from proton transfer to the C-5 position[15]. The formation of the photohydrate is highly unfavoured for polynucleotides or DNA as a result of the other competing photoreactions mentioned previously. For polynucleotide or DNA, base stacking would be more conducive to photoaddition while an unstacked structure would favour the photohydration photoreaction[15].

1.4 Molecular Beacons

Molecular beacons are molecules that have been used as an emerging detection tool, primarily through hybridization to complementary sequences. Molecular beacons, first developed by Tyagi and Kramer[20], are probes that produce measurable fluorescence signal when hybridized with a complementary target[16]. Molecular beacons are composed

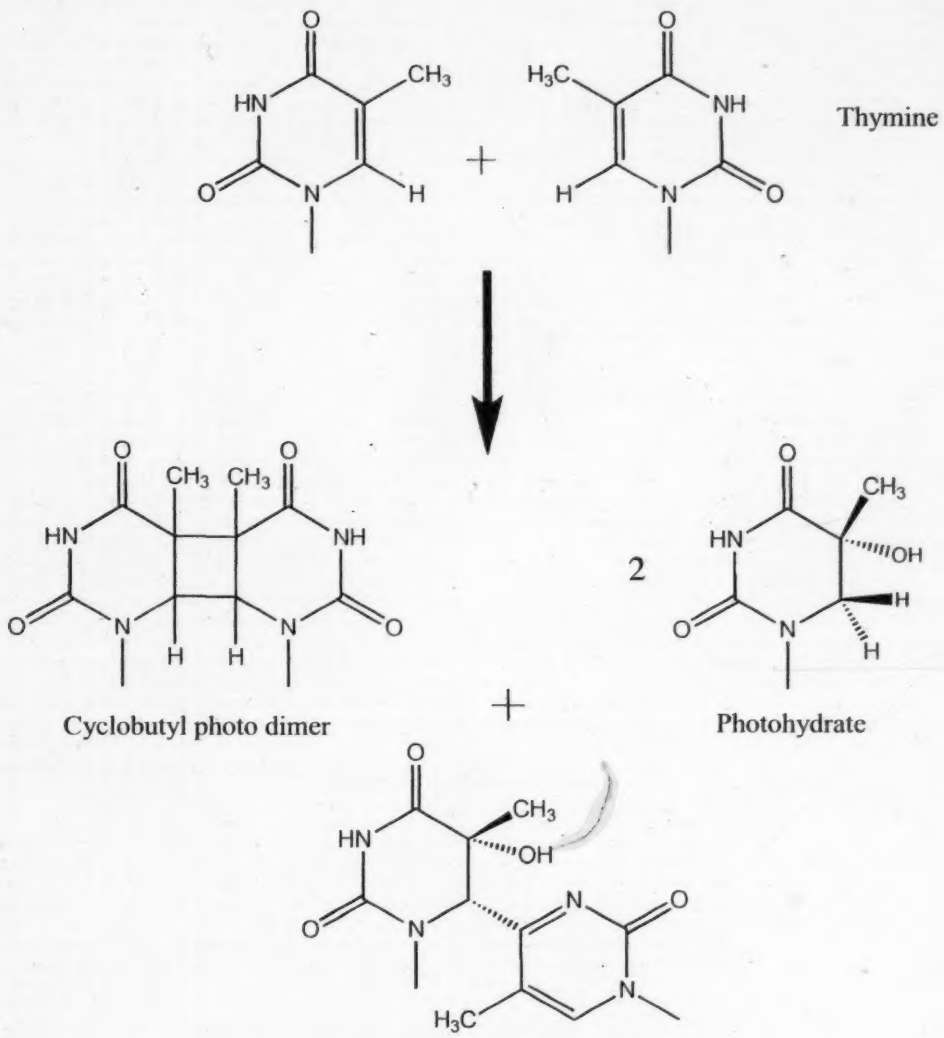

Figure 1.4 – Major photoproducts of thymine upon UV irradiation.

of a single-stranded oligonucleotide, usually of approximately 25 nucleotides, which form a stem and loop structure (Figure 1.5), where the 3' and 5' ends are self-complementary for ~5-7 bases, and the center sequence is complementary to a chosen target[17,18,19]. The dual-labeled oligonucleotide has a fluorophore coupled to the 5' end and a fluorescent quencher coupled to the 3' end of the stem[16,20]. In the absence of target, the self-complementary stem anneals, which brings the fluorophore and quencher in close proximity resulting in the quenching of fluorescence[19,21,22]. When the loop sequence hybridizes with the target sequence, the stem portion of the probe is forced to unfold, spatially separating the fluorophore and quencher, and restoring fluorescence upon excitation[16,19,23,24].

There are three major advantages of molecular beacons due to their innovative structure. The first is the freedom to detect samples without immobilization to solid supports. The hybridization of a nucleic acid to its complement has been used in many areas, employing different types of DNA fluorescent probes. One area it has been used is in nucleic acid blotting techniques where a solid support is used to immobilize DNA fragments. A labeled probe containing the sequence of interest is used to hybridize with its counterpart. For the success of this technique, a solid support must be used, and as such, poses a problem for monitoring real time synthesis of nucleic acids, or nucleic acids within a living cell.

Second, the inherent signal transduction mechanism possessed by molecular beacons allows for high sensitivity[17,20]. They are able to act as sensitive probes with high signal-to-background ratios. The fluorescence intensity can increase more than 200-fold when hybridized to a target under optimal conditions[17,25]. In addition to this, when

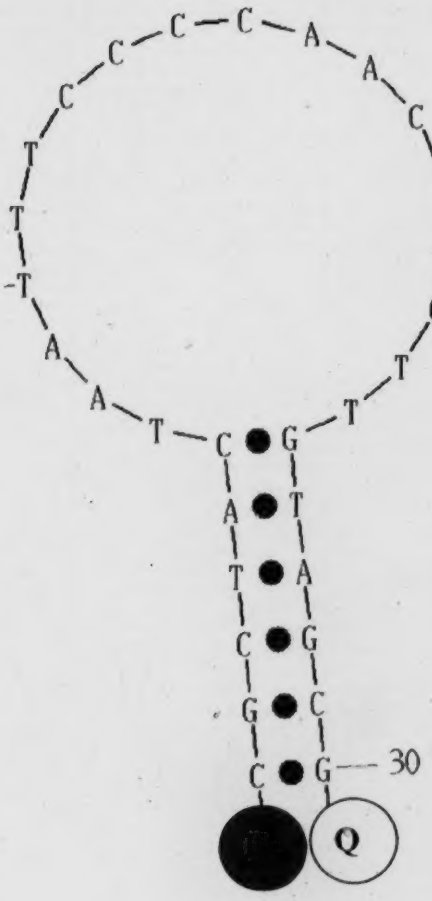

Figure 1.5 – Schematic of a classic molecular beacon. The covalently linked fluorophore and quencher, F, and Q, respectively, are attached at the 5' and 3' ends of the stem.

with molecular beacons one has the ability to detect target hybridization in situations where the separation of hybridized from nonhybridized probes is either not possible or desired[16,17,20,23,,26] such as real-time monitoring of polymerase chain reactions (PCRs) in sealed containers or the detection of mRNAs within living cells[25]. This characteristic allows one to monitor the synthesis of nucleic acids in sealed tubes or in living specimens, without additional manipulation.

The third advantage of molecular beacons is their molecular recognition specificity. They are extremely target-specific, compared to traditional linear probes, distinguishing between nucleic acid target sequences that differ by as little as a single nucleotide[17,21,27]. This extraordinary selectivity of molecular beacons is a result of the loop and stem structure, since the stem hybrid is able to shift the equilibrium from the loop-target hybrid. These molecules follow a well-documented melting curve or thermal denaturation profile as shown in Figure 1.6. This allows us to monitor the effects of temperature on the secondary structure of the molecular beacons through fluorescence. When a solution of molecular beacons is incubated in the absence of target at lower temperatures (below 20°C), the predominant structural conformation is the 'closed' form. Here the fluorophore and the quencher are brought in close proximity to one another. Fluorescence is quenched, through energy transfer between the fluorophore and the quencher, and minimal emission is observed in this phase. When the temperature is increased and the required energy for stem denaturation is met, opening the stem and spatially separating the fluorophore from the quencher (Figure 1.6A, trace a). If the temperature continues to increase, the beacon goes into a random coil structure where the

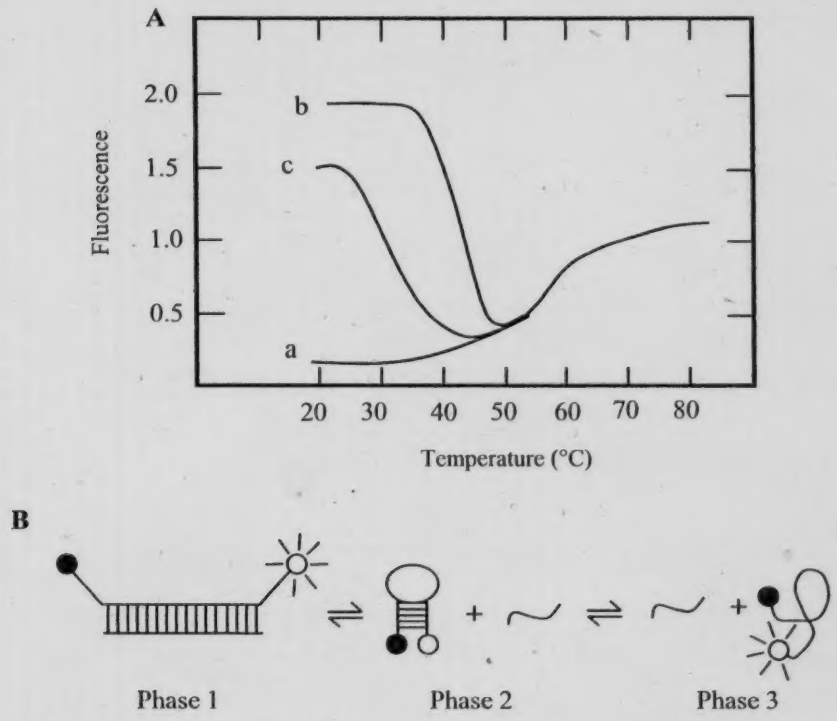

Figure 1.6 – Phase transitions for molecular beacons. (A) represents a thermal denaturation profile. Trace (a) depicts the fluorescence change for a molecular beacon incubated in the absence of targets, trace (b) depicts the fluorescence change for a molecular beacon incubated with perfectly complementary targets, and trace (c) depicts the fluorescence change for a molecular beacon incubated with mismatched targets. (B) is a schematic of molecular beacons in different phases. Phase 1 represents the open "light" phase where the molecular beacon is hybridized with target. Phase 2 represents the closed "dark" phase in the presence of target and increased temperature. Phase 3 represents the random coil phase where the molecular beacon stem denatures as a result of high temperatures.

fluorescence emission levels off and remains relatively constant with increasing temperature to ~80°C[23].

Upon the addition of a perfectly matched target sequence the thermal denaturation profile will follow a different melting trend (Figure 1.6 A, trace b). In this case, when excess target is in solution with the molecular beacon, the equilibrium will favor the 'open' form of the molecular beacon, where the fluorophore and the quencher are spatially separated the most, resulting in maximum fluorescence. As the temperature is increased, the hybrid duplex will reach its inflection point where the probe-target hybrid will begin to denature and the molecular beacon stem will begin to reanneal decreasing the fluorescence intensity. With a further addition of heat, the molecular beacon will once again go into the random coil phase[23].

Interestingly, if an excess of target, which is not perfectly complementary to the loop portion of the molecular beacon, is incubated with the solution of molecular beacon, the melting curve will closely resemble the curve with the matched target except for one key point. The inflection point demonstrating the temperature where the probe-target hybrid begin to denature shifts to a lower temperature, indicating that less heat energy is required to denature the mismatched hybrid duplex (Figure 1.6A, trace c). Molecular beacons have been found to be sensitive enough to detect a difference as small as a single base mismatch through the difference in the melting temperature[23]. The use of molecular beacons dismisses the need for separation chemistry. Since the closed form molecular beacon is dark when it is not hybridized to the target, it will only minimally contribute to the signal.

Variations to the classic molecular beacon structure have been reported, often including different quencher molecules or changes to the length of complementarity between the stem of the molecular beacon and the target sequence. One of the interesting developments to molecular beacon design is the immobilization of a molecular beacon on to the surface of a silica plate through avidin linkages for the development of a solid-state biosensor[28]. In this example, both a fluorophore and a quencher are still used. However, when the molecular beacon is attached to a metal surface, such as gold, the need for a quencher molecule is eliminated. The closed molecular beacon phase is not able to emit due to the quenching properties of the gold surface[29,30,31]. Another modification to the classic molecular beacon design attacks the problem of nonspecific binding occurring on the stem portion when used in a natural biological environment[31]. To solve this problem Kim *et al* designed a molecular beacon, which uses non-standard bases like L-DNA in the stem portion of the probe[31]. L-DNAs are enantiomers of natural D-DNA and as such are unable to bind with naturally occurring DNA within the sample. With this design the stem is prevented from engaging in any intramolecular or intermolecular nonspecific interactions other than the hairpin structure desired[31]. Current work with molecular beacons has shown their extensive use as damage detecting molecules. This includes the detection of oxidative damage[32] and DNA damage induced by ionizing radiation[33].

1.5 Summary of Research

Advancements in microarray technology have allowed DNA/or RNA hybridization research to broaden our understanding of gene expression, single nucleotide polymorphisms, and even genetic identification. Unfortunately, the quality of current

microarrays has not been fully developed, allowing them to be used as analytical tools. In Chapter 2, we investigate the numerous parameters, which can be optimized to reduce the amount of error resulting from spot-to-spot printing variation. The use of an internal standard and the optimization of target and probe concentrations are explored. Chapter 3 contains detection of UVC-induced DNA damage using fluorescently-labeled hairpin probes on microarrays, from which the rates of photodamage of three different DNA sequences are determined. The quantification of the fluorescent properties of Si nanoparticles as potential DNA fluorophores is discussed in Chapter 4. Chapter 5 provides some conclusions and ideas for future work from the results obtained in Chapters 2-4.

1.6 References

[1] Lemieux, B.;Aharoni, A.; Schena, M. *Molecular Breeding* **1998**, 4, 277-289.

[2] Kumar, A.; Goel, G.; Fehenbach, E.; Puniya, A. K.; Singh, K. *Eng. Life Sci.* **2005**, 5, 215-222.

[3] Guo, Z.; Guilfoyle, R. A.; Thiel, A. J.; Wang, R.; Smith, L. M. *Nuc. Acid. Res.* **1994**, 22, 5456-5465.

[4] Zammatteo, N.; Jeanmart, L.; Hamels, S.; Courtois, S.; Louette, P.; Hevesi, L.; Remacle, *Anal. Biochem.* **2000**, 143-150.

[5] Venkatasubbarao, S. *Trends Biotechnol.* **2004**, 22, 630-637.

[6] Lipshutz, R.; Fodor, S. P. A.; Gingeras, T. R.; Lockhart, D. J. *Nature Genet.* **1999**, 21, 20-24.

[7] Barbulovic-Nad, I.; Lucente, M.; Sun, Y.; Zhang, M.; Wheeler, A.; Bussmann, M. *Critical Reviews in Biotechnology* **2006**, 26, 237-259.

[8] McGall, G.; Labadie, J.; Brock, P.; Wallraff, G.; Nguyen, T.; Hinsberg, W. *Proc. Natl. Acad. Sci. USA* **1996**, 93, 13555-13560.

[9] Pease, A. C.; Solas, D.; Sullivan, E. J.; Cronin, M. T.; Holmes, C. P.; Fodor, S. P. A. *Proc. Natl. Acad. Sci. USA* **1994**, 91, 5022-5026.

[10] Schena, M.; Heller, R. A.; Theriault, T. P.; Konrad, K.; Lachenmeier, E.; Davis, R. W. *Trends Biotechnol.* **1998**, 16, 301-306

[11] Belaubre, P.; Guirardel, M.; Leberre, V.; Pourciel, J.; Bergaud, C. *Sens. and Actuators A* **2004**, 110, 130-135.

[12] Dugan, D. J.; Bittner, M.; Chen, Y.; Meltzer, P.; Trent, J. M. *Nature Genetics Supplement*, **1999**, 21, 10-14

[13] Nelson, D. L.; Cox, M. M. *Lehninger Principles of Biochemistry, 3rd edition*; Worth Publishers: New York, NY, 2000; pp 325-358.

[14] Rahn, R. O.; Patrick, M. H. In *Photochemistry and Photobiology of Nucleic Acids*; Editor, Wang, S. Y.; Academic Press, Inc: New York, NY, 1976; Vol. 2, p98.

[15] Mitchell D. L., In *CRC Handbook of Organic Photochemistry and Photobiology*; Editor, Horspool, W. H.; Editor, Song, P.-S.; CRC Press: New York, NY, 1995, pp 1297-1328.

[16] Goel, G.; Kumar, A.; Puniya, A. K.; Chen, W.; Singh, K. *Appl. Microbiol.* **2005**, 99, 435-442.

[17] Yao, G.; Tan, W. *Anal. Biochem.* **2004**, 331, 216-223.

[18] Drake, T. J.; Tan, W. *Appl. Spectrosc.* **2004**, 58, 269-280A.

[19] Tsourkas, A.; Behlke, M. A.; Rose, S. D.; Bao, G. *Nuc. Acid. Res.* **2003**, 31, 1319-1330.

[20] Tyagi, S.; Kramer, F. R. *Nat. Biotechnol.* **1996**, 14, 303-306.

[21] Liu, X.; Tan, W. *Anal. Chem.* **1999**, 71, 5054-5059.

[22] Dubertret, B.; Calame, M.; Libchaber, A. J. *Nat. Biotechnol.* **2001**, 19, 365-370.

[23] Bonnet, G.; Tyagi, S.; Libchaber, A.; Dramer, F. R. *Proc. Natl. Acad. Sci. USA* **1999**, 96, 6171-6176

[24] Marras, S. A. E.; Krammer, F. R.; Tyagi, S. *Genet. Anal. – Biomol. Eng.* **1999**, 14, 151-156.

[25] Fang, X.; Li, J. J.; Perlette, J.; Tan, W.; Wang, K. *Anal. Chem.* **2000**, 72, 747-753A.

[26] Xi, C.; Raskin, L.; Boppart, S. A. *Biomed. Microdevices* **2005**, 7, 7-12.

[27] Tan L.; Li, Y.; Drake, T. J.; Moroz, L.; Wang, K.; Li, J.; Munteanu, A.; Yang, C. J.; Martinez, K.; Tan, W. *Analyst* **2005**, 130, 1002-1005.

[28] Borisov, S. M.; Wolfbeis, O. S. *Chem. Rev.* **2008**, 108, 423-461.

[29] Strohsahl, C. M.; Miller, B. L.; Krauss, T. D. *Nat. Prot.* **2007**, 2, 2105-2110.

[30] Fang, X.; Liu, X.; Schuster, S.; Tan, W. *J. Am. Chem. Soc.* **1999**, 121, 2921-2922.

[31] Kim, Y.; Yang, C. J.; Tan, W. *Nuc. Acid. Res.* **2007**, 35, 7279-7287.

[32] Mah, A.; Loppnow, G. R. in preparation.

[33] Sparling, S.; Loppnow, G. R. in preparation.

2 Reducing the Error on DNA Microarrays

2.1 Introduction

Microarrays are a technique used to study biomolecular samples [1]. Microarrays consist of a modified microscope glass slide, with deoxyribonucleic acid (DNA) or ribonucleic acid (RNA)[1] attached to the surface in a highly dense array pattern. Modifications to the slide surface often contain molecules that covalently bind DNA, such as epoxides, 1,4-phenylene diisothiocyanate[2], and sulfo-succinimidyl 4-(N-maleimidomethyl) cyclohexane-1-carboxylate[3]. Typically, a target sequence of DNA is covalently attached to the surface of a microarray slide. A complementary fluorescently labeled sequence can be hybridized with the surface-bound target sequence. The hybridized probe produces its maximum fluorescence signal maximum when the probe DNA sequence and the target sequence are perfectly complementary. However, with the appropriate hybridization conditions this technique can be used to discriminate between a target DNA differing in sequence by only a single base[2,4], resulting in a decrease in fluorescence signal. This technique allows one to determine the presence or relative amount of a specific DNA sequence on the slide.

Microarrays are a commonly used technique in gene expression research, which correlates gene expression levels to DNA sequence[5]. Changes in gene expression levels are associated with important biological phenomena[5] such as cancer, aging, and disease states. These studies are able to show how gene expression levels change between the normal and abnormal states of the cell. Microarrays have been developed as a more advantageous alternative to the more limited RNA blots, assays that are dependent upon gel electrophoresis[5]. In DNA microarray experiments, one is able to screen thousands of

genes simultaneously in a single experiment[6]. DNA microarrays have become increasingly important in accelerating genetic analysis due to their ability to conduct almost an unlimited amount of experiments simultaneously[7, 8]. Microarrays have been used to measure a selected set of genes expression levels, which have been correlated to specific diseases. These gene expression levels are either activated ("up-regulated"), or suppressed ("down-regulated") compared to a control[9]. Although microarrays are becoming the leading technique over assays and blots[5], the expression results obtained are validated with other techniques such as RNA blots and qRT-PCR[10]. These two alternative techniques (RNA blots and qRT-PCR) are both more sensitive than DNA microarrays. With this, gene up- or down- regulation are the same for all three techniques, while the dynamic range for these techniques can differ significantly - where qRT-PCR may span five orders of magnitude, a DNA microarray may only span three[10].

Current DNA microarray results are obtained through normalization of signal intensities and are qualitative. There are many problems associated with this method, such as the current inability to determine the differences in the amount of DNA in the probe preparation, the variations that may exist in label efficiencies, and protocols of hybridization and washing[5]. The susceptibility of data to large amounts of error due to lack of control and quality involved in the immobilization techniques[7] is another problem. This difficulty in standardizing microarray results from different research groups makes the current microarray platform somewhat unreliable and irreproducible.

Previous microarray work[11] involving internal standards used a two-step hybridization method where fluorescence was used to detect each hybridization process. Fluorescence detection made it possible to visualize the hybridization of labeled viral

RNA fragments to a capture sequence bound to a microarray slide. This was followed by a second hybridization step between the labeled viral RNA and a labeled probe, resulting in a second signal which could be measured. This technique provides a means to evaluate the capture efficiency of both hybridization steps[11]. However, this method utilized linear probes, which have been found to be less specific compared to a hairpin structure[12]. This technique would not allow for dynamic experiments to be conducted on the microarray slide, where environmental conditions are altered, resulting in a change in the sequence.

This chapter discusses a novel method, and its optimization, to obtain quantitative data from DNA microarray experiments. Using a short single stranded deoxyribonucleic acid (ssDNA) oligonucleotide, labeled with an organic dye and modified to bind to the microarray glass surface as an internal standard, we attempted to reduce the large variations within single sets of data. Optimization of the target and probe concentrations were investigated in order to obtain maximum signal intensity. The results show that 35 μM is the optimal concentration for the fluorescently labeled probe. The target concentration found to correlate to the most reliable signal intensity when bound to the fluorescent probe was 50 μM. Data analysis was completed using two different techniques, in order to determine the most reliable method. All of these factors decreased errors by approximately a factor of 2 or more.

2.2 *Experimental*

Materials. NaH_2PO_4, Na_2HPO_4, and sodium citrate were obtained from Fisher Scientific (Ottawa, ON). NaCl was obtained from EMD (San Diego, CA). Bovine serum albumin was obtained from Sigma (Oakville, ON). Tris-HCl was obtained from ICN (Biomedicals Inc., Irvine, CA). All chemicals were used as received. Nanopure water from a Barnstead NanoPure (Boston, MA) water purification system was used for all solutions. The 5' amino-modified target and probe DNA oligonucleotides (Tables 2.1 and 2.2), FAM internal standard (Figure 2.1 and 2.2), and the complementary 5'-Cy-5 modified DNA probe sequences (Figure 2.3 and 2.4) were obtained from Integrated DNA Technologies (Coralville, IA). The amino modified target sequences (Table 2.1) were purified using standard desalting. The 5'-Cy-5 modified DNA probe sequences (Table 2.2) and the FAM internal standard (Table 2.1) were purified with standard desalting and HPLC. The model 40041 epoxide-coated slides with bar codes were purchased from Corning (Neepan, ON).

Buffers. The 300 mM phosphate buffer was prepared by adding 300 mM NaH_2PO_4 dropwise to 300 mM Na_2HPO_4 to reach a final pH of 8.6, then filtered with a 0.2 μm membrane filter. A 0.1 X NaCl-Sodium citrate solution (SSC) (wash 1) was prepared by a 200-fold dilution of 20 X SSC (3 M NaCl, 0.3 M sodium citrate, pH adjusted to 7.4) and filtered through a 2 μm membrane filter. The wash 2 buffer was prepared by adding 0.2% SDS (sodium dodecyl sulfate) to a 10-fold dilution of 20 X SSC, adjusting the pH to 7.4, and filtering through a 0.2 μm membrane filter. The 0.2 %

Table 2.1 - Amino terminated target sequences

Name	Sequence
ATTA	5'-/Am/CGT GCA AAA AAA TTA AAA AAA A-3'
GTTG	5'-/Am/CGT GCA AAA AAG TTG AAA AAA A-3'
AAAA	5'-/Am/CGT GCA AAA AAA AAA AAA AAA A-3'
dFAM	5'-/Am/TGA GC/FAM/-3'

Each of the target sequences are terminated at the 5' end with an amino (Am) group. The dFAM internal standard sequence is modified on the 3' end with the fluorescent dye 6-carboxyfluorescein (FAM).

Table 2.2 - Complementary Cy5 modified DNA hairpin probe sequences

Name	Sequence
ATTA probe	5'- /5Cy5/CGT GCT TTT TTT TAA TTT TTT TGC ACG -3'
GTTG probe	5'- /5Cy5/CGT GCT TTT TTT CAA CTT TTT TGC ACG -3'
AAAA probe	5'- /5Cy5/CGT GCT TTT TTT TTT TTT TTT TGC ACG -3'

Each of the DNA probe sequences is modified on the 5' end with the fluorescent dye thiadicarbocyanine (Cy5).

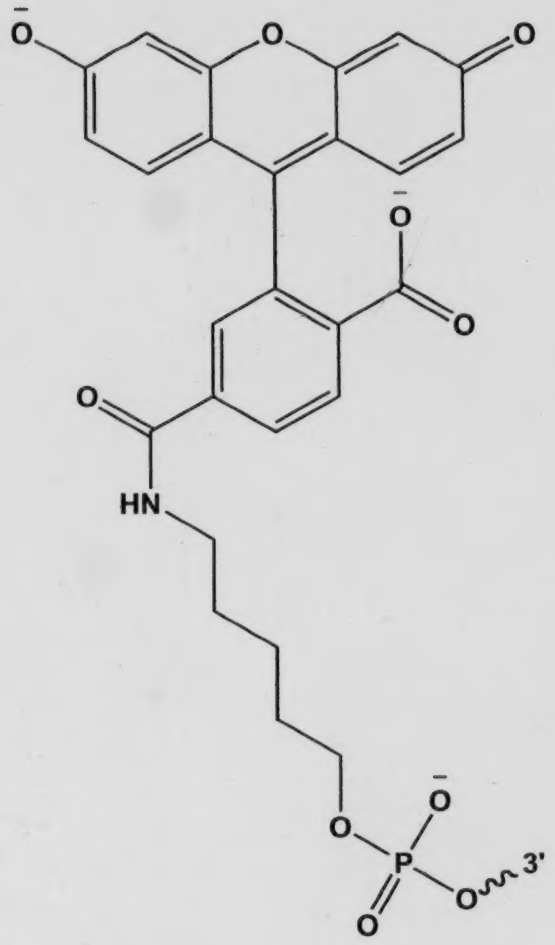

Figure 2.1 - Structure of 6-carboxyfluorescein (FAM) used as the internal standard. It absorbs 488 nm light and fluoresces at a wavelength of 530 nm. Scanner presets for excitation and emission of the FAM fluorophore are 480 nm and 530, respectively.

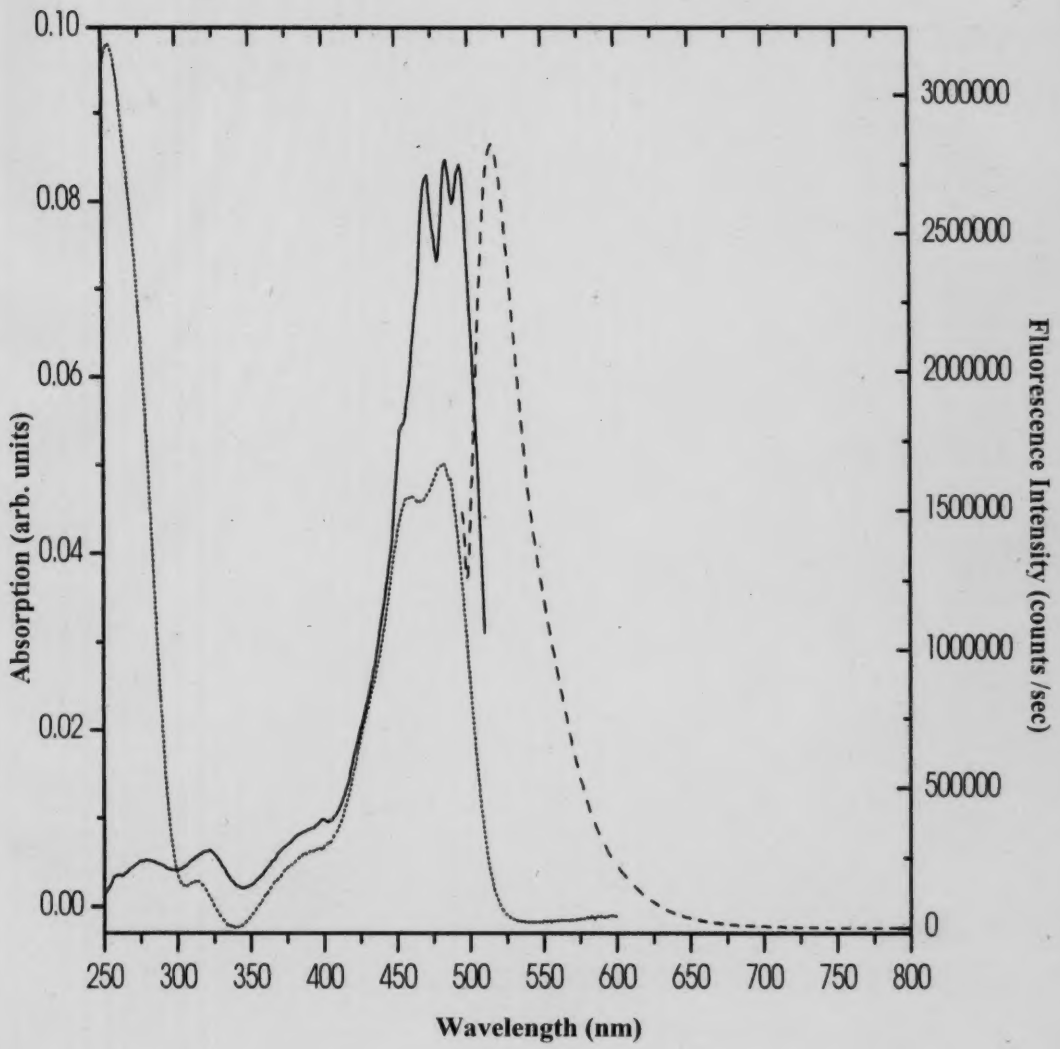

Figure 2.2 - FAM internal standard absorption (dotted), excitation (solid), and emission (dashed) spectra (FAM labeled target). Internal standard concentration was 2 µM. An excitation wavelength of 495 nm was used for the emission spectrum. An emission wavelength of 515 nm was used to monitor the excitation spectrum.

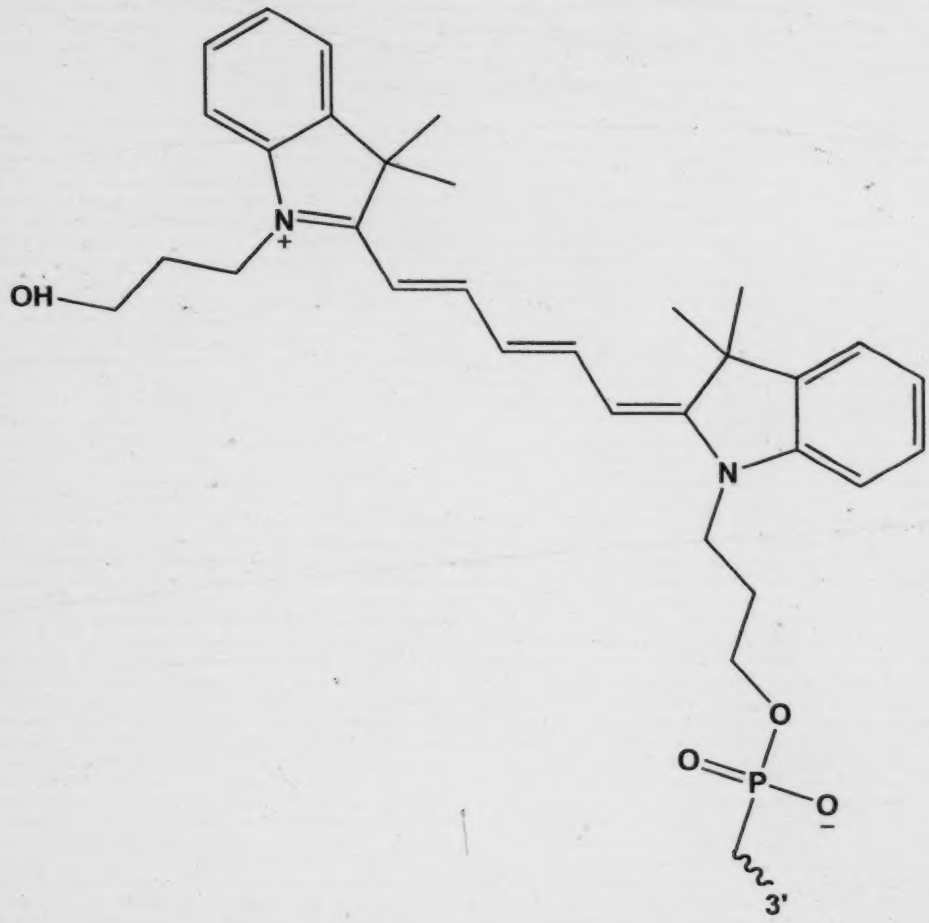

Figure 2.3 - Structure of the thiadicarbocyanine (Cy5) organic dye modification to DNA, used on the hairpin probes. This dye absorbs light at 648 nm and fluoresces at a wavelength of 668 nm. Scanner presets for excitation and emission of the Cy5 probe are 635 nm and 685 nm, respectively.

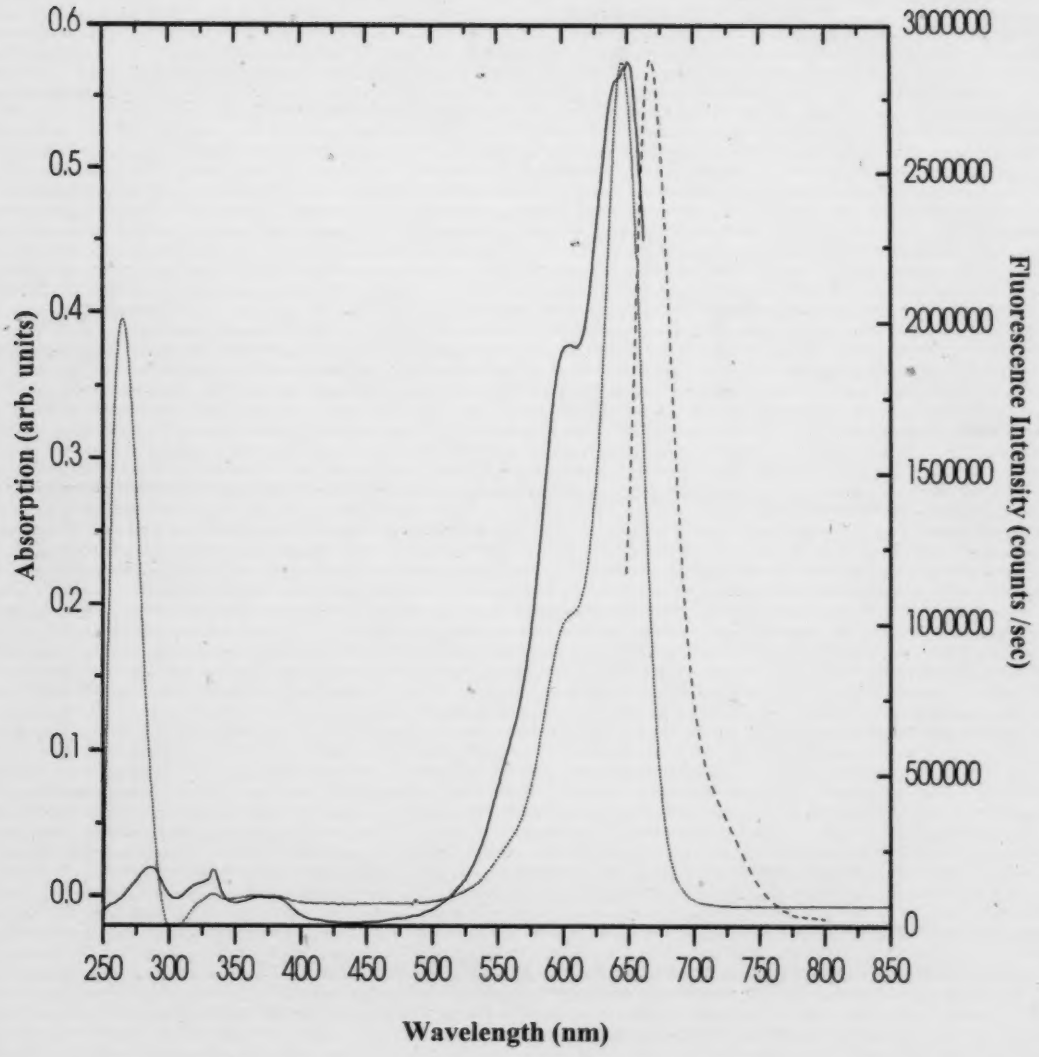

Figure 2.4 – As in Figure 2.2 but for the Cy5 probe. Here an excitation wavelength of 648 nm was used for the emission spectrum and an emission wavelength of 668 nm was monitored for the excitation spectrum.

(w/v) bovine serum albumin (BSA) solution was prepared with 5X SSC and 1% SDS. The hybridization buffer was prepared by combining 1 mM $MgCl_2$ and 10 mM Tris-HCl, adjusting the pH to 7.4, and filtering through a 0.2 μm membrane filter.

Microarrays. The amino-terminated target DNA sequences were diluted with 150 mM phosphate buffer and 0.5 μM FAM internal standard to the following concentrations: 5, 10, 25, 50, 100, 250, and 500 μM. A multifunctional, liquid-handling robotic microarrayer OmniGrid100™from GeneMachines, (San Carlos, CA) in the Microarray and Proteomics Facility at the University of Alberta was used to print the DNA onto the Corning epoxide-coated slides (Figure 2.5). The capillary printing pins were Stealth 3 Micro Spotting Pins from TeleChem International, Inc. (Sunnyvale, CA), the pin speed was 2 cm/s, and the dwell time on the slide was 100 ms for each spot. For all the printings, the humidity was maintained at 50%. Sonication and pin washings were carried out between samples to avoid sample cross-contamination. After printing, the DNA was left to dry and react with the epoxide groups on the surface of the glass slide for approximately 1 hour. Fluorescent scans of the slides were obtained with an arrayWoRx Standard scanner from Applied Precision, LLC (Issaquah, WA). These scans were used to measure the fluorescent intensities of the fluorophores used in the experiments.

Pre-Treatment and Washes of DNA Array Slide. BSA solutions were preheated in 30 mL conical slide holders from Starplex Scientific Inc. (Etobicoke, ON) for 1 hour at 42-45 °C. The DNA microarray slides were then incubated in the BSA solution for one hour at 42 °C. Once the slides were removed from the BSA solution, they were immersed in a 0.1X SSC solution contained in a conical slide holder at room

temperature for 5 minutes. Immersion was done into two more fresh 0.1X SSC solutions contained in separate 30 mL conical slide holders. Slides were then washed in nanopure water in a conical slide holder, to remove any residual SSC salt, for 5 minutes at room temperature. Slides were then removed with tweezers and inserted into dry conical slide holders with Whatman filter paper at the bottom and centrifuged for 3 minutes at 1400 rpm. Slides were immediately removed from the 30 mL conical slide holder with tweezers and visually examined for any dirt deposits. All or most of any remaining water droplets were allowed to evaporate, preventing them from showing up on subsequent scans and damaging the slide. This procedure resulted in a dry slide, which was stored under dry nitrogen.

DNA Hybridization and Washing. Each slide was placed in a separate Corning® #2551 Hybridization Chamber (Neepan, ON). Two drops of nanopure water were placed in the chamber holes in order to maintain a level of humidity throughout incubation. The complementary probes were used at concentrations of 0, 5, 15, 35, 71, or 142 μM in hybridization buffer. The diluted DNA probe solution was heated to 80°C for a short period of time in a water bath and allowed to cool to room temperature to re-anneal. Three 30 μL aliquots of DNA probe solution were pipetted onto the center of each slide, spacing the aliquots equally on the experimental surface. The slide was then quickly covered with a 24 X 60 mm hybri-slip from Sigma-Aldrich (H0784-100EA), placed in the hybridization chamber, and incubated in a dark, heated water bath at 32 °C for 16 hours. Two 30 mL conical slide holders of wash 2 solution were preheated at 42 °C for 1 hour. Once the slides were removed from the hybridization chamber they were immediately immersed with the hybri-slip into one of the wash 2 solutions until the

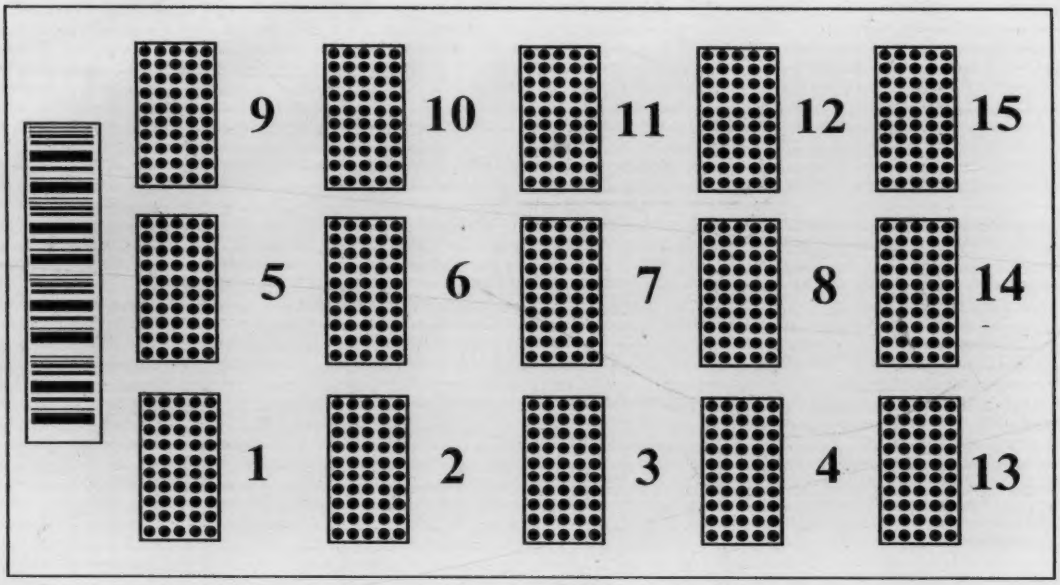

Figure 2.5 - Schematic of experimental slide. Each subarray represents 50 DNA spots. Subarrays 1-15 contain 0.5 μM FAM internal standard. Subarrays 1-4 also contain 50 μM of the ATTA target sequences, subarrays 5-8 contain 50 μM of the AAAA target sequence, and subarrays 9-12 contain 50 μM of the GTTG target sequence. The bar code is shown at the left.

hybri-slip separated from the slide. The hybridized slide was then transferred into the second wash 2 solution and immersed for 5 minutes. The slides were then transferred to a room temperature wash 1 solution for 5 minutes, and then repeated twice more in two more wash 1 solution jars. The slide was once again dried in the centrifuge at 1400 rpm for 3 minutes.

Spectroscopy. All absorption spectra were obtained with a Hewlett Packard 8452 UV-Vis Diode Array Spectrophotometer. Fluorescence measurements of solutions were obtained on a Photon Technology International MP1 System. Fluorescence detection scans were obtained intensity optimization to prevent saturating the detector. Cy5 and FAM samples were diluted and blanked with nanopure water. Absorption and fluorescence measurements were obtained in a 2 cm quartz cuvette. A slit width of 0.5 mm and corresponding bandpass of 2 nm was maintained for all fluorescence measurements.

Microarray Data Analysis. TIGR Spotfinder, part of the TM4 Microarray Software Suite, provides rapid analysis of microarray images, allowing us to quantitatively measure the amount of fluorescence emitted from the hybridized probe. This program reads TIFF images produced from the microarray scanner. Using the TIFF image, a grid was composed, containing all the spots in a sub-array (Figure 2.6). Within each coordinate grid position a boundary around a spot was determined with an algorithm dependent on a manually entered spot size. The program used the following equation determine the spot intensity within the boundary region:

$$\text{Intensity} = \text{Integral} - \text{BKG}^*\text{A} \qquad (1)$$

Where, A is the spot area, and is equal to the number of pixels within the defined spot boundary, BKG is the median pixel value within the cell (excluding the spot pixels), and Integral is the sum of all spot pixels excluding saturated pixels. Spots containing pixels that were fully saturated or too faint (Figure 2.7) were automatically flagged and removed from the data set.

Error Analysis. Error bars used in Figures 2.11, 3.7, 3.8, 3.9, 3.11, and 3.12 were calculated through a data filtration process described below. Each sub-array was composed of 50 spots, each of which produced a fluorescence intensity after hybridization with the DNA probe and scanning. The fluorescence values underwent three filters. The first was that any fluorescence value less than or equal to zero was removed. Second, any fluorescence intensity values which were greater than the calculated upper limit were removed. Finally, any fluorescence values which were less than the determined lower limit were removed from the data set. A large portion of our data followed a skewed distribution, hindering the use of the standard t-confidence interval upper and lower limits. Instead, we used the non-specific 1.5 x interquartile range (IQR) rule to determine the upper and lower limits. The IQR value is determined by measuring the difference between the 3rd quartile and the 1st quartile of the data. The upper limit was then calculated by adding 1.5 x IQR to the median intensity, while the lower limit had the 1.5 x IQR value subtracted from the lower limit. From this final data set, the standard deviation of each sub-array was calculated and plotted as an error bar on the median.

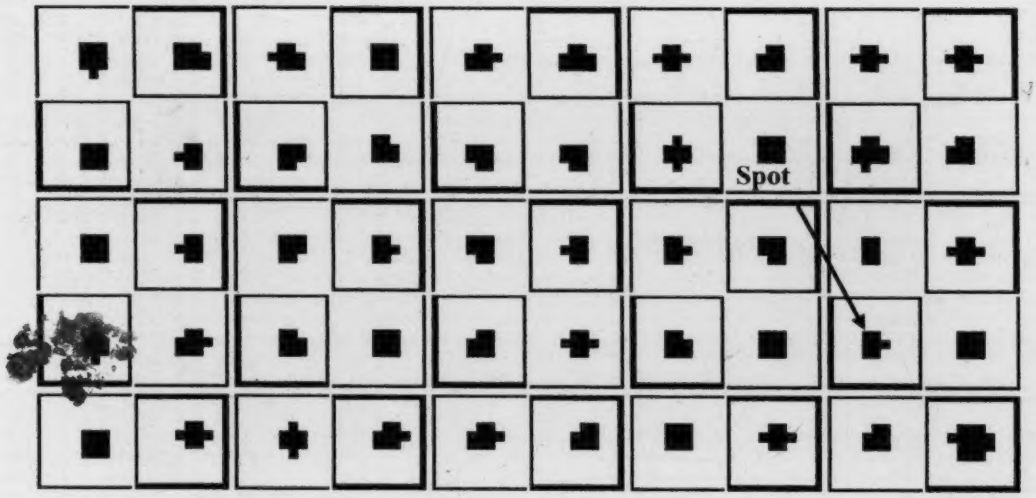

Figure 2.6 – Image of TIGR Spotfinder analysis of a microarray slide. DNA spots are from one subarray fit into a grid to obtain a local background.

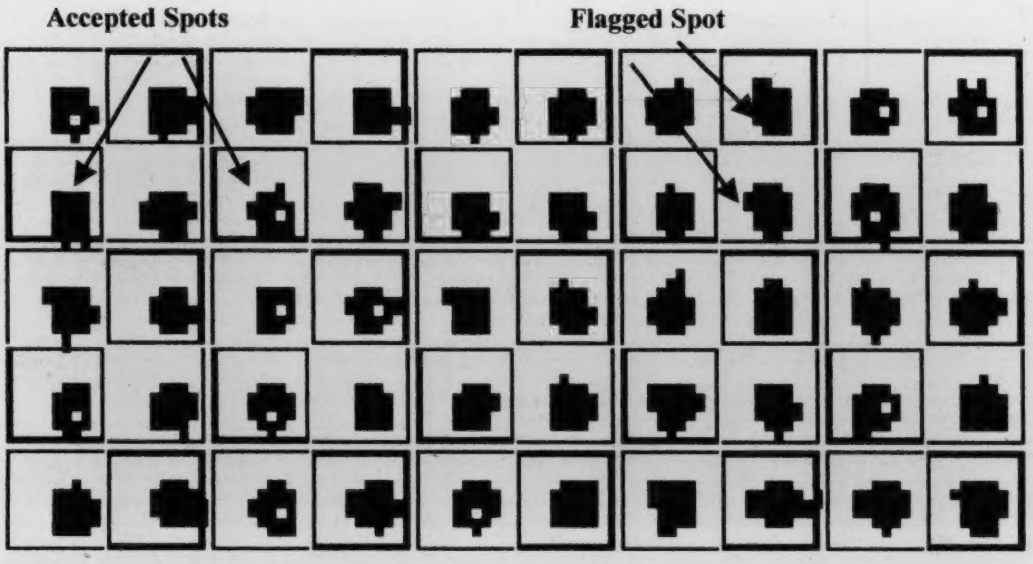

Figure 2.7 – Image of TIGR Spotfinder analysis of a subarray. DNA spots after processing, purple represents spots with acceptable pixel values, green represents flagged DNA spots with inconsistent pixel values.

2.3 Results and Discussion

Internal Standard. An internal standard correction on microarray slides is being considered here in order to reduce the spot-to-spot variation. Our internal standard was a FAM-labeled short ssDNA (dFAM), which was covalently attached to the slide during spotting in addition to the target DNA sequence. The dFAM concentration was constant for all target sequence solutions, thus the ratio of internal standard vs. target should remain constant for each spot. In other words, the fluorescence intensity observed from the internal standard should reflect the concentration of the target DNA bound to the slide. A decrease in the FAM fluorescence would either correspond to a loss of DNA on the slide during our experimental procedure or UV photobleaching of FAM.

Since the scanner used here contains only four "channels" (a set of emission and excitation wavelength bands), we were restricted in the fluorescent dyes which could be used as the internal standard and probe. The four fluorophore channel presets available were FAM, Cy5, Cy3, and Alexa 350. FAM (Figure 2.1) was chosen as the internal standard due to its efficiency and its emission at 530 nm. This emission was considered to be at a sufficiently different wavelength from the excitation maximum of Cy5 at 648 nm (Figure 2.2 and 2.4) to minimize Förster Resonance Energy Transfer (FRET) occurrence.

In order to determine the benefits of implementing an internal standard, it was important to develop criteria to ensure its usefulness. First, we had to observe a definite need for this tool in our experiments. Figure 2.8 shows a plot of the Cy5 fluorescence

intensities for each of the three DNA probe sequences as a function of spot position on the slide. This plot demonstrates the large fluctuations incurred on the slide from spot to spot (Figure 2.8), producing an experimental error of 48.9%. Notice that there is also a gradual decrease in the overall Cy5 fluorescence as a function of spot position, and, therefore DNA sequence (Figure 2.8). In contrast, Figure 2.9 shows the plot of the Cy5/FAM fluorescence intensity ratio as a function of spot position. This figure displays a great deal less scatter in data from spot to spot on the microarray slide and a reduced experimental error of 25.4%. Spikes in Cy5 fluorescence (e.g. spots 117, 150 and 300) that were observed in Figure 2.8 are no longer present in Figure 2.9. Also, the drops in fluorescence for the AAAA and the ATTA (spots 201-600) probe sequences were no longer visible once Cy5 was divided by the FAM internal standard.

Second, we had to determine a way to quantify improvements once the internal standard was used. For this, we compared the percent error, or coefficient of variation, to measure the dispersion of data points in each of the subarrays. The percent error was obtained for the Cy-5 fluorescence alone after hybridization and then compared with the ratio of the Cy-5 fluorescence and the FAM internal standard fluorescence after hybridization. Figure 2.10 shows the calculated percent error as a function of each subarray. The percent error was calculated for each subarray, after the three data filters were applied, then dividing the standard deviation with the subarray mean value. Three slides were used. One slide was used as a control in a dessicator, another was the irradiated slide, and the third was a slide in the photoreactor that was not irradiated. The dessicator control was kept in a dessicator purged with N_2 gas. The subarrays on the experimental slide were irradiated with UVC light. The experimental conditions will be

discussed further in Chapter 3. The control in the dessicator (Figure 2.10A) has an average Cy5 error of 18%. The introduction of the FAM data reduced the average error to 9%. The control slide in the photoreactor (Figure 2.10B) has an average Cy5 error of 17%, which was reduced to 7% when the Cy5/FAM fluorescence intensity ratio was used. Finally, the photoreactor experimental slide (Figure 2.10C) has an average Cy5 error of 17%, while the error for the ratio was reduced to 10%. A decrease in the percent error was observed when the ratio of Cy5 / FAM was applied for all three experimental slide conditions. As a consequence of this reduction in error, an increase in the amount of target bound to the slide will lead to an increased Cy5 fluorescence intensity compared to that of dFAM. This ratio can be used to normalize the fluorescence intensities after hybridization with the Cy5 labeled probes.

Figure 2.10C does show some discrepancies, however. The fluorescence intensity ratios errors for subarrays 11 and 12 (20 and 29 % respectively) were either greater or equal to the Cy5 error. This may be a result of the lower mean dFAM fluorescence intensity for these subarrays. The raw data for subarrays 11 and 12 (not shown) contained the most spots with 0 intensity values; subarray 12 raw data contained a statistical mode of 0 intensity. This might have been caused by the order of printing, as subarrays 11 and 12 were the last to be printed, and thus may not be an accurate representation of the dFAM in solution. This leads to the conclusion that the dFAM is being deposited onto the slide at a constant relative amount with the target DNA sequence.

Third, we had to ensure that the data obtained (see also Chapter 3) was maintained after implementation of the internal standard. Developed more in the next chapter but

shown here for completeness, the effects of UV light on our target sequence DNA was investigated with the use of the Cy5 labeled hairpin probe. A comparison of UV damage data using the two methods of analysis is shown in Figure 2.11. Figure 2.11A shows the Cy5 fluorescence intensities as a function of UVC irradiation time, while Figure 2.11B shows the fluorescence intensities of the ratio of Cy5/FAM intensities also as a function of UVC irradiation time. Clearly, the results show a decrease in the error for each of the experimental sub-arrays when the internal standard fluorescence is used in the ratio. As further discussed in the next chapter, the general trend of the data was also maintained with the inclusion of the internal standard.

From these preliminary tests, we were able to determine that the high degree of fluctuation in the Cy-5 fluorescence intensity, on account of the printing errors, leads to large spot-to-spot percent errors. This large spot-to-spot percent error may result in improper interpretation of experimental data. The internal standard provides a means of quantitatively reducing the amount of variation in the results, particularly in the variations due to printing. While reducing the error within each sub-array, the internal standard did not alter the general trend of the data, which shows that it does not introduce distortions of the data set in the experimental results.

Target concentration and spot position optimization. Optimization of the target concentration was attempted in order to saturate the epoxide residues on the slide with target DNA. High concentrations could reduce the effects of printing error on our results. Saturating the binding sites and reducing the number of spots that could potentially give lower values, due to a lack of target attached to the slide, could reduce the spot-to-spot variation. If the epoxide sites on the slide are not saturated, then fewer

target molecules will be available to hybridize with probe DNA, thus producing a limited amount of fluorescence from the probe. However, if the epoxide sites are maximally saturated more target molecules are available to be bound with DNA probe, increasing fluorescence emission. At the same time, it would also be possible to determine if the spot position on the slide influences reproducibility.

The target concentration optimization was attempted through sequential variations of the AAAA target concentrations from 0-500 μM. The position of each sub-array was also varied on the slide (see Figure 2.12 for a schematic) to examine the position dependence of spotting errors. Figure 2.13 shows an image of the microarray slide after hybridization with the 5 μM AAAA probe. The 0 μM target concentration positions on the slide show zero fluorescence for all of the different positions on the slide, as expected. The positioning of the spots on the slide did not significantly alter the Cy-5 intensity emitted. The morphology of the spots did appear slightly improved around the center of the slide, however no quantitative differences were observed (Figures 2.13). The results observed in Figure 2.14 for the Cy5 scan after hybridization with 5 μM probe DNA did not show any significant differences based on target concentrations. Rather, all of the intensities were clustered within a range of 250 000 – 750 000. As a result, no general trends were observed; instead a high degree of fluctuations within each concentration which we attribute to the lack of internal standard. From these results, it appears that we are saturating our binding sites on the microarray slide and that increasing the target concentration from 5 μM on the slide is not necessary since no significant increase in fluorescence was observed.

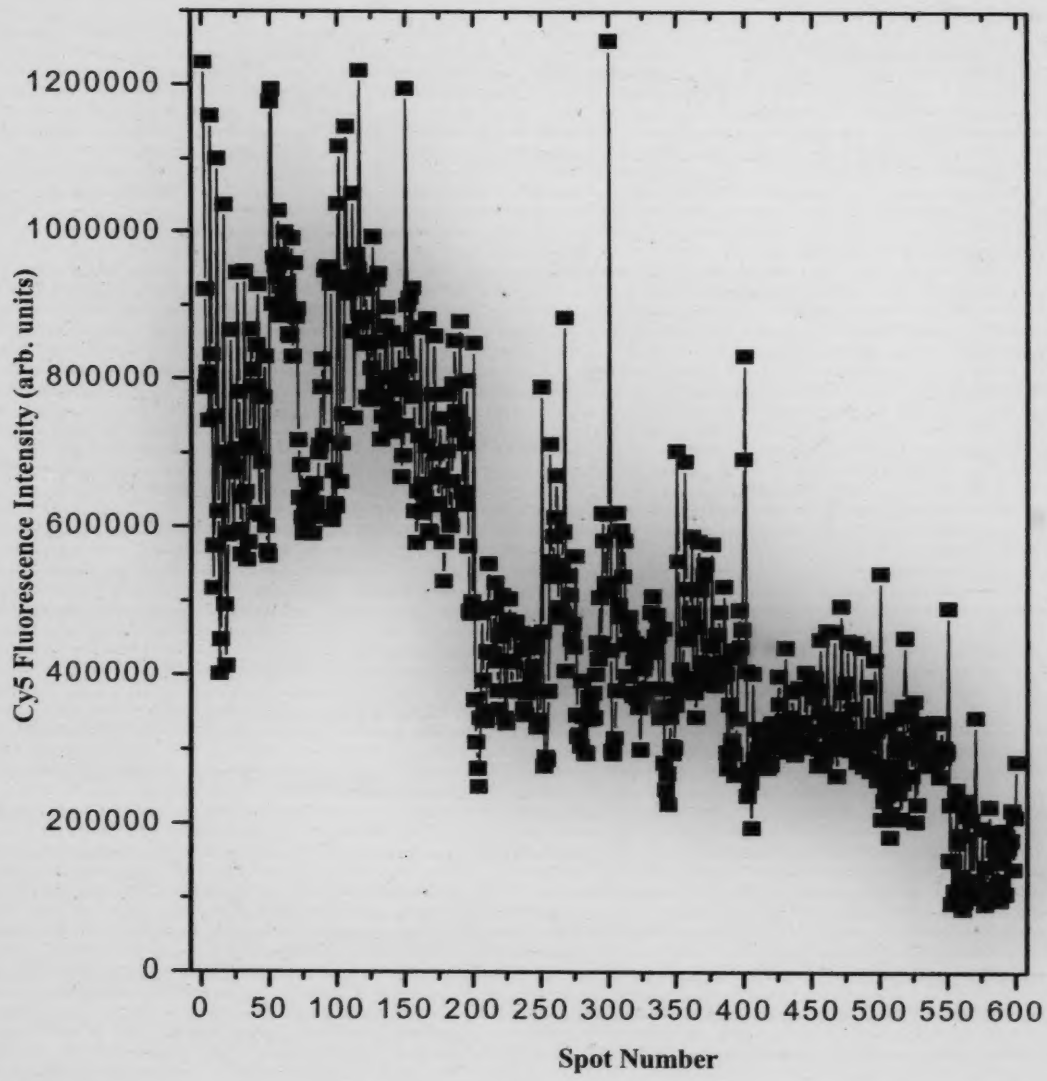

Figure 2.8 – Cy5 fluorescence intensities of the GTTG probe (spots 1-200), AAAA probe (spots 201-400) and ATTA probe (spots 401-600) hybridized to GTTG, AAAA, and ATTA target sequences, respectively. The probe sequence concentrations were 5 μM and the target sequence concentrations were 50 μM.

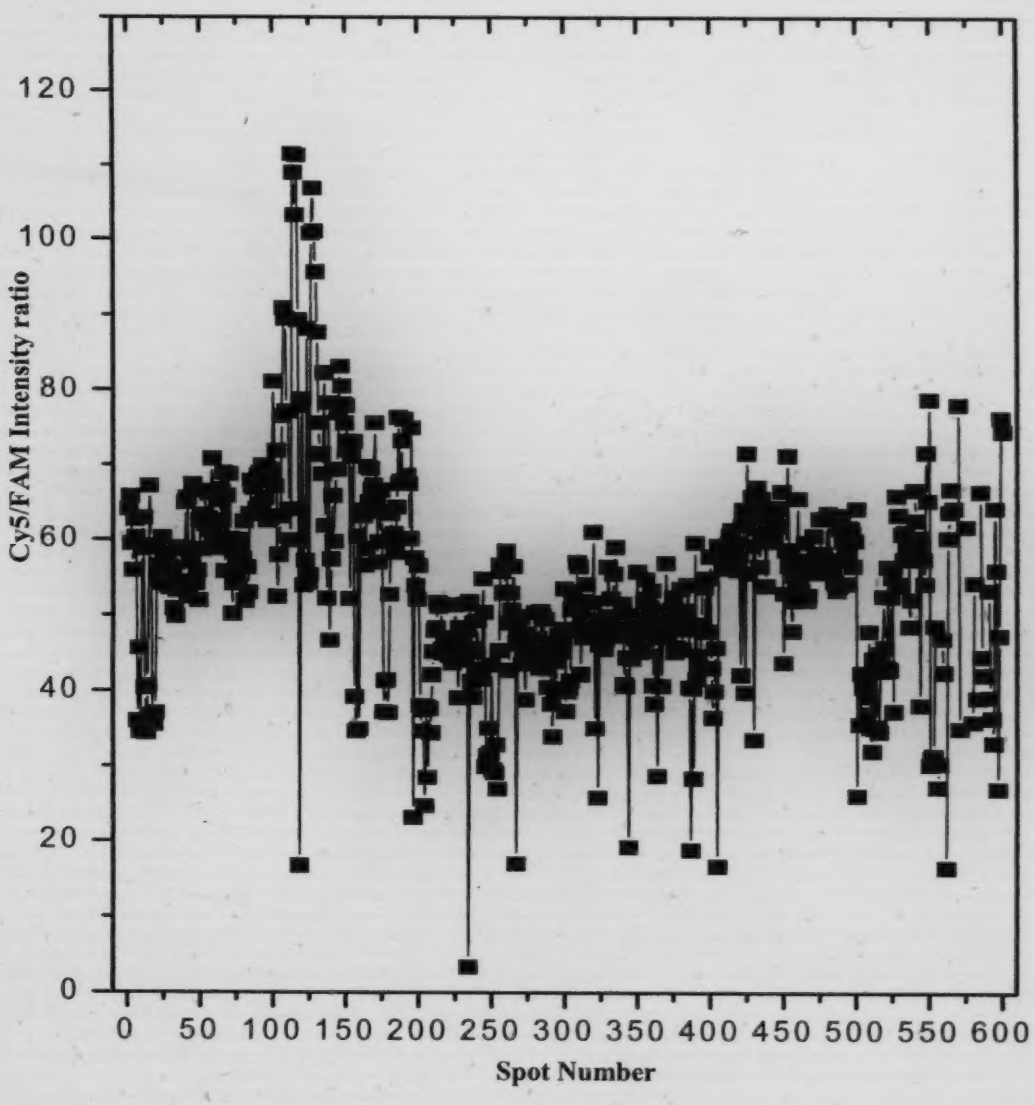

Figure 2.9 – Cy5/FAM ratio of fluorescence intensities of the GTTG probe and dFAM (spots 1-200), AAAA probe and dFAM (spots 201-400) and ATTA probe and dFAM (spots 401-600) hybridized to GTTG, AAAA, and ATTA target sequences, respectively. The probe sequence concentrations were 5 μM, the target sequence concentrations were 50 μM, and the dFAM concentrations were 0.5 μM.

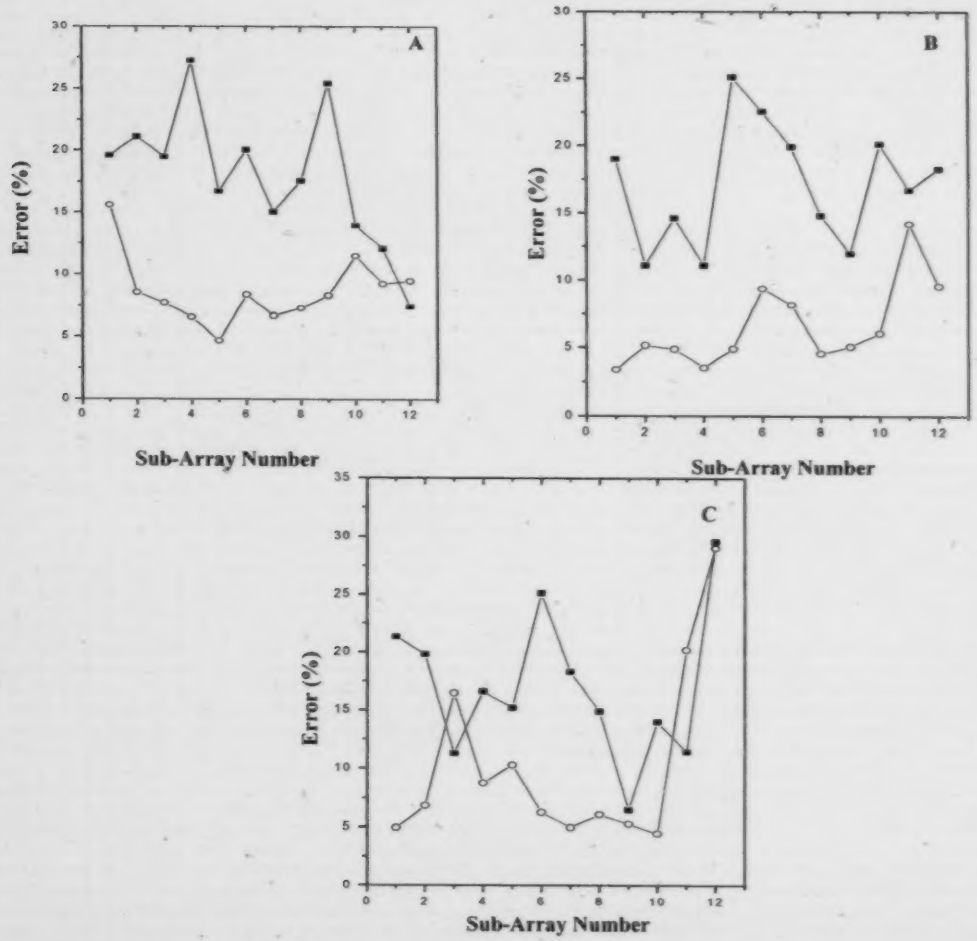

Figure 2.10 - Comparison of percent error by sub-array number for (A) dessicator control slide, (B) photoreactor control slide, and (C) experimental slide. The filled squares are the average error of the Cy5 fluorescence for sub-arrays containing 50 spots after three data filters using only the Cy5 intensities. The open circles represent average error for the Cy5/FAM fluorescence ratio for the respective sub-arrays. The Cy5 probe concentration for hybridization was 5 μM, the dFAM concentration was 0.5 μM, and the target concentrations were 50 μM.

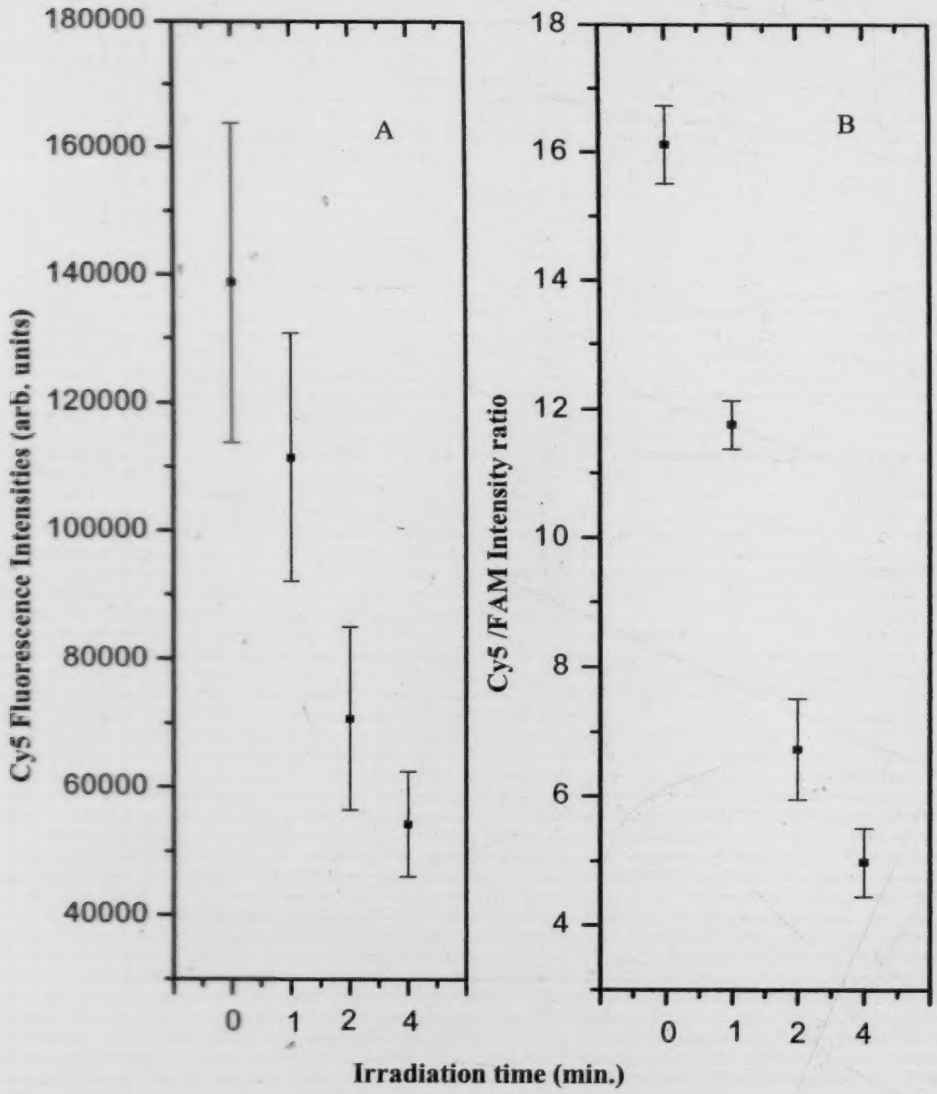

Figure 2.11 - Median fluorescence intensities and ratios of ATTA sub-arrays as a function of UV irradiation time. The Cy5 probe concentration for hybridization was 5 μM, the dFAM concentration was 0.5 μM, and the target concentrations were 50 μM. (A) is the median Cy5 fluorescence intensities and (B) represents the Cy5/FAM fluorescence ratios.

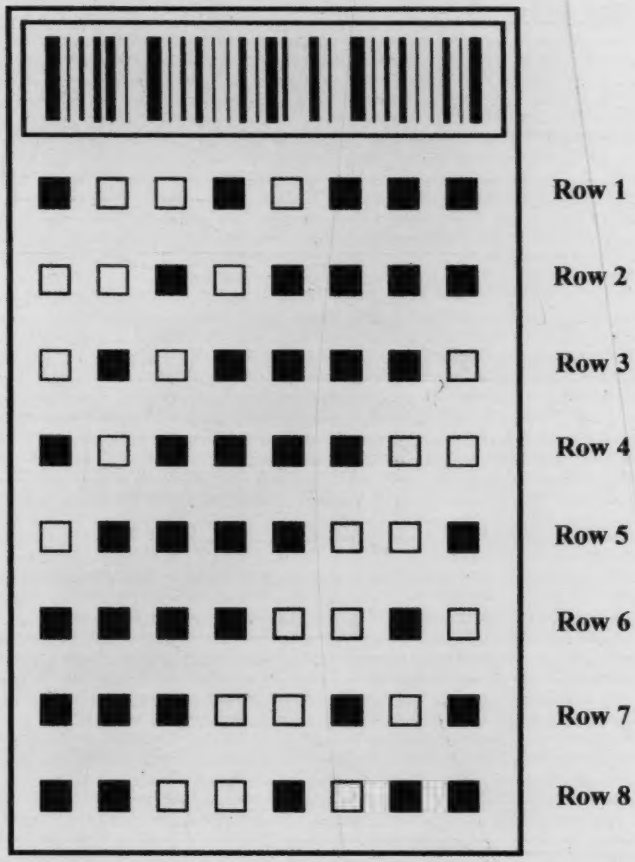

Figure 2.12 – Schematic of the slide, measuring target concentration dependence. Each square represents 25 spots of the following concentrations: 0 μM (red), 5 μM (orange), 10 μM (yellow), 25 μM (green), 50 μM (white), 100 μM (dark blue), 250 μM (purple), and 500 μM (magenta).

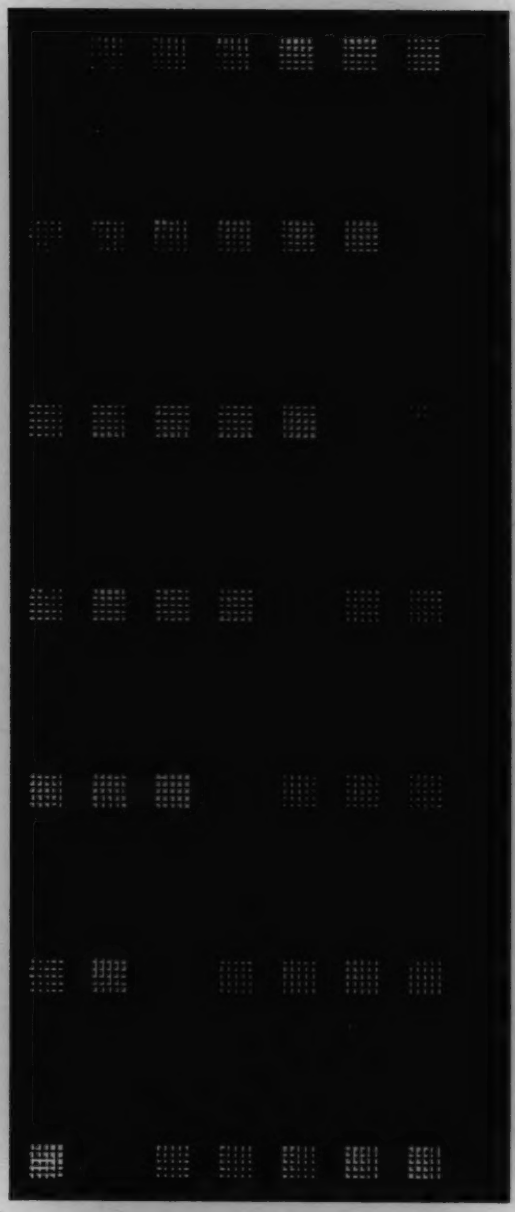

Figure 2.13 - Slide image after hybridization with 5 μM concentration AAAA probe at 635 nm excitation. Concentrations within each row correspond to the schematic in Figure 2.12.

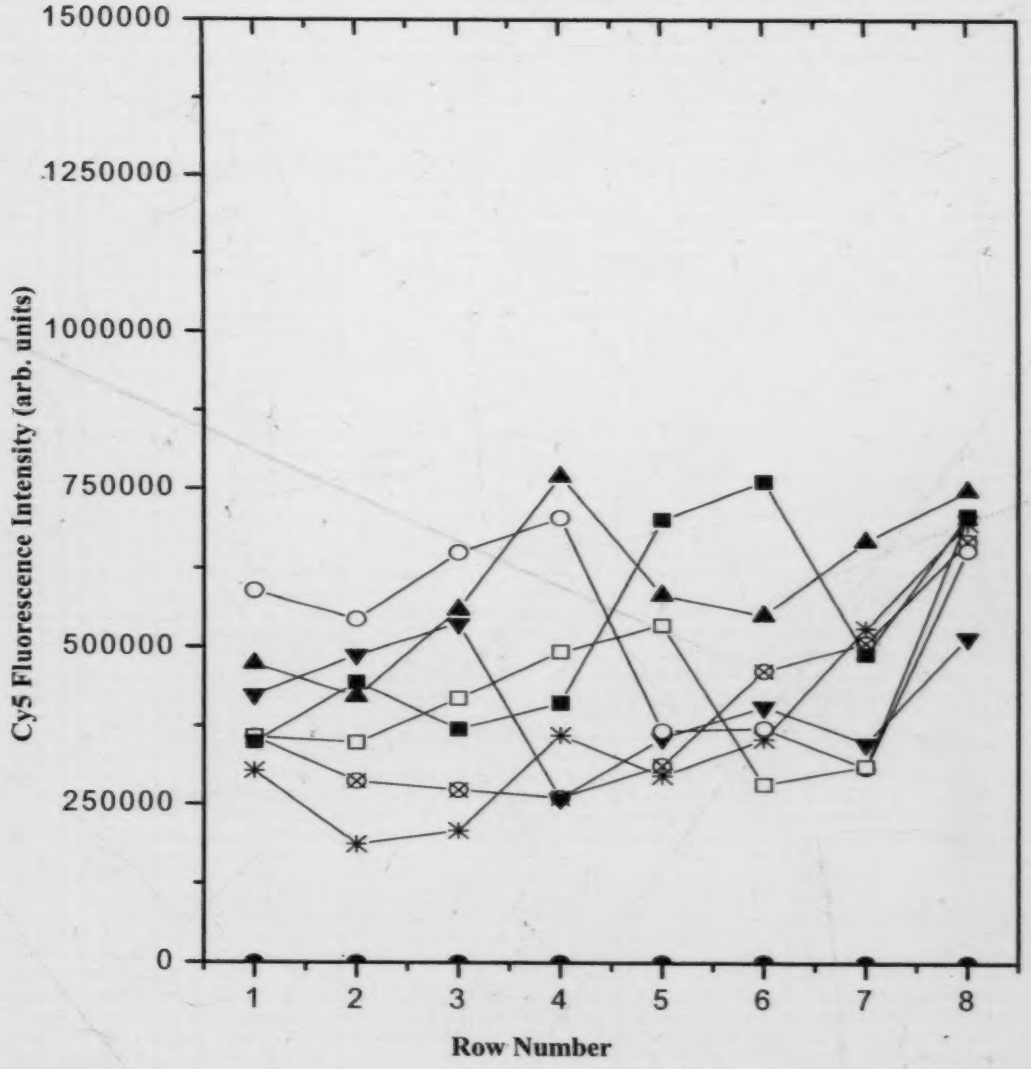

Figure 2.14 – Cy5 Fluorescence intensity of AAAA probe with a concentration of 5 μM as a function of sub-array position on the glass slide. AAAA target concentrations were (●)0 μM, (✳)5 μM, (⊗)10 μM, (▼) 25 μM, (○)50 μM, (□)100 μM, (■)250 μM, and (▲) 500 μM.

Probe concentration optimization. The lack of variation in the fluorescence intensities with the changing concentrations led to the revised thought that perhaps saturating the target DNA with probe DNA on the slide would be more effective at reducing the spot-to-spot error. We next investigated the affects of altering the ratio of probe molecules to target molecules printed on the microarray slide. The AAAA target DNA was printed onto 6 microarray glass slides in eight concentrations. The position of the different concentrations were cycled on the slide, as previously discussed and shown in Figure 2.12. Each slide was hybridized with a different concentration (1, 5, 15, 35, 71, and 142 μM) of AAAA probe DNA.

Figure 2.15A shows the Cy5 fluorescence intensity of AAAA probe at a concentration of 1 μM for each subarray target concentration as a function of row number. The fluorescence emission intensities for the different target concentrations 5, 10, 25, and 50 μM appear to cluster together. The remaining higher target concentrations 100 and 250 μM show a steady increase in fluorescence intensities as we move further down the slide, (this more clearly observed in Figure 2.14). Figure 2.16A shows the average fluorescence intensity for the 1 μM AAAA probe concentration as a function of AAAA target concentration. Here, each point represents the combined intensities for all of the subarrays with a specific target concentration. This plateau followed by increasing fluorescence trend continues with probe concentrations of 5 μM and 15 μM (Figures 2.15B and C). An additional target concentration of 500 μM was used for the higher probe concentrations (Figures 2.17A, B, and C) in order to see if any differences would occur. Figures 2.18A, B, and C also showed the plateau at 50 μM target concentration followed by increasing fluorescence trend, with a continual increase in fluorescence

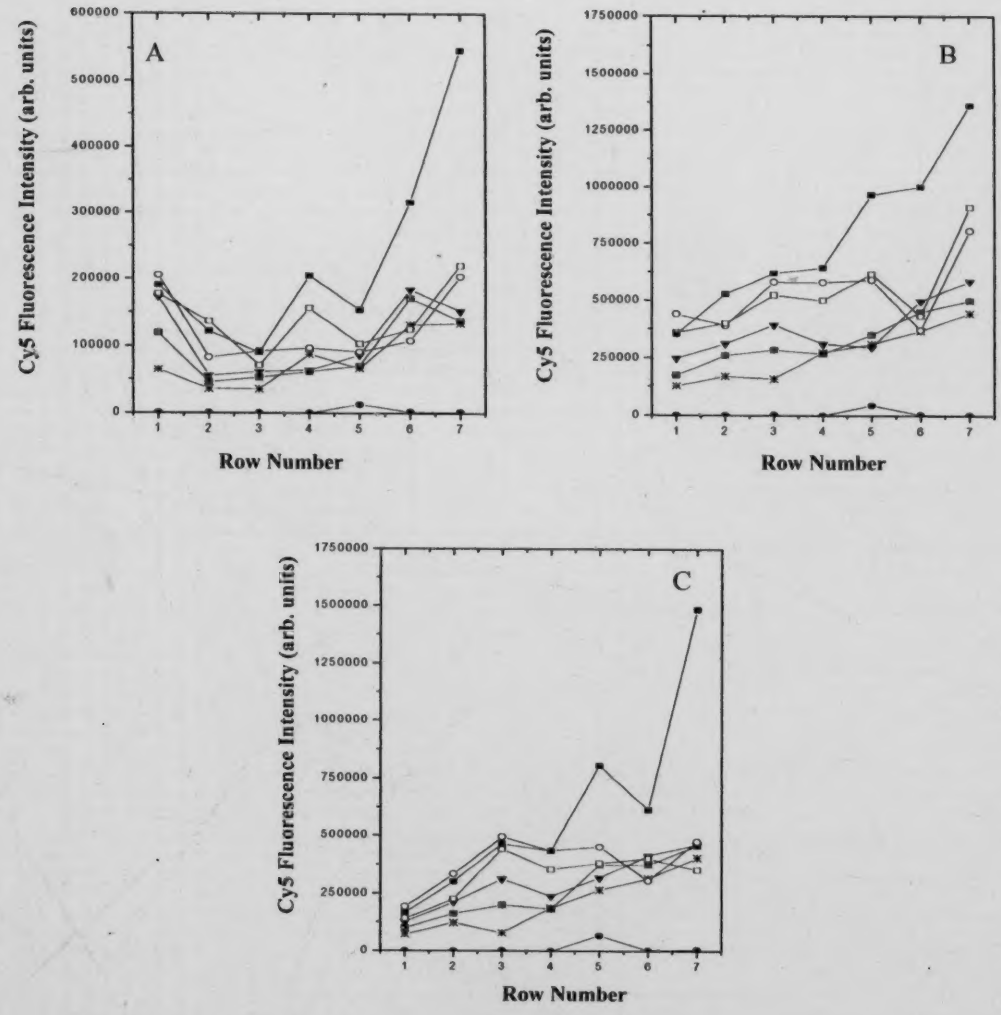

Figure 2.15 – Cy5 Fluorescence intensities of AAAA probe at a concentration of (A) 1 μM, (B) 5 μM, and (C) 15 μM as a function of sub-array position on the glass slide. AAAA target concentrations were 0 μM (●), 5 μM (✳), 10 μM (⊗), 25 μM (▼), 50 μM (○), 100 μM (□), and 250 μM (■). Row number corresponds to slide positions as in Figure 2.12.

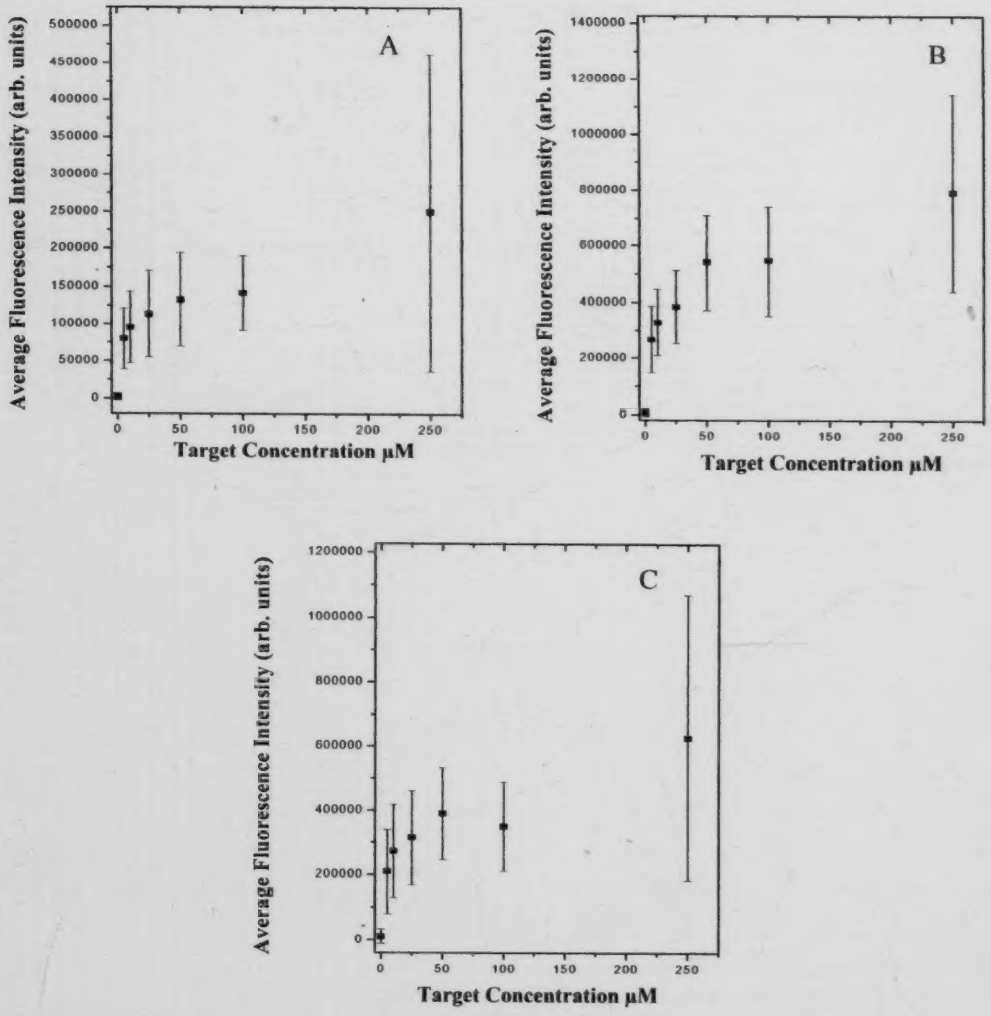

Figure 2.16 - Average fluorescence intensity of AAAA probe with a concentration of (A) 1 µM, (B) 5 µM, and (C) 15 µM as a function of target concentration. Error bars were determined as ± the standard deviation of all the spot intensities.

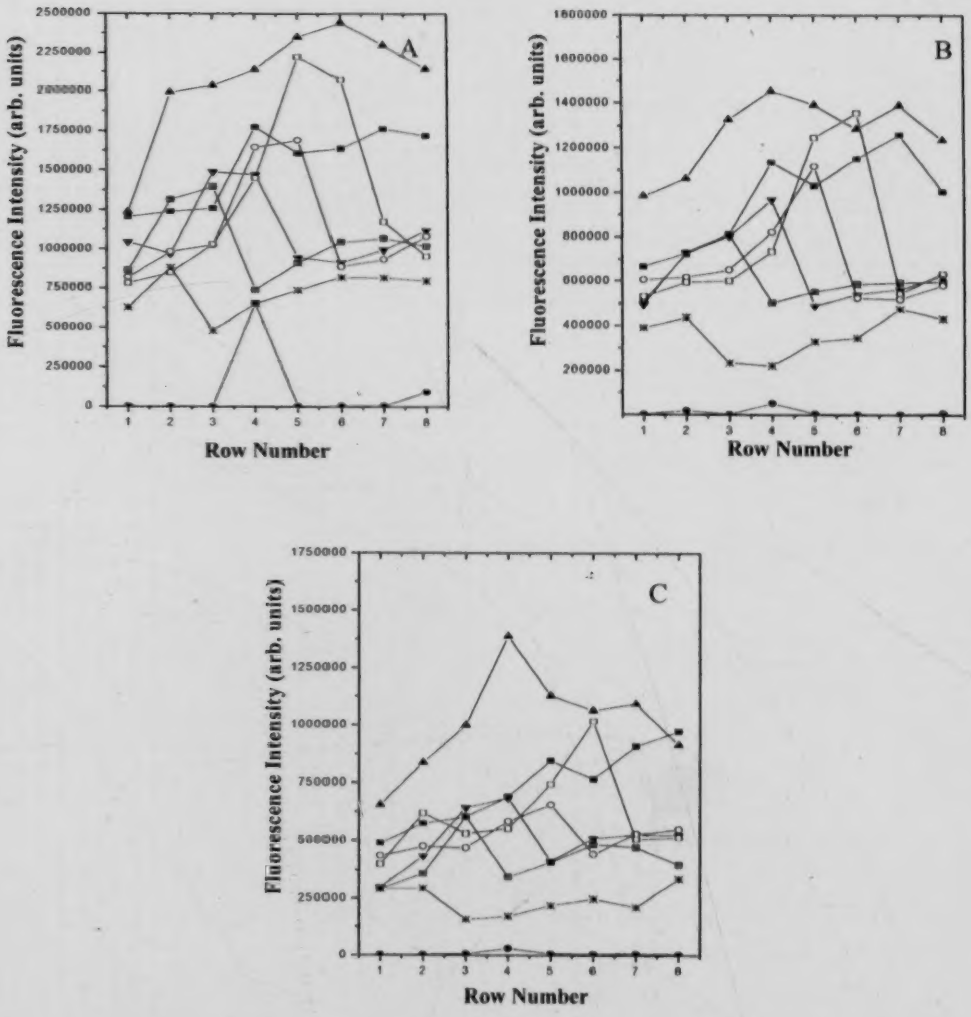

Figure 2.17 – As Figure 2.15, but with an AAAA probe concentrations (A) 35 μM, (B) 71μM, (C) 142 μM and an additional AAAA target concentration of 500 μM (Row 8).

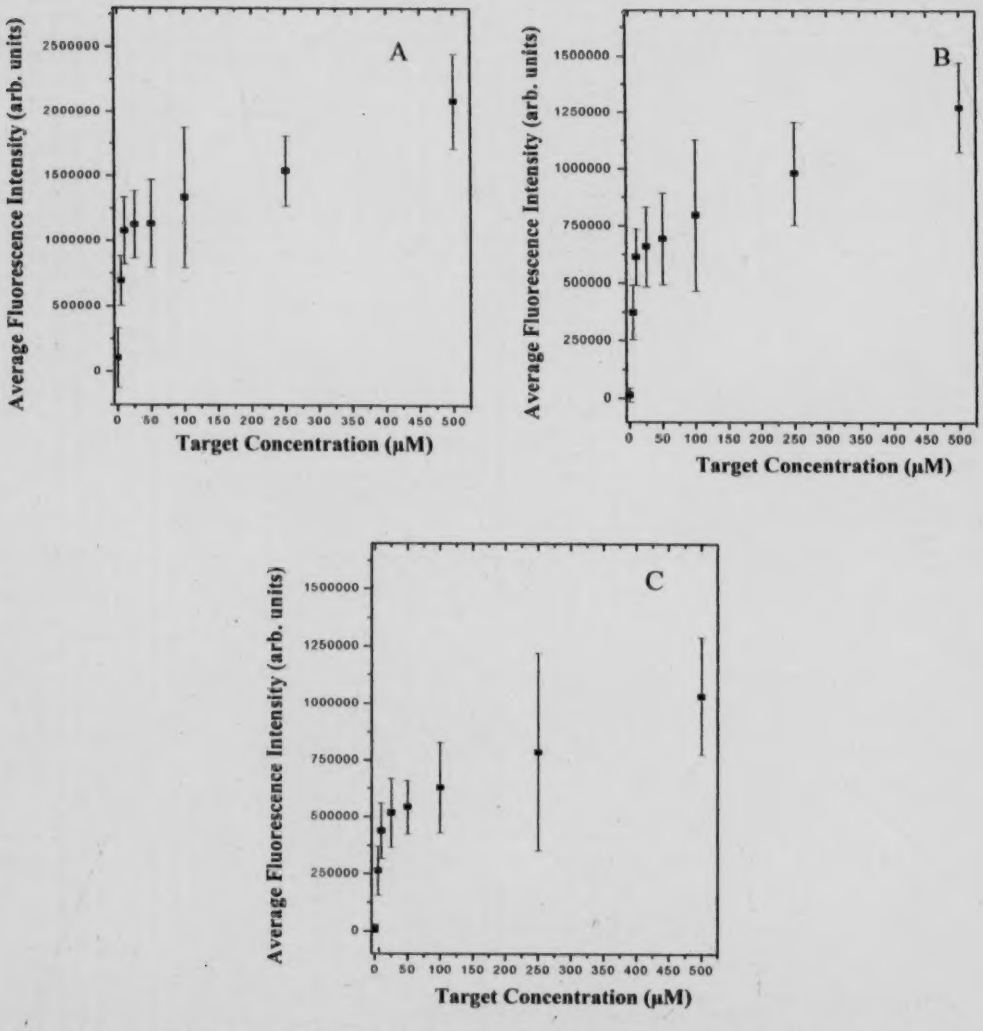

Figure 2.18 – As Figure 2.16, but with an AAAA probe concentrations (A) 35 μM, (B) 71μM, (C) 142 μM and an additional AAAA target concentration of 500 μM (Row 8).

intensity for concentration 100 to 500 μM. Large error bars were observed at the higher probe concentrations. We believe that the use of the internal standard would have reduced the error observed significantly. However, we did not want to increase the number of variables in these experiments by potentially introducing an additional target to compete for binding sites on the slide.

The average fluorescence intensity of the hybridized probe DNA shows an initial increase for target concentrations 0 to 25 μM (Figure 2.16A). The probe intensity then plateaus when hybridized with target concentrations of 50 and 100 μM. Probe concentrations of 5, 15, 35, 71, and 142 μM show similar results in Figures 2.16B, and C, Figure 2.18A, B, and C. Figure 2.19 shows the average Cy5 AAAA probe fluorescence when hybridized to the 50 μM AAAA target. Each different probe concentration was hybridized to one of 6 microarray slide. The hybridization with the 50 μM AAAA target averages resulted in an increase in fluorescence intensity from 1 to 35 μM followed by a decrease in fluorescence to the 142 μM probe concentration. This trend was observed for all of the remaining target concentrations (5, 10, 25, 100, 250, and 500 μM) with the exception of the 0 μM target concentration. The 0 μM target concentration maintained zero average fluorescence intensity for all of the probe concentrations used.

The results obtained may be to due to many factors involved in hybridization of probe DNA to the target and in the binding of target DNA to microarray slide. The fact that the probe emission increases as the concentration of target DNA was increased proves that an increase in the number of probe molecules successfully hybridizing to the printed target. The plateaus observed in each plot in Figures 2.16 and 2.18 may reflect

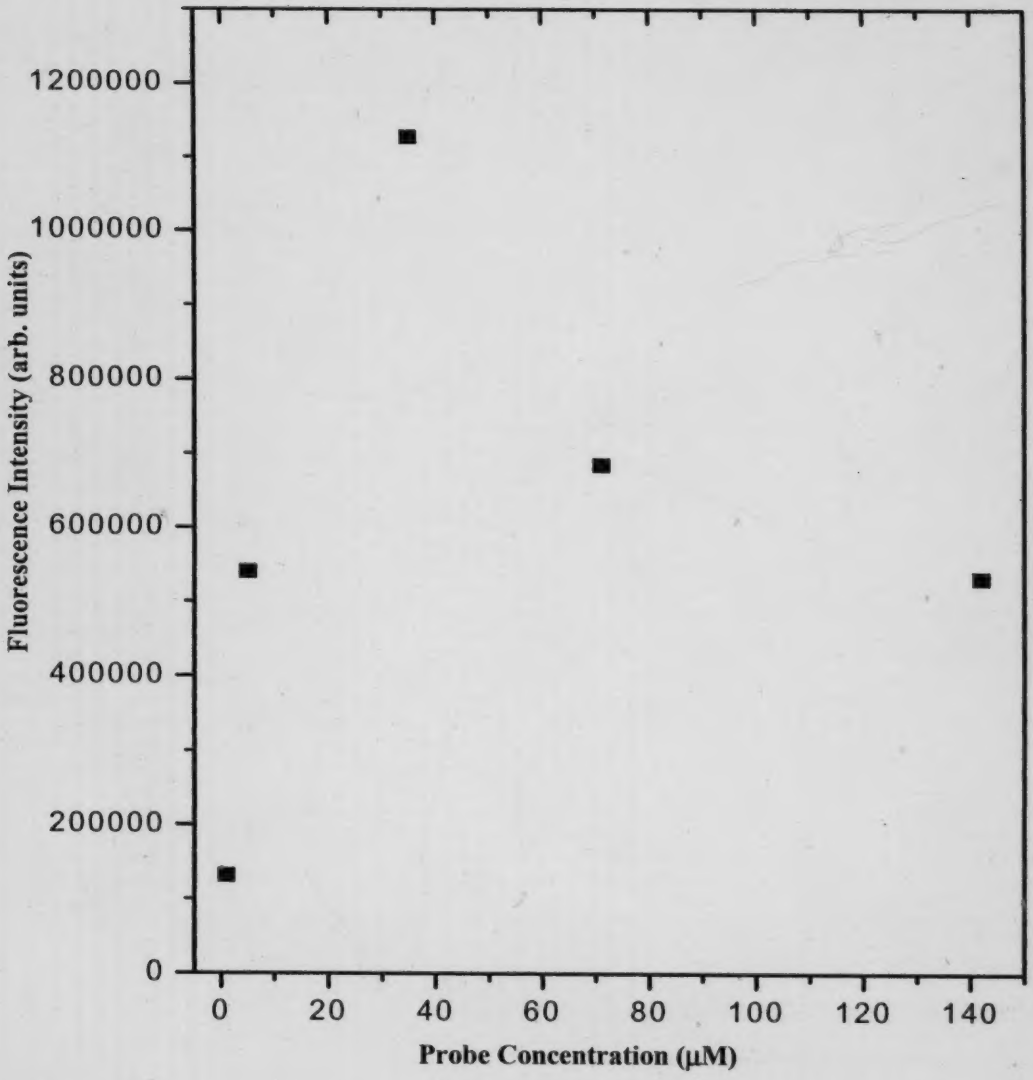

Figure 2.19 – Average AAAA probe Cy5 fluorescence intensity as a function of the probe concentration when hybridized to 50 μM target concentration on 6 microarray slides.

the optimized concentration of target for which the probe can be bound. The continued increase in fluorescence, following the plateau, may occur as a result of multiple probe DNA molecules binding to the target or Hoogstein base-pairing[13], increasing the presence of fluorescent molecules on the slide. Consequently, as the layers of probe DNA build from the increasing probe concentrations; self-quenching may occur between the bound probe fluorophores, resulting in a decrease of fluorescence emission observed for the 71 μM and 142 μM probe concentrations Figure 2.19. From these results, we determined that the optimal probe and target concentrations are 35 μM and 50 μM, respectively.

Data analysis. We tried to determine the accuracy of the data we were obtaining from the software analysis program TIGR Spotfinder. To do this, we compared the TIGR Spotfinder results to those obtained from a method we developed in Microsoft Excel. This latter method eliminated the boundary line surrounding each spot, resulting in the inclusion of all the pixel values from each spot. In order to accomplish this, the raw data from a sub-array was acquired from the scanner and converted to a pivot table in Microsoft Excel. The median value of the background was determined from the intensity values of pixels surrounding the spots. This value was removed from all of the pixel values, visually exposing each spot within the Excel pivot table. The sum of each spot was calculated and compared with the calculated spot intensity determined with TIGR Spotfinder. The comparison between the Microsoft Excel data and the TIGR Spotfinder are shown in Table 2.3. The pivot table data obtained from one subarray on a slide produced a mean and median intensity of 46425 ± 6993 counts/sec and 47736 ± 6993 counts/sec, respectively and a range of 25742 counts/sec. From the TIGR Spotfinder data

Table 2.3 - Comparison of pivot table and TIGR Spotfinder statistics

Statistic	Pivot Table Data	TIGR Spotfinder Data
Mean	46425	45817
Median	47736	46970
Range	25742	24200
Standard Deviation	6993	6993
Experimental Error	15%	15%

we obtained a mean and median intensity of 45817 ± 6993 counts/sec and 46970 ± 6993 counts/sec, respectively. Both methods produced an experimental error of 15%. The mean values for the pivot table and TIGR Spotfinder were within a standard deviation of each other and the median values of each were well within range of the other. These results show that the two methods of data analysis had no statistically significant difference. Thus, the two methods of data analysis resulted in similar quantitative results that did not position one technique as superior to the other. The Microsoft Excel method was more time consuming, however, and intensive for the data collector. The TIGR Spotfinder software was chosen as the more reliable and user-friendly method at this stage in our analysis.

2.4 Conclusions

We have demonstrated the use of FAM as an internal standard in microarray experiments as a way to reduce the spot-to-spot error associated with DNA printing on microarray glass slides. The ratio between the median signal intensity for Cy5 spots divided by median FAM signal intensity provided significantly lower spot-to-spot percent errors. Optimization of the concentrations for target DNA and probe DNA were determined, thus providing maximized signal intensity for future experiments. The development of a boundary free method for determining spot intensity was deemed unnecessary. Spot Finder was found to be a reliable and time efficient tool for calculating spot intensity on the microarray slide.

2.5 References

[1] Lemieux, B.; Aharoni, A.; Schena, M. *Molecular Breeding* **1998**, 4, 277-289.

[2] Guo, Z.; Guilfoyle, R. A.; Thiel, A. J.; Wang, R.; Smith, L. M. *Nuc, Acid, Res.* **1994**, 22, 5456-5465.

[3] Strother, T.; Hamers, R. J.; Smith L. M. *Nuc, Acid, Res.* **2000**, 28, 3535-3541.

[4] Yarasi, S., McConachie, C., Loppnow, G. *Photochemistry and Photobiology*, **2005**, 467-473

[5] Deyholos, M. K.; Galbraith D. W. *Cytometry Rev.* **2001**, 43, 229-238.

[6] Baggerly, K.; Mitra, R.; Grier, R.; Medhane, D.; Lozano, G.; Kapoor, M *Analytica Chimica Acta.* **2004**, 506, 117-125.

[7] Park, S. H.; Krull, U. *Analytica Chimica Acta.* **2006**, 564, 133-140.

[8] Gerion, D.; Chen, F.; Kannan, B.; Fu, A.; Parak, W. J.; Chen, D. J.; Majumdar, A.; Alivisatos, A. P. *Anal. Chem.* **2003**, 75, 4766-4772.

[9] Bild, A. H.; Yao, G.; Chang, J. T.; Wang, Q.; Potti, A.; Chasse, D.; Joshi, M.; Harpole, D.; Lancaster, J. M.; Berchuck, A.; Olson, J. A. Jr; Marks, J. R.; Dressman, H. K.; West, M.; Nevins, J. R. *Nat. Letters* **2006**, 439, 353-357.

[10] Clarke, J.D.; Zhu, T. *The Plant Journal.* **2006**, 45, 630-650.

[11] Mehlmann, M.; Townsend, M. B.; Stears, R. L.; Kuchta, R. D.; Rowlen, K. L. *Anal. Biochem.* **2005**, 347, 316-323.

[12] Bonnet G.; Tyagi, S., Libchaber, A.; Kramer, F. *Proc. Natl. Acad. Sci. USA* **1999**, 96, 6171-6176.

[13] Nelson, D. L.; Cox, M. M. *Lehninger Principles of Biochemistry* 3rd Edition; Worth Publishers: New York, NY, 2000; pp 340-341.

3 Photochemistry of DNA on a Microarrays

3.1 Introduction

UV light is typically separated into three regions, UVA (320-400nm), UVB (290-320 nm), and UVC (200-290 nm)[1]. Each of the three regions of the UV spectrum possesses the power to create damage within the biological system. Fortunately, the earth's ozone layer serves as a shield against harmful solar ultraviolet radiation[2]. UVA is able to penetrate this layer, reaching the earth's surface[1] while the UVB photons, which reach the surface are largely reduced by the amount of stratospheric O_3[2]. In addition, atmospheric O_2 and O_3 absorb UVC light, preventing the majority of these photons from reaching the ground. However, UVC can still be present when produced by artificial light, such as mercury lamps.

Ultraviolet (UV) light has been shown to have harmful consequences on cellular life. The absorption of UV light by DNA has been correlated with photoproduct synthesis, cell killing, mutation induction and tumorigenesis[3]. Each region of the UV spectrum is able to penetrate human skin to varying degrees. UVC light penetrates only to the stratum corneum[1], while UVB light penetrates to living tissue and its wavelengths span the photoabsorption spectrum of DNA[2]. Consequently, UVB radiation is a more efficient mutagen in vivo on a per photon basis[1,4], and capable of producing deleterious biological effects, including skin cancer[2]. DNA contains an absorption peak around 260 nm, which is in the UVC region of the electromagnetic spectrum, making UVC radiation a more efficient in vitro mutagen. When DNA is exposed to UVC light, the most abundant photoproduct is the cyclobutane pyrimidine dimer (CPD)[5], forming 70% of the

total photoproducts. Cyclobutane photodimers (CPDs) are formed through a [2π+2π] cycloaddition reaction between adjacent pyrimidine bases at the C_5-C_6 position on both bases. This reaction occurs through a cyclic transition state[5]. In addition to CPD formation, UVC light also leads to the formation of a [6-4]-photoproduct between adjacent pyrimidine bases with a yield of 20%. The [6-4]-photoproduct also arises from a [2π+2π] cycloaddition, involving either the C_4-O_4 carbonyl of thymine or the C_4-N_4 imino tautomer of cytosine and the C_5-C_6 double bond of the adjacent 5' base. The third photoproduct produced through UVC irradiation is the photohydrate. The photohydrate, which accounts for approximately 2% of the total photoproducts, does not affect any neighbouring bases. This photoproduct is limited to pyrimidine bases and is the nonstereospecific nucleophilic addition of water across the C_5-C_6 double bond[6].

Previous work has shown that the CPD lesion causes disruptions in the DNA helix to the extent that the hydrogen bond distance of the 5' thymine to its complementary adenine base increases to 2.5 Å and the hydrogen bond angle increases to 125°[7]. In addition, the base stacking is also affected between the two thymine bases. The presence of the T<>T dimer in a DNA duplex has also been found to induce a kink or bend in the DNA helix, and may go as far as to flip out the base extrahelically from the duplex[8].

We have developed fluorescently-labeled DNA probes, which possess similar structures and characteristics as molecular beacons. Similar to the molecular beacons, these DNA probes were designed such that they fluoresce when they bind to a complementary nucleic acid sequence. The DNA probe possesses the characteristic stem and loop structure of hairpins and molecular beacons. However, unlike the molecular

beacon, only a fluorophore was tagged to one end of the DNA sequence. The opposite end of the hairpin structure does not contain a quencher as in a typical molecular beacon. When the probe sequence in the loop anneals to a complementary target sequence the longer and stronger probe – target duplex unwinds the stem portion of the hairpin[9]. Molecular beacons have been shown to discriminate targets with as few as one mismatch in the nucleic acid sequence[9,10]. As such, following the formation and hybridization between targets containing photodamage and the DNA probe, sufficient destabilization in the target – probe duplex would allow the DNA probe to be easily removed from the microarray surface, decreasing the fluorescence observed.

In this work, we investigate the effects of UV irradiation on the FAM internal standard. We measured the change in fluorescence before and after UVC irradiations. We found that the FAM labeled internal standard fluorescence was reduced, as a result of photobleaching, induced by UV light irradiation. We also found indirect evidence that the slide's exposure to ambient levels of ozone in the atmosphere during the experimental procedures can result in reduced fluorescence emission. We also discuss a method developed to use fluorescently-labeled hairpin probes to detect the formation of DNA damage, induced by UVC irradiation on microarray slides. By exposing a glass surface containing 3 different immobilized DNA target sequences to UVC light, we were able to measure the rate at which DNA damage was formed. The rates of DNA damage for three different DNA target sequences (ATTA, GTTG, and AAAA) were determined. The time constants were determined as 51.59113 ± 2.14881 min (R^2 = 0.95881) for the ATTA, 47.78764 ± 3.5573 min (R^2 = 0.83409) for the AAAA, and 53.52365 ± 1.26358 min (R^2 = 0.96956) for the GTTG DNA sequences.

3.2 Experimental

Materials. NaH_2PO_4, Na_2HPO_4, and sodium citrate were obtained from Fisher Scientific (Ottawa, ON). NaCl was obtained from EMD (San Diego, CA). Bovine serum albumin was obtained from Sigma (Oakville, ON). Tris-HCl was obtained from ICN (Biomedicals Inc., Irvine, CA). All chemicals were used as received. Nanopure water from Barnstead NanoPure (Boston, MA) water purification system was used for all solutions. The 5' amino - modified target DNA oligonucleotides (Table 2.1), FAM internal standard (Figure 2.1, Figure 2.2, and Table 2.1), and the complementary 5'-Cy5 modified DNA probe sequences (Figure 2.3, Figure 2.4, and Table 2.2) were obtained from Integrated DNA Technologies (Coralville, IA). The amino modified target sequences (Table 2.1) were purified using standard desalting. The 5'-Cy-5 modified DNA probe sequences (Table 2.2) and the FAM internal standard (Table 2.1) were purified with standard desalting and HPLC. The model 40041 epoxide-coated slides with bar codes were purchased from Corning (Neepan, ON).

Buffers. The 300 mM phosphate buffer solution was prepared by adding 300 mM NaH_2PO_4 dropwise to 300 mM Na_2HPO_4 to reach a final pH of 8.6, then filtered with a 0.2 μm membrane filter. A 0.1 X SSC (wash 1 buffer solution) was prepared by a 200-fold dilution of 20 X SSC (3 M NaCl, 0.3 M sodium citrate, pH adjusted to 7.4) and filtered through a 2 μm membrane filter. The wash 2 buffer solution was prepared by adding 0.2% SDS (sodium dodecyl sulfate) to a 10-fold dilution of 20 X SSC, adjusting the pH to 7.4, and filtering through a 0.2 μm membrane filter. The 0.2 % (w/v) bovine serum albumin (BSA) solution was prepared with 5X SSC and 1% SDS. The

hybridization buffer was prepared by combining 1 mM $MgCl_2$ and 10 mM Tris-HCl, adjusting the pH to 7.4, and filtering through a 0.2 μm membrane filter.

Microarrays. The amino-terminated target DNA was diluted with 150 mM phosphate buffer and 0.5 μM FAM internal standard to concentrations of either 5 or 50 μM. A multifunctional, liquid-handling robotic microarrayer OmniGrid100™ from GeneMachines, (San Carlos, CA) in the Microarray and Proteomics Facility at the University of Alberta was used to print the DNA onto the Corning epoxide-coated slides (Figure 3.1). The capillary printing pins were Stealth 3 Micro Spotting Pin from TeleChem International, Inc. (Sunnyvale, CA), the pin speed was 2 cm/s, and the dwell time on the slide was 100 ms for each spot. For all the printings, the humidity was maintained at 50%. Sonication and pin washings were carried out between samples to avoid sample cross-contamination. After printing, the DNA was left to dry and react with the epoxide groups on the surface of the glass slide for approximately 1 hour. Fluorescent scans of the slides were obtained with an arrayWoRx Standard scanner from Applied Precision, LLC (Issaquah, WA).

Pre-Treatment and Washes of DNA Array Slide. A diamond pen was used to mark important positions on the microarray slide prior to the BSA pre-treatment. BSA solutions were preheated in 30 mL conical slide holders from Starplex Scientific Inc. (Etobicoke, ON) for 1 hour at 42-45°C. The DNA microarray slides were then incubated in the BSA solution for one hour at 42°C. Once the slides were removed from the BSA solution, they were immersed in a 0.1X SSC solution contained in a conical slide holder at room temperature for 5 minutes. Immersion was done into two more fresh 0.1X SSC solutions contained in separate 30 mL conical slide holders.

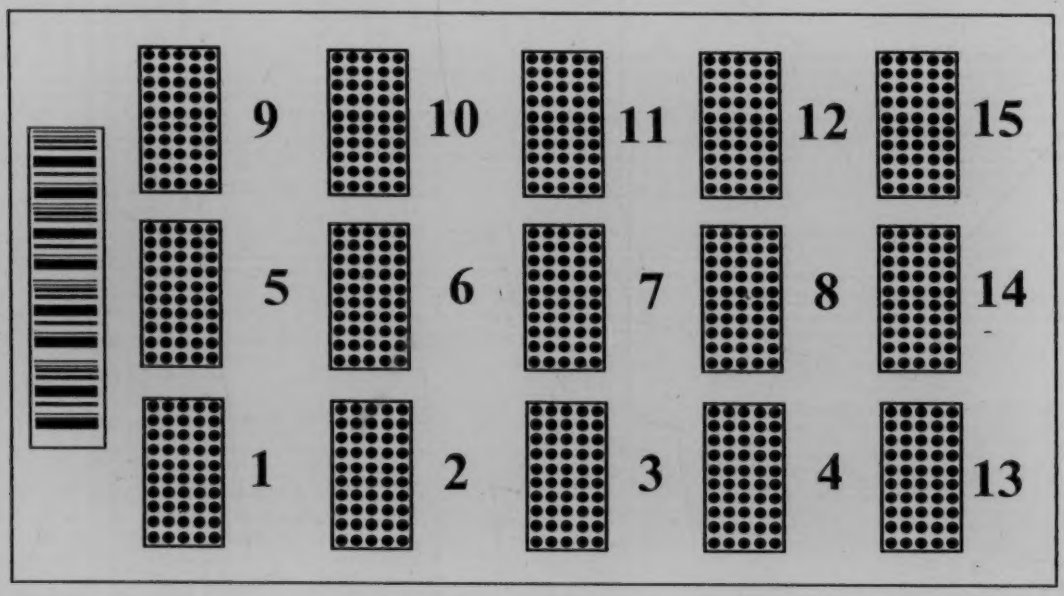

Figure 3.1 - Schematic of experimental slide. Each subarray represents 50 DNA spots. Subarrays 1-15 contain 0.5 μM FAM internal standard. Subarrays 1-4 also contain 50 μM of the ATTA target sequences, subarrays 5-8 contain 50 μM of the AAAA target sequence, and subarrays 9-12 contains 50 μM of the GTTG target sequence. Target sequences are given in Table 2.1. The bar code is shown at the left.

Slides were then washed with nanopure water in a conical slide holder, to remove any residual SSC salt, for 5 minutes at room temperature. Slides were then removed with tweezers and inserted into dry conical slide holders with Whatman filter paper at the bottom and centrifuged for 3 minutes at 1400 rpm. Slides were immediately removed from the 30 mL conical slide holder with tweezers and visually examined for any dirt deposits. All or most of any remaining water droplets were allowed to evaporate, preventing them from showing up on subsequent scans and damaging the slide. This procedure resulted in a dry slide, which was stored under dry nitrogen.

UVC Irradiation. Corning® 5 Slide Holders (Corning model 40082) were altered such that the hinged lid and one side were removed. This alteration allowed the chamber to act as a slide holder for irradiation experiments. These altered holders were used as received, then later spray painted black to reduce the translucency inherent to the orange plastic. A metal blocker was also used as is, then later painted black to reduce unwanted reflections within the holder. UVC light irradiations were carried out in a Luzchem (Ottawa, ON) EDU/DEV photoreactor, which contained 4 UVC lamps with a dosage power of 16.5 W m^{-2} each positioned on the top of the photoreactor, above the microarrays. N_2 gas was used to purge the photoreactor of any oxygen species during irradiations. Three irradiation time sequences were used, one sequence of 0, 1, 2, and 4 minutes (sequence 1), one of 0, 3, 6, 12, 17, 22, 27, 32 minutes (sequence 2), and one of 0, 15, 45, 75, 105, 135, 165 minutes (sequence 3). Prior to the beginning of each irradiation and in between each time interval, the photoreactor was purged with N_2 gas for 6 minutes. In addition, at each time interval, the metal blocker was also shifted above the microarray slide to expose a new section of the slide to UVC light. For controls, one

slide remained covered with a metal blocker, and an additional slide was placed in a dark dessicator purged with N_2 gas for times equivalent to those of the irradiated slide.

DNA Hybridization and Washing. Each irradiated or control slide was placed in a separate Corning® #2551 Hybridization Chamber (Neepan, ON). Two drops of nanopure water were placed in the chamber holes in order to maintain a level of humidity throughout incubation. The complementary probes were used at concentrations of either 5 or 35 μM in hybridization buffer. The diluted DNA probe solution was heated to 80°C for a short period of time in a water bath and allowed to cool to room temperature to re-anneal. Three, 30-μL aliquots of DNA probe solution were pipetted onto the center of each slide, spacing each aliquot at 1/3 of the length of the slide, then it was quickly covered with a 24 X 60 mm hybri-slip from Sigma-Aldrich (H0784-100EA), placed in the hybridization chamber, and incubated in a dark, heated water bath at 32 °C for 16 hours. Two 30 mL conical slide holders of wash 2 solution were preheated at 42 °C for 1 hour. Once the slides were removed from the hybridization chamber they were immediately immersed with the hybri-slip into one of the wash 2 solutions until the hybri-slip separated from the slide. The hybridized slide was then transferred into the second wash 2 solution and immersed for 5 minutes. The slides were then transferred to a room temperature wash 1 solution for 5 minutes, and then repeated twice more in two more wash 1 solution jars. The slide was once again dried in the centrifuge at 1400 rpm for 3 minutes.

Spectroscopy. All absorption spectra were obtained with a Hewlett Packard 8453 UV-Vis Diode Array Spectrophotometer. Fluorescence measurements of solutions were

obtained on a Photon Technology International MP1 System. Cy5 and FAM samples were diluted and blanked with nanopure water.

Error Analysis. Error bars used in Figures 3.7-3.11 were calculated through a data filtration process described below. Each sub-array was composed of 50 spots, each of which produced a fluorescence intensity after hybridization with the DNA probe and scanning. The fluorescence values underwent three filters. The first was that any fluorescence value less than or equal to zero was removed. Second, any fluorescence intensity values which were greater than the calculated upper limit were removed. Finally, any fluorescence values which were less than the determined lower limit were removed from the data set. A large portion of our data followed a skewed distribution, hindering the use of the standard t-confidence interval upper and lower limits. Instead, we used the non-specific 1.5 x interquartile range (IQR) rule to determine the upper and lower limits. The IQR value is determined by measuring the difference between the 3rd quartile from the 1st quartile. The upper limit was then calculated by adding 1.5 x IQR to the median intensity, while the lower limit had the 1.5 x IQR value subtracted from the lower limit. From this final data set, the standard deviation of each sub-array was calculated and plotted as an error bar on the median.

3.3 Results and Discussion

Effects of UV irradiation on the FAM internal standard. The stability of the FAM internal standard is of high importance to ensure that data obtained following UVC irradiation is reproducible and reliable. Preliminary results obtained in Chapter 2 have

led to the conclusion that the FAM internal standard will be stable throughout our experimentation, however, further investigation is required for confirmation. We tried to see the effects of UV irradiation on the FAM internal standard fluorescence. One slide was irradiated for different time intervals to a maximum of 4 minutes. A second slide was used as a positive control and was placed in the photoreactor covered presumably from any UVC light reaching the slide.

Figures 3.2, and 3.3 show plots of the FAM fluorescence intensities for each spot on the slide both before and after UV irradiation. The fluorescence intensity observed for the FAM internal standard in each DNA target sequence after UV irradiation was similar to the patterns observed prior to irradiation. Spikes in fluorescence intensities before UV irradiation were located at the same spot position as after UV irradiation, but at lower intensities. Figures 3.4, and 3.5 show plots for the ratio of pre UV/post UV irradiation as a function of each spot position on the slide. With the exception of a few spots, the ranges of the ratios were quite narrow. The lower half of each of the above-mentioned figures contains a narrower range of y-axis values in order to view the amount of scatter that occurred.

The fluorescence scatter in Figures 3.2A, B, C, and D before and after UV irradiation may be due to the variation of volumes spotted during the printing sequence or subsequently, dirt, or printing error. Approximately every 50^{th} spot results in an increase in observed fluorescence. Thus, although most of the spots contain similar amounts of solution, there are patterned exceptions where the last spot of each subarray contains more. The drop in the observed intensities, after irradiation, may be a result of the conditions in which the photoreactor was operated, for example a build up of ozone or

other reactive oxygen species which may cause other forms of damage to our DNA sequences or to the coupling between the DNA and slide. Cy5 was previously found to be negatively effected by certain environmental factors such as ambient ozone levels[11]. Ozone at a concentration of 12.5 ± 2.5 ppb was found to reduce fluorescence intensity emitted during the drying period[11] after washing slides with the post hybridization wash buffers. Investigations comparing the susceptibility of Cy5 and Cy3 to lower levels of ozone (60 to 85 ppb) found that Cy5 was more susceptible, reducing in intensity by 30 % after 10 minutes of exposure[12]. As a result of Cy5 and FAM's slight structural similarities (i.e. high degree of conjugation and rigidity), the drying process may also affect FAM by decreasing fluorescence in the presence of ozone.

The ratio of the pre and post UV irradiation is greater than unity for the majority of the spots in each of the target sequences. The UV irradiation may decrease the stability of the FAM fluorescence through photobleaching or photodecomposition[1314]. Photobleaching occurs when a fluorophore is repeatedly excited or irradiated, resulting in an excited-state reaction, where electrons, excited from the ground singlet state S_0 to an excited singlet state S_1 dissipate via intersystem crossing to the triple state T_1 followed by relaxation back to the ground state S_0 or reaction to reduce or eliminate fluorescence[15,1617]. Surprisingly, both the control and the experimental slides show similar results, even though the control was not exposed to UV light. Therefore, there must be additional parameters affecting the fluorescence intensity and/or DNA target robustness, which were not controlled in our preliminary experiments.

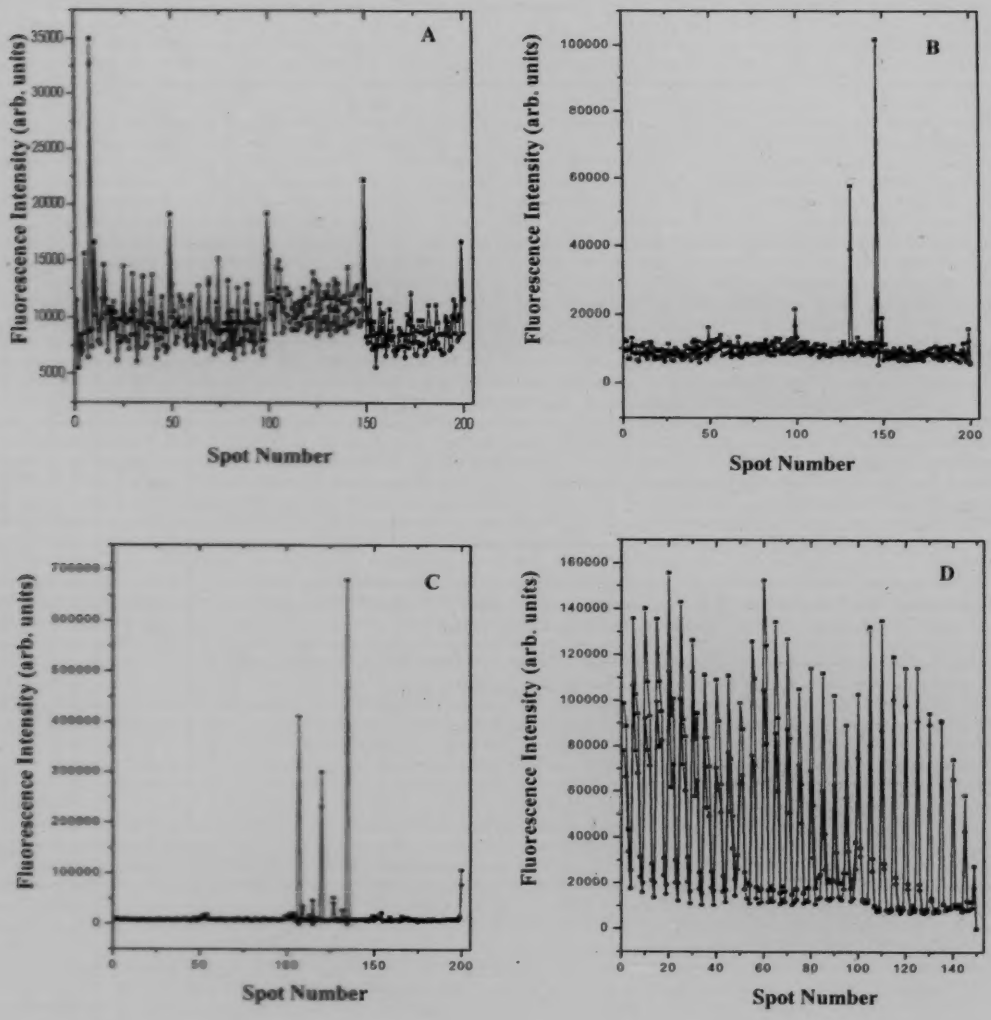

Figure 3.2 – FAM fluorescence intensities for the photoreactor control slide, where plot A represents ATTA, (B) GTTG, (C) AAAA, and (D) dFAM target sequences (■) prior to UV irradiation and (●) post UV light irradiation. The FAM concentration was 0.5 μM and target concentrations were 50 μM.

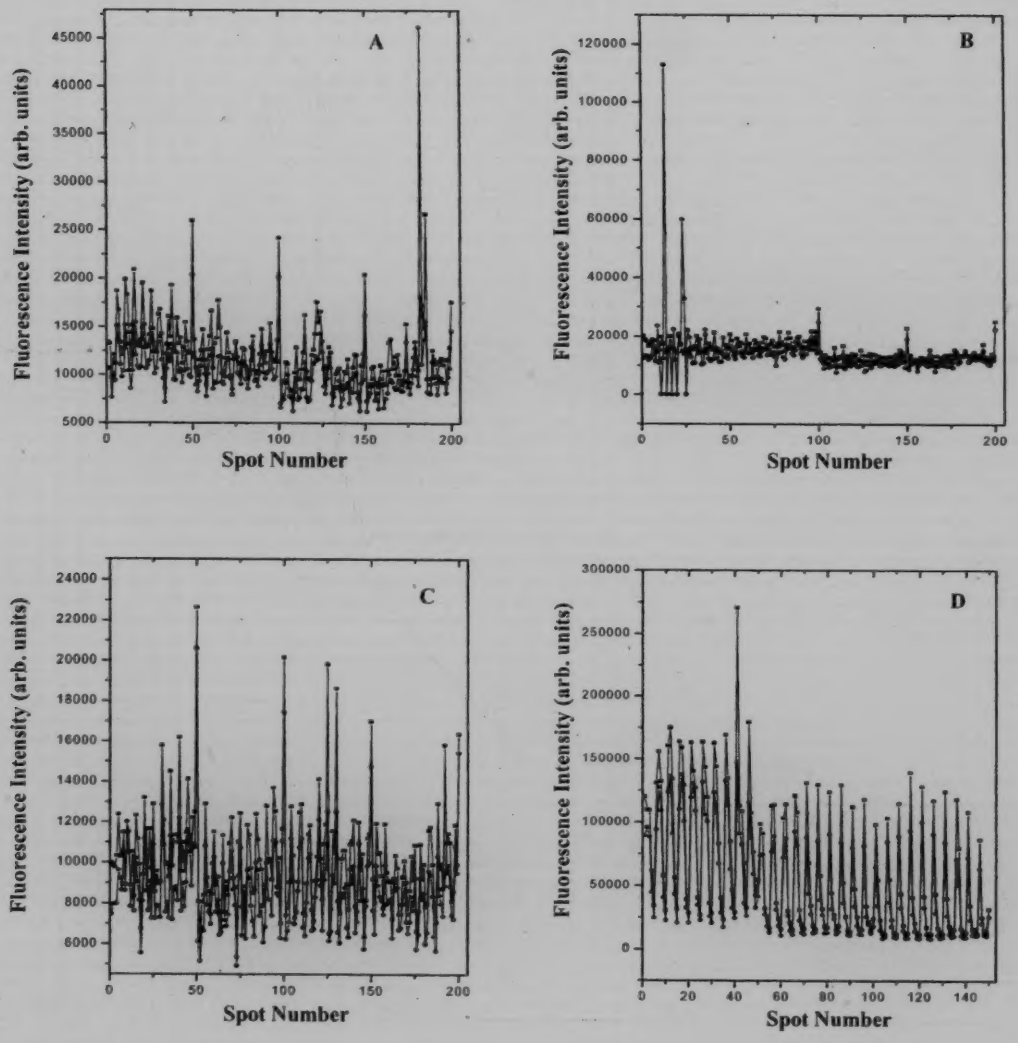

Figure 3.3 – FAM fluorescence intensities for the experimental slide, where plot A represents ATTA, (B) GTTG, (C) AAAA, and (D) dFAM target sequences (■) prior to UV irradiation and (●) post UV light irradiation. The FAM concentration was 0.5 μM and target concentrations were 50 μM. Spots 1-50 were irradiated for 4 minutes, spots 51-100 were irradiated for 2 minutes, spots 101-150 were irradiated for 1 minute, and spots 151-200 were irradiated for 0 minutes.

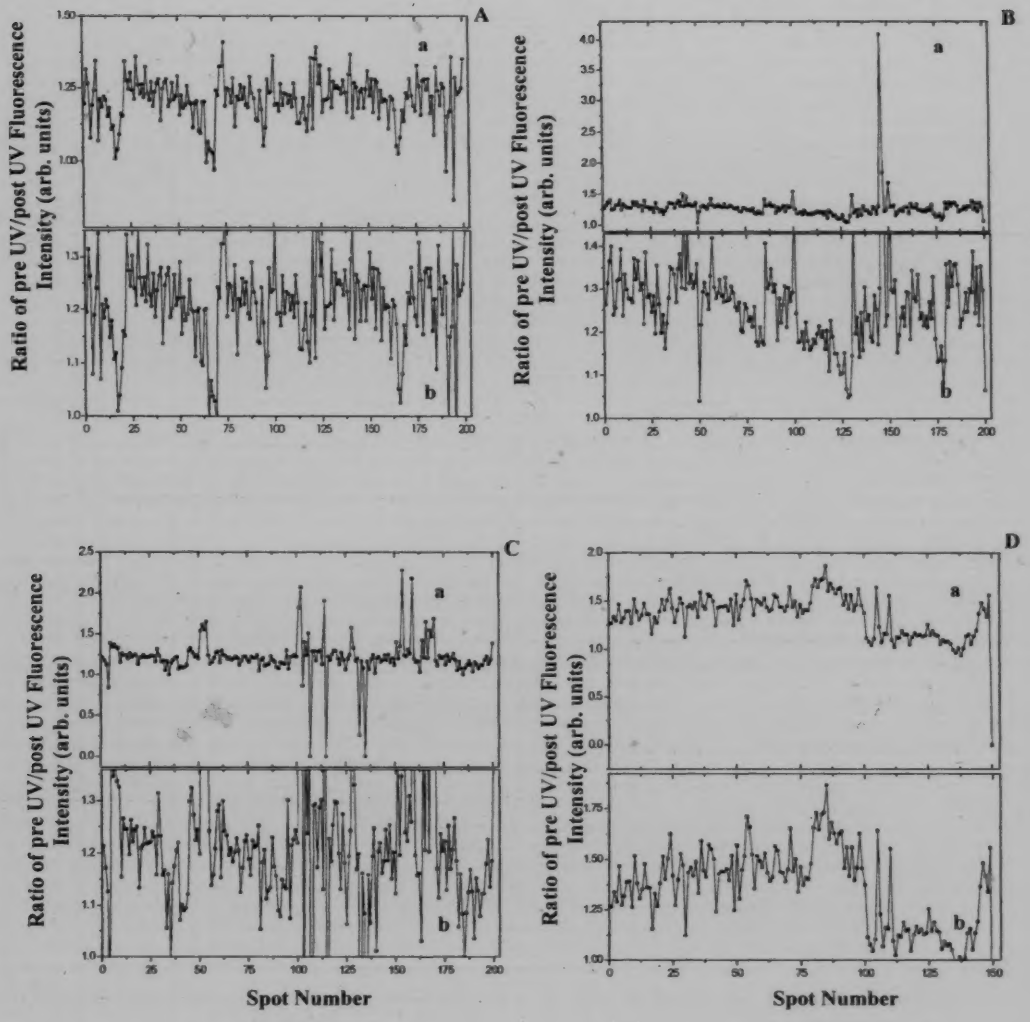

Figure 3.4 - Ratio of FAM fluorescence intensities for the photoreactor control slide prior to and after UV irradiation, where plot A represents ATTA, (B) GTTG, (C) AAAA, and (D) dFAM target sequences. The FAM concentration was 0.5 μM and target concentrations were 50 μM. The full range of values is given in (a), while a zoomed in range is given in (b).

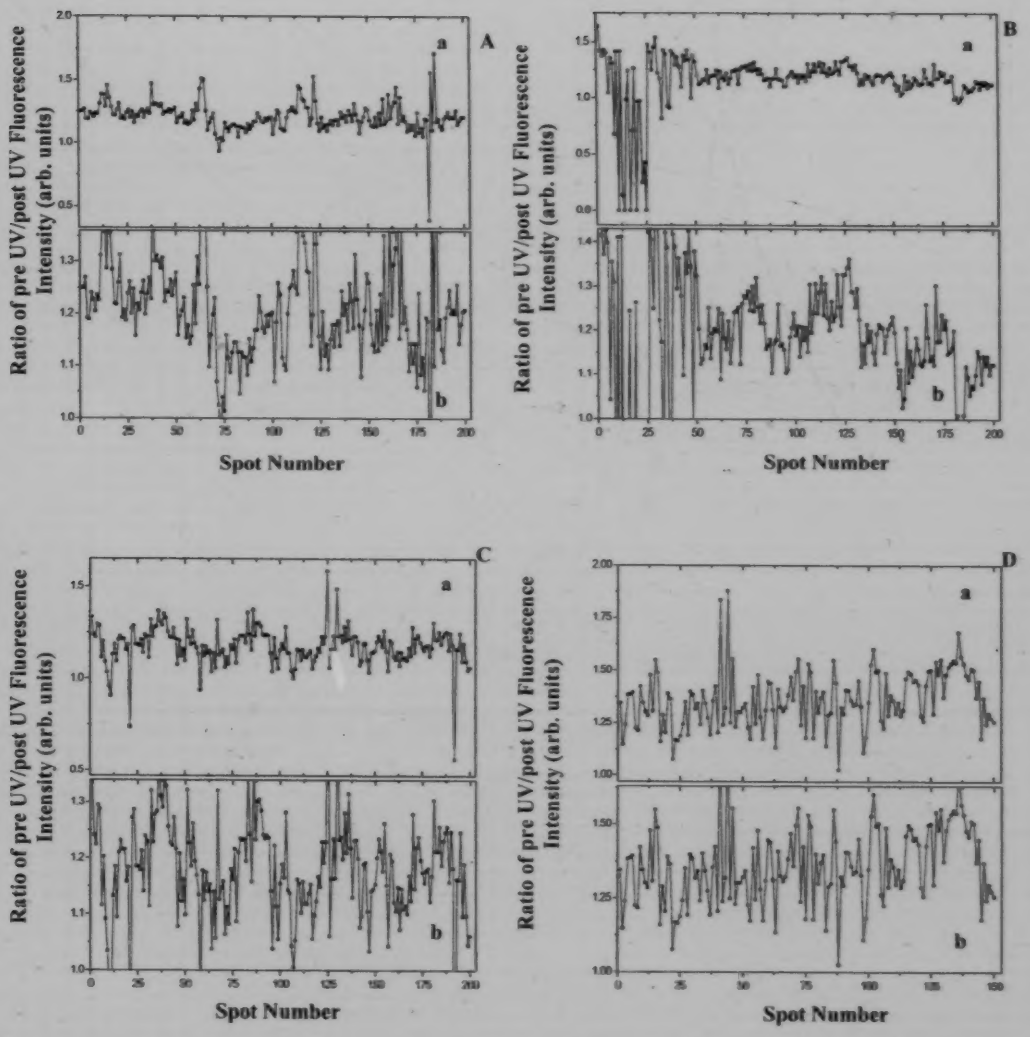

Figure 3.5 – Ratio of FAM fluorescence intensities for the experimental slide prior to and after UV irradiation, where plot A represents ATTA, (B) GTTG, (C) AAAA, and (D) dFAM target sequences. The FAM concentration was 0.5 μM and target concentrations were 50 μM. The full range of values is given in (a), while a zoomed in range is given in (b). Spots 1-50 were irradiated for 4 minutes, spots 51-100 were irradiated for 2 minutes, spots 101-150 were irradiated for 1 minute, and spots 151-200 were irradiated for 0 minutes. The full range of values is given in (A), while the zoomed in range is given in (B).

Detection of DNA damage. The main goal of this work was to determine the rate at which thymine damage would occur when two adjacent thymine nucleotides are flanked on both sides by either guanines (GTTG target sequence) or adenines (ATTA target sequence). The AAAA target sequence was used as the control sequence. The schematic of the microarray slide is shown in Figure 3.6.

Figure 3.7A shows the Cy5/FAM fluorescence ratio of the three DNA sequences as a function of UV irradiation time to a maximum of 4 minutes. As the UVC irradiation time increases, the Cy5/FAM fluorescence intensity apparently decreases for each of the DNA sequences. The photoreactor control slide depicted in Figure 3.7B was covered with a metallic blocker in the photoreactor during the irradiation of the experimental slide. Similar to the experimental slide, the Cy5/FAM emission on the control slide decreased as the UV irradiation time was increasing. This result was entirely unexpected.

The decrease in the Cy5/FAM fluorescence in the experimental slide was considered to be a result of thymine photodamage. However, the conflicting control results led to the belief that all possible control parameters were not considered prior to the execution of this experiment. It was postulated that the control slide was being damaged either by ambient light in the laboratory or reflected light within the photoreactor itself, or by some other condition in the photoreactor (e.g. ozone damage).

Enhanced controls. We attempted to correct for the parameters, which had not been controlled in the previous experiment. To do this, we instituted several changes in the experimental setup and procedure. First, each of the slide holders used in the photoreactor were painted black, preventing the transmittance of light through the holders. This transmittance of light may have occurred with the previous orange

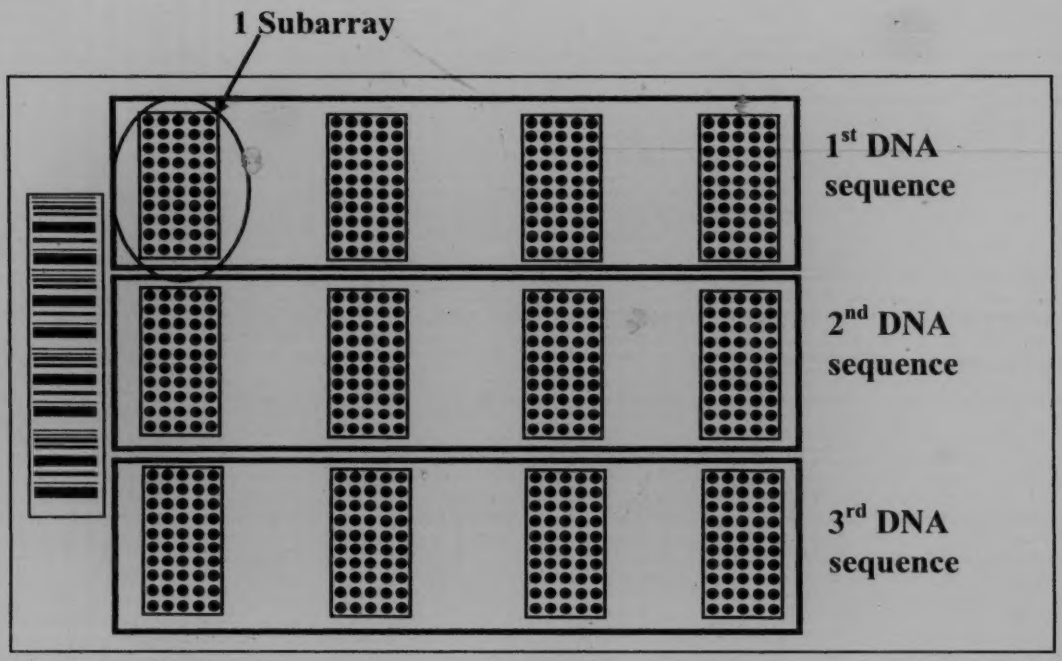

Figure 3.6 - Schematic of DNA microarray slide. Each row contained either ATTA, GTTG, or AAAA DNA target sequence (Table 2.1). One subarray is composed of fifty DNA target spots. Each spot is approximately 7 nL of solution and creates a spot diameter of 100 μm. All of the DNA spots contain 50 μM amino-terminated target DNA. The barcode is located on left side of the slide in this schematic.

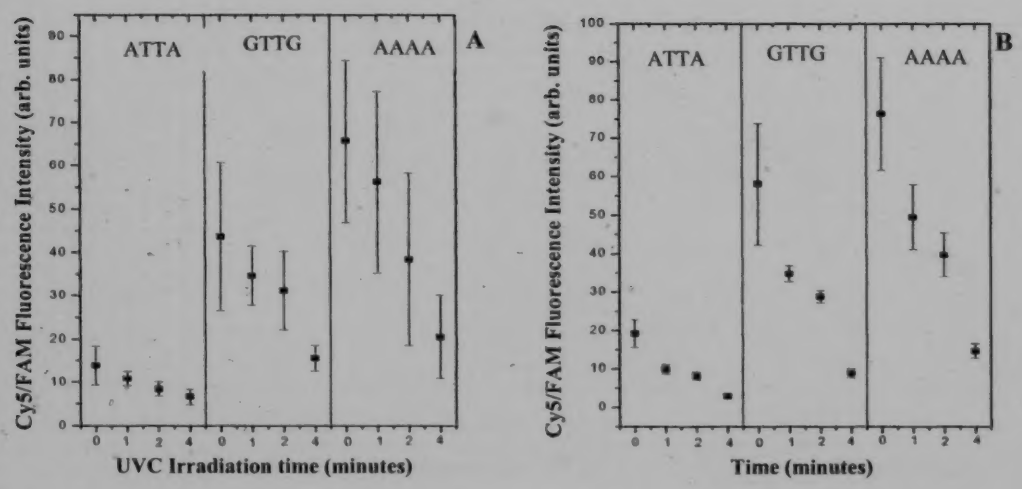

Figure 3.7 - Median Cy5/FAM fluorescence intensities for the experimental slide (A) and photoreactor control slide (B). Each point represents one subarray, the error bars represent the calculated standard deviation. The concentration of three target sequences ATTA, GTTG, and AAAA were 50 μM, the concentration of the FAM internal standard was 0.5 μM and the complementary probes was 5 μM.

translucent slide holders. Second, the metallic blockers were also painted black, inhibiting reflected light from reaching the slide. Third, the floor and walls of the photoreactor were covered with paper towels throughout the experiment, to reduce reflections within the photoreactor.

Repeating the photochemistry experiment with these new controls in place, the photoreactor control data (Figure 3.8B) from this experiment shows general scattering of the Cy5/FAM fluorescence intensity data, independent of the sub-array position on the slide. This result suggests that no photochemistry is occurring in the control slide. Unfortunately, the fluorescence intensity graph of the experimental slide (Figure 3.8A) also shows a random scattering independent of UVC irradiation time.

The scattering of the Cy5/FAM fluorescence for both the photoreactor control and experimental slide may be due to the correction of controls in the procedure and setup. The resulting general scattering of the Cy5/FAM was expected for the photoreactor slide since it meant that the new controls were preventing damage and the control was in fact acting as a control. However, the corrections also prevented any damage from being observed on the experimental slide (Figure 3.8B). Longer UV irradiation times were considered in order to observe a greater effect on the Cy5/FAM fluorescence by creating DNA damage on the experimental slide. In the next experiment, we attempted to increase the irradiation time on the experimental slide to a maximum of 32 minutes.

The experimental slide represented in Figure 3.9A was exposed to UV light for a maximum of 12 minutes. As a result, only the ATTA sequence showed any significant effects from the irradiation times used, decreasing in fluorescence as the irradiation time was increased. Figure 3.9B, the second slide in this experiment, shows the results from

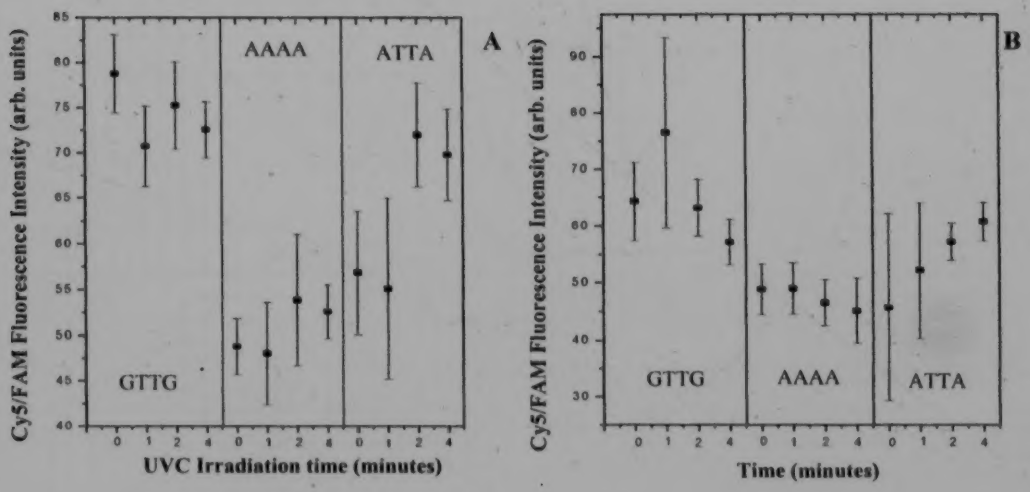

Figure 3.8 – Median Cy5/FAM fluorescence intensities for the photoreactor control slide (A) and the experimental slide (B). Each point represents one subarray, the error bars represent the calculated standard deviation. The concentration of three target sequences ATTA, GTTG, and AAAA were 50 μM, the concentration of the FAM internal standard was 0.5 μM and the complementary probes was 5 μM. Enhanced controls were used (see text for details).

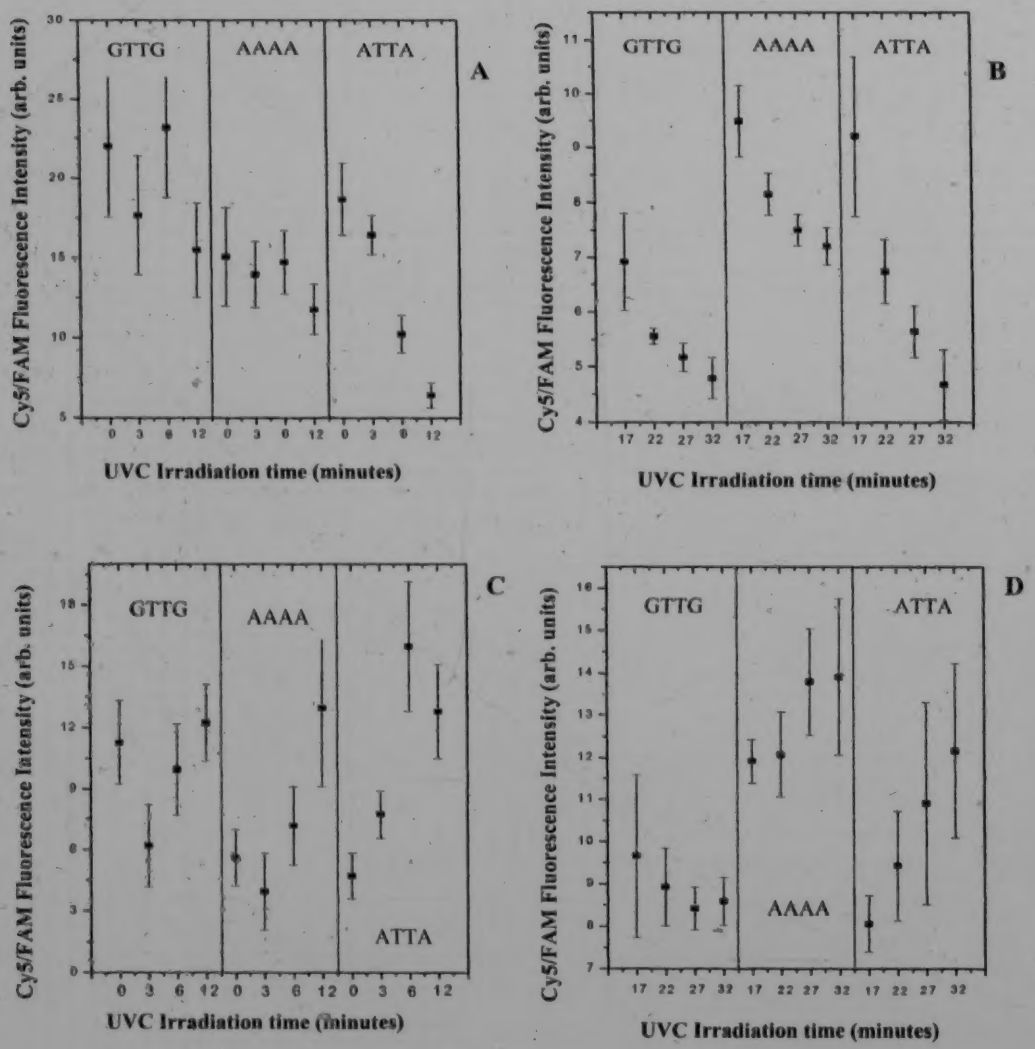

Figure 3.9 – Median Cy5/FAM fluorescence intensity as in Figure 3.8, but for the experimental slides with further enhanced controls (see text for details). The experimental slide irradiation times were from 0-12 minutes (A and C) and 17-32 minutes (B and D). Plots C and D are for replicate experiment of the conditions used in A and B.

longer irradiation times, up to 32 minutes. Here all three of the DNA target sequences decrease in Cy5/FAM fluorescence as the irradiation time increased. In contrast, Figures 3.9C and D, replicates of the experimental procedures for Figure 3.9A and B, show scattered Cy5/FAM intensities independent of the UV irradiation time used. Inexplicably, the ATTA control in Figure 3.9D displayed increasing Cy5/FAM fluorescence as the irradiation time increased. Control slides showed constant Cy5/FAM fluorescence intensities independent of the time the slide spent in the photoreactor (data not shown).

Initially, it was believed that the increases in irradiation times used were sufficient since the result obtained in Figure 3.9A and B were as expected. However, the counter-intuitive results observed for the ATTA sequence in Figure 3.9D led us to the conclusion that there may be other factors contributing to the unreliable results. One possible factor may be the affect of ozone content in the atmosphere and in the photoreactor. Research has shown that even minimal ozone concentrations may negatively affect the quality of microarrays[12]. To reduce the effects of ozone on the slides N_2 gas was blown over the slides immediately after centrifugation. Slide exposure to air during the drying steps was also reduced. Finally, the irradiation times were increased. The time used for the UV irradiations was increased to 75 minutes on and one slide to 165 minutes on a second slide. Both of the slides had a 0 minute irradiation time on them to maintain a baseline fluorescence intensity which was exclusive to each slide. The DNA probe concentrations were also increased as per results obtained in Chapter 2. The concentrations of each probe sequence were increased from 5 μM to 35 μM. Slide exposure to ambient light was removed and purging with N_2 continued for the length of time of irradiations. A summary flow chart of our experimental process and results is shown in Figure 3.10.

The results for the photoreactor control slide for this experiment (Figure 3.11) show that the Cy5/FAM fluorescence intensity ratios are independent of the sequence position on the slide and are independent of the amount of time in the photoreactor. In Figures 3.12A and C we have plotted the Cy5/FAM fluorescence as a function of UV irradiation time for each of the three DNA target sequences. The error bars shown are the standard deviation of each subarray. The results show a clear decreasing trend for each DNA sequence. The 0 and 15 minute irradiation times for AAAA sequence show slight fluorescence data scatter (Figure 3.12A) followed by a significant decrease in fluorescence intensity for the 45 and 75 minute times. The remaining two DNA sequences (GTTG and ATTA) show the greatest fluorescence intensity at the 0 minute irradiation time. The scatter in data in Figure 3.12A and C may reflect that extended UV irradiation times may have caused damage or photobleaching to the FAM fluorophore, as discussed previously. The resulting deflation in the FAM emission can correspondingly inflate the Cy5/FAM ratios, masking any damage.

In Figure 3.12B and D we have plotted only the Cy5 fluorescence intensity after hybridization as a function of UVC irradiation time. The determined time constants for each of the three DNA sequences for the 0-75 min. irradiations were 55.94652 ± 34.81171 min (R^2 = 0.99968) for ATTA, 43.49542 ± 28.79901 min (R^2 = 0.98107) AAAA, and 22.86783 ± 7.11634 min (R^2 = 1) for GTTG (all exponential curve fits are shown in Chapter 6). The time constants determined for the 0-165 min irradiations were 51.59113 ± 2.14881 min (R^2 = 0.95881) for ATTA, 47.78764 ± 3.5573 min (R^2 = 0.83409) for AAAA, and 53.52365 ± 1.26358 min (R^2 = 0.96956) for GTTG DNA sequence. All of these slides show a decrease of fluorescence intensity upon irradiation.

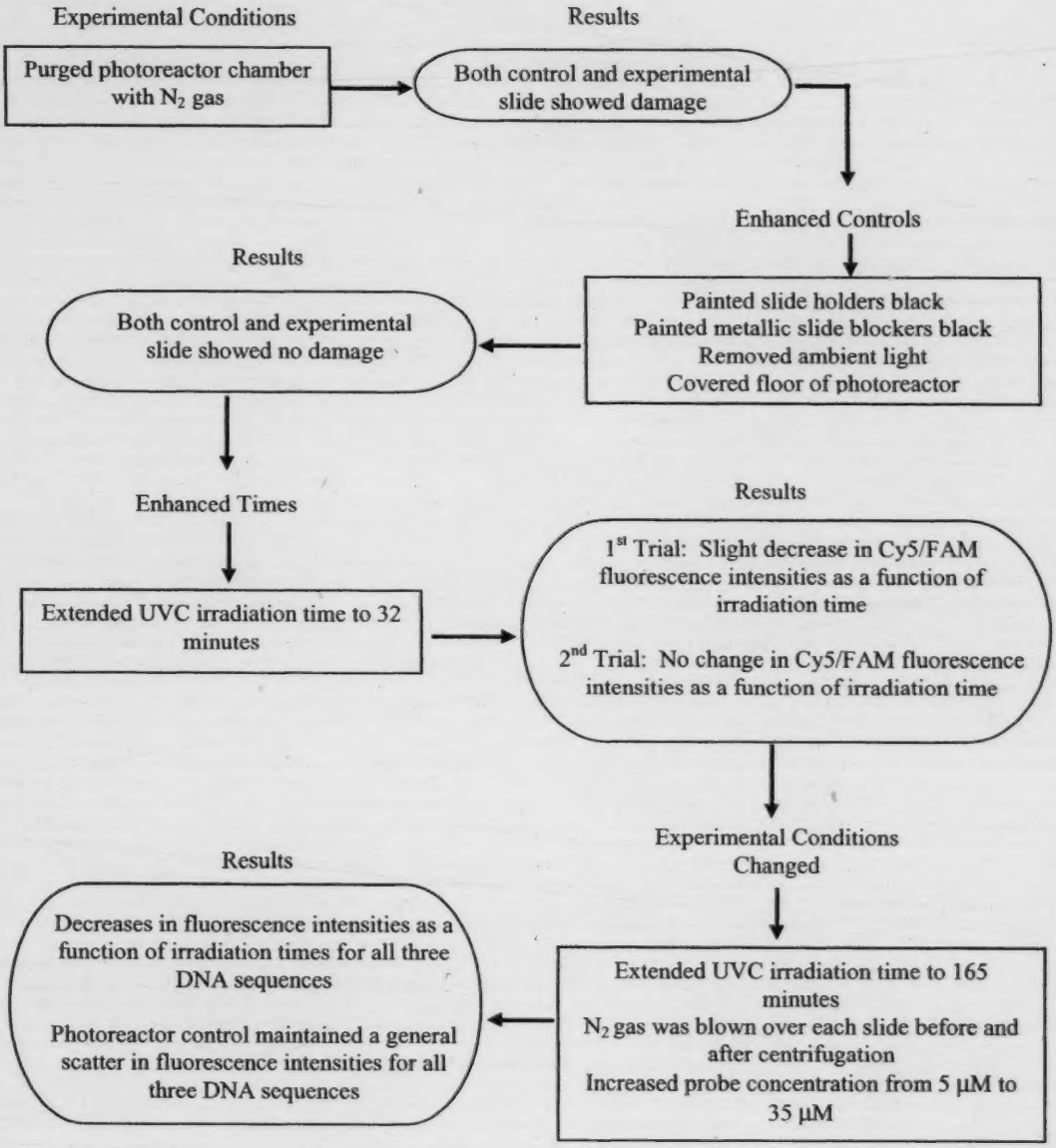
Experimental Conditions
Purged photoreactor chamber with N_2 gas
Results
Both control and experimental slide showed damage
Enhanced Controls
Painted slide holders black
Painted metallic slide blockers black
Removed ambient light
Covered floor of photoreactor
Results
Both control and experimental slide showed no damage
Enhanced Times
Extended UVC irradiation time to 32 minutes
Results
1st Trial: Slight decrease in Cy5/FAM fluorescence intensities as a function of irradiation time
2nd Trial: No change in Cy5/FAM fluorescence intensities as a function of irradiation time
Experimental Conditions Changed
Extended UVC irradiation time to 165 minutes
N_2 gas was blown over each slide before and after centrifugation
Increased probe concentration from 5 µM to 35 µM
Results
Decreases in fluorescence intensities as a function of irradiation times for all three DNA sequences
Photoreactor control maintained a general scatter in fluorescence intensities for all three DNA sequences

Figure 3.10 – Summary flow chart of the experimental process.

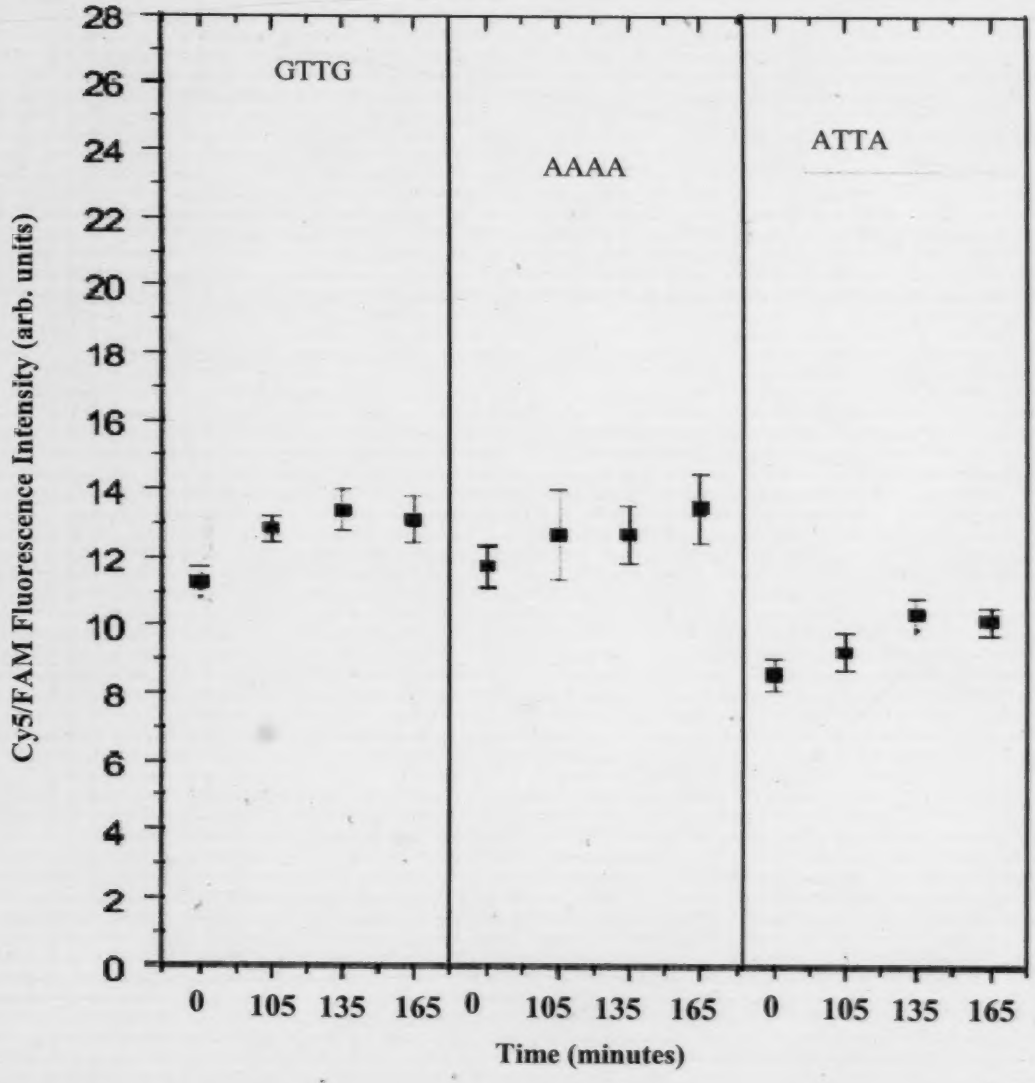

Figure 3.11 – Median Cy5/FAM fluorescence intensities for the photoreactor control slide. Each point represents one subarray, the error bars represent the calculated standard deviation. The concentration of three target sequences ATTA, GTTG, and AAAA were 50 μM, the concentration of the FAM internal standard was 0.5 μM and the complementary probes was 5 μM. Ambient light exposure to the slide was removed and air exposure during drying steps was reduced.

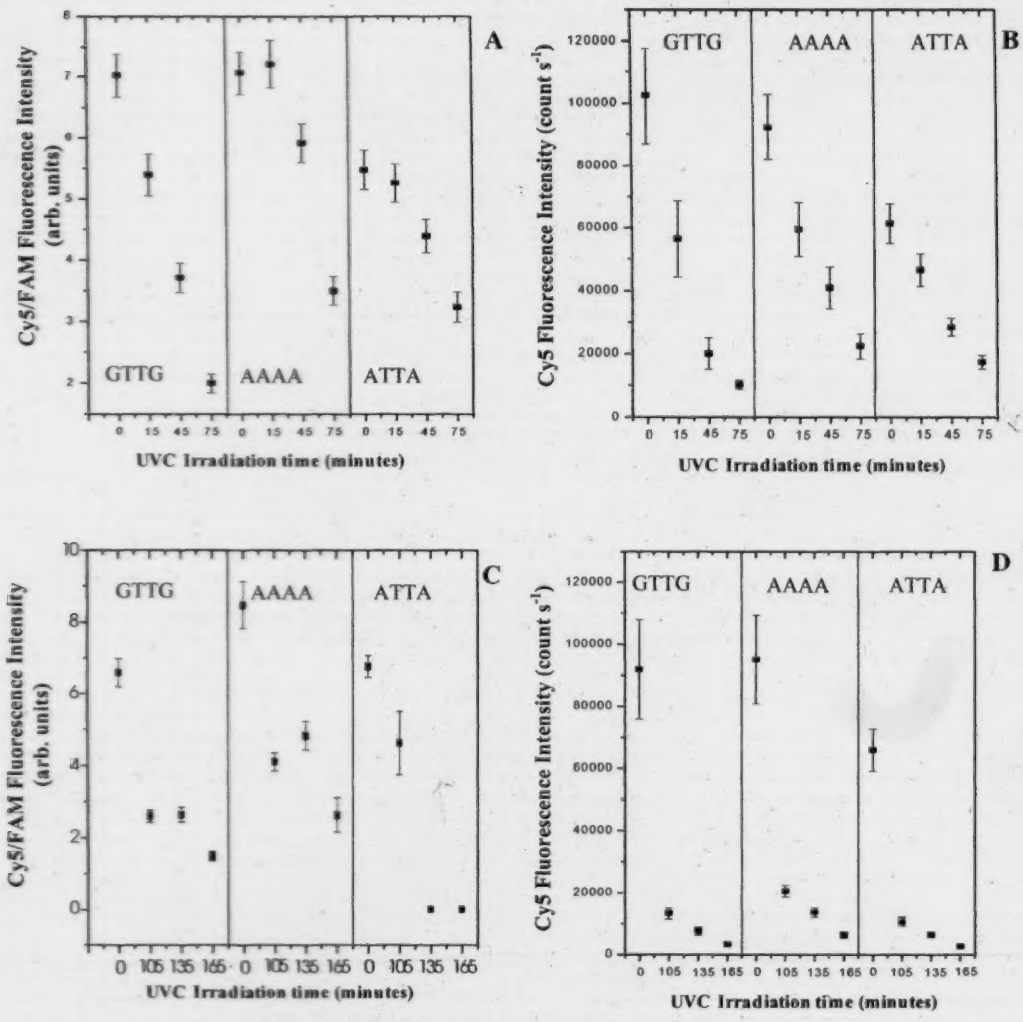

Figure 3.12 – Median Cy5/FAM fluorescence intensities for the experimental slide. Each point represents one subarray, the error bars represent the calculated standard deviation. The concentration of three target sequences ATTA, GTTG, and AAAA were 50 μM, the concentration of the FAM internal standard was 0.5 μM and the complementary probes was 35 μM. Ambient light exposure to the slide was removed and air exposure during drying steps was reduced.

Also, it is interesting to not that the R^2 values are much closer to 1 without the FAM standard, suggesting that FAM may indeed be damaged in these photochemical experiments.

As briefly mentioned previously, the AAAA target sequence was initially designed as a control, since purines are generally considered to be stable against radiation[18,19]. However, there have been reports of purine photodamage, induced by UV irradiation at 254 nm[20]. Similar to their pyrimidine counter-parts adenine can also undergo photocycloaddition with adjacent thymine residues. This photodimerization reaction between adjacent adenines and thymines produces a highly strained unstable azetidine intermediate, which breaks down through two competing pathways to form two distinct photoproducts[18,20]. These strained intermediates make the photodimerization a less favourable reaction in double stranded or native DNA[20], although the reaction may occur much more readily on more flexible ssDNA. Thus, our perceived control target shows considerable photodamage in most of the experiments.

We attribute the decrease in fluorescence intensity, when the irradiation time was increased, to UV-induced damage to the DNA target sequences. The fluctuations observed in the decreasing trend may be a result of the FAM correction used for each subarray. In contrast, the trends observed when only the Cy5 probe intensity was plotted as a function of UVC irradiation time show a definite exponential decay due to photochemical damage. The rate constants for the ATTA and AAAA were similar for both the 0-75 minutes and 0-165 minutes.

3.4 Conclusions

We have demonstrated the numerous controls that are required in order to obtain reliable data from a microarray experiment. This included the reduction of ambient light exposed to the microarrays, the presence of atmospheric ozone, and reflected light within the photoreactor. We immobilized three DNA target sequences, ATTA, AAAA, and GTTG onto glass slides and induced DNA photodamage with UVC light. A method was developed to detect the formation of DNA damage on the microarrays using fluorescently labeled hairpin probes. The exponential decay rate constants of the three DNA sequences were calculated and were most reliable when obtained from the probe fluorescence alone. The rate constants determined were 51.59113 ± 2.14881 min (R^2 = 0.95881) for ATTA, 47.78764 ± 3.5573 min (R^2 = 0.83409) for AAAA, and 53.52365 ± 1.26358 min (R^2 = 0.96956) for GTTG DNA sequence. The fluorescence emitted from the internal standard FAM was found to decrease when the slide were irradiated for longer periods of time (0-165 min) this may be a result of photobleaching from over exposure to UV light. In order to use a fluorophore as an internal standard in these experiments a more photostable fluorophore will need to be considered.

3.5 References

[1] Coohill, T. P. *Journal of Toxicology* **1998**, 17, 559-565.

[2] Cicerone, R. J. *Science* **1987**, 237:35-42.

[3] Mitchell D. L., in *CRC Handbook of Organic Photochemistry and Photobiology*, edited by W. H. Horspool and P.-S. Song (CRC Press, New York), p1326.

[4] Ravanat, J., Douki, T., Cadet, J. *Journal of Photochemistry and Photobiology B: Biology* **2001**, 63, 88-102.

[5] Schreier, W. J., Schrader, T. E., Koller, F. O., Gilch, P., Crespo-Hernandez, C. E., Swaminanthan, V. N., Carell, T., Zinth, W., Koller, B. *Science*, **2007**, 315, 625-629.

[6] Ruzsicska, P.; Lemair, E., in *CRC Handbook of Organic Photochemistry and Photobiology*, edited by W. H. Horspool and P.-S. Song (CRC Press, New York), pp. 1298-1305 1326–1328.

[7] Miaskiewicz, K.; Miller, J.; Cooney, M.; Osman, R., *J. Am. Chem. Soc.* **1996**, 118, 9156-9163.

[8] O'Neil, L. L., Grossfield, A., Wiest, O. *J. Phys. Chem. B*, **2007**, 111, 11843-11849.

[9] Bonnet, G., Tyagi, S., Libchaber, A., Kramer, F. R., *Proc. Natl. Acad. Sci. USA*, **1999**, 96, 6171-6176.

[10] Yarasi, S., McConachie, C., Loppnow, G. R. *Photochemistry and Photobiology*, **2005**, 81, 467-473.

[11] Burgoon, L. D., Passow, J. E., Gennings, C., Boverhof, D. R., Burt, J. W., Fong, C. J., Zacharewski, T. R., *Nucleic Acids Research*, **2005**, 33, e172-e183.

[12] Fare, T. L., Coffey, E. M., Dai, H., He, Y. D., Kessler, D. A., Kilian, K. A., Koch, J. E., LeProust, E., Marton, M. J., Meyer, M. R., Stoughton, R. B., Tokiwa, G. Y., Wang, Y., *Analytical Chemistry*, **2003**, 75, 4672-4675.

[13] Malicka, J.; Gryczynski, I.; Fang, J., Lakowicz J. R., *Analytical Biochemistry*, **2003**, 317, 136-146.

[14] Reinikuntla, B. R.; Rose, H. C.; Eldo, J.; Waggoner, A. S.; Armitage, B. A., *Organic Letters*, **2004**, 6, 909-912.

[15] Füreder-Kitzmüller, E.; Hesse, J.; Ebner, A.; Gruber, H. J.; Schütz G. J., *Chemical Physics Letters*, **2005**, 404, 13-18.

[16] Eggeling, C.; Widengren. J.; Brand, L.; Schaffer, J.; Felekyan, S.; Seidel, C. A. M., *Journal of Physical Chemistry A*, **2006**, 110, 2979-2995.

[17] Mondal, P. P. *Applied Physics Letters* **2008**, 92, 13902-1-3.

[18] Porschke, D. *Proc. Nat. Acad. Sci. USA* **1973**, 70, 2683-2686

[19] Porschke, D. *J. Am. Chem. Soc.* **1973**, 95, 8440-8446.

[20] Clingen, P. H.; Davies, R. J. H. *Journal of Photochemistry and Photobiology B: Biology 1997, 38, 81-87.*

4 Silicon Nanoparticles

4.1 Introduction

One of the challenges involved in microarray techniques is the necessity that fluorophores be compatible with the experimental conditions used. This may require obtaining fluorophores with appropriate spectral properties (i.e. absorption and emission wavelengths) and enhanced photostability. Investigations into novel, more robust fluorophores has led us to semiconductor nanoparticles, and their development in fluorescent probe research.

Semiconductor nanoparticles have recently become of great interest; they are believed to someday significantly contribute to the fields of biology and biochemistry because of their attractive luminescence properties[1]. The synthesis of various types of nanoparticles have been realized[6] such as CdS, CdSe, and InP. For example, silicon coated with silica has been prepared through the combustion of silane, followed by hydrogen fluoride etching. Also, GaN has been made through the thermolysis of $[H_2GaNH_2]_3$ in supercritical ammonia and CdS has been synthesized via arrested precipitation in the presence of polyphosphates[2]. Silicon, in particular, is of great technological importance since it has been the basis of the computer revolution and has found applications in photovoltaic devices[3]. Silicon nanoparticles have been found to display particle size dependent optical and electronic properties[3,4,5]. Work performed by the Veinot group at the University of Alberta has led to the development of a method that produces noncrystalline silicon particles from a commercially available hydrogen silsesquioxane (HSQ)[6]. Their particles, like those of many other groups have been found

to be highly photoluminescent. The silicon nanoparticles have been shown to emit light in the near IR region of the electromagnetic spectrum and in some cases (as shown here) also in the UV region.

The use of these nanoparticles as probes to provide insight into biological systems possesses some advantages. The detection of biological samples often requires the use of labels that can be detected with high sensitivity. Current fluorescent labels available include cyanine dyes, enzymes and now nanoparticles[7]. Semiconductor nanoparticles possess properties such as a broad excitation spectrum with a narrow emission that is tunable with size variations. Nanoparticles also exhibit negligible photobleaching, fairly high quantum yields, stability, and negligible phototoxicity[7,8]. Nanoparticles have been considered for use as multiple genetic markers[9,12], unachievable with existing fluorophores due to their narrow excitation spectrum and their broad emission spectrum with long tails at red wavelengths. These characteristics can introduce cross talk between different detection channels, complicating quantification of different probes when used simultaneously[7].

The ability to bind nanoparticles to biological molecules is a significant step towards the integration of nanotechnology and biology, as it can lead to advancements in medical diagnostics, targeted therapeutics, microbiology and cell biology[9]. Biomolecular-nanoparticles conjugates such as Cd/Se – Zn/S core – shell nanoparticles, capped with an organic layer to prevent aggregation and conjugated to DNA[10], immunoglobulin G and ovalbumin[11] have been successfully synthesized. Unfortunately, these bioconjugates have resulted in a decrease in the quantum yield of the nanoparticles and in some cases undesired aggregation[11]. In addition to these complications, the

cytotoxicity of inorganic nanoparticles containing Cd, Se, Zn, Te, Hg, and Pb have led to some concerns for their use in biological systems. Depending on the dosage, these chemicals can be potent toxins and neurotoxins, capable of accumulating in the liver and/or the nervous system[12] and have lead to investigations of nontoxic alternatives such as silicon. Similar to other inorganic nanoparticles, silicon nanoparticles also possess broad absorption bands and tunable narrow-band emission, but are bioinert.

The cause behind the emission of silicon nanoparticles is still currently debated. It was generally believed that the many unique properties exhibited by the nanoparticles was as a result of quantum confinement effects[1,13,14,15], occurring when the size of the particles become comparable to the exciton diameter of the bulk semiconductor material[13]. However, some researchers are not convinced of this fact[16]; some have observed discrepancies between the luminescence energy from Si nanocrystals and the width of the energy band gap calculated with quantum confinement theory. These discrepancies have been explained by considering a defect center at the Si nanocrystal/ SiO_2 interface[17].

Here we look at the stability of silicon nanoparticles by observing the effects of aging on the emission spectrum. We measured the absorption and emission spectra of silicon nanoparticle samples over 14 days. We found that the absorption and emission were highly stable for samples with a narrow particle size distribution. The average observed emission from the sealed samples displayed larger quantum yield for the UV region (17%) and near IR region (1.27%) compared to the exposed SiH samples 4.18% and 0.48% respectively. Slight decreases in quantum yield values were observed after a period of 14 days. Thus, silicon nanoparticles may be useful as a biochemical label for

techniques involving detection of biological samples once their functionalization and bioconjugation have been further developed.

4.2 Experimental

Materials. FOX® 15 was obtained from Dow Corning Corporation (Midland, MI). NaCl was obtained from EMD (San Diego, CA). Hydrofluoric acid was obtained from JT Baker (Anachemia Science Edmonton, AB). Pentane was obtained from Caledon Laboratory Chemicals (Georgetown (Halton Hills), ON). The octane, and toluene were obtained from Fisher Scientific (Ottawa, ON). $CaCl_2$ was obtained from Aldrich (Oakville, ON). All reagents were used as received.

Silicon nanoparticle synthesis. Within a glove box, a 5 mL aliquot of FOX® 15, containing methyl isobutyl ketone, hydrogen silsesquioxane, and toluene was poured into a Schlenk flask with a stir bar. After removing the Schlenk flask from the glove box the flask was attached to a vacuum line and placed under a positive flow of argon gas to ensure no air seeped into the flask. Vacuum lines and the stopcock to the Schlenk flask were closed and the argon gas flow was stopped. The vacuum line was cleared and the stopcock was slightly opened until gentle bubbling of the hydrogen silsesquioxane (HSQ) commenced. The HSQ was left bubbling for approximately one hour to remove the solvent. The stir bar was removed from the highly viscous HSQ solution while under argon gas. This solution was left to sit overnight under vacuum. The following day the Schlenk flask containing the dried solid HSQ was purged once more with Ar (g) then removed from the vacuum line. A small amount of this solid HSQ product was crushed and placed onto a weighing paper then transferred into a furnace boat under atmospheric

conditions. The boat was placed into the furnace with a set maximum temperature of 1100 °C and a flow of a 4% H_2 and 96% N_2 through the furnace tube. The temperature was increased at 20 °C/min until the set temperature was reached. The temperature remained at 1100 °C for 1 hr after which the sample was left to cool overnight[18]. The annealed HSQ was removed from the furnace and ground with a nonporous mortar and pestle to a fine crystal under atmospheric conditions. The 2:1 NaCl/HSQ mixture was ground until the NaCl became visibly homogenous. Approximately 0.5 g of the dried sample was etched in a 10 mL mixture of 1:1:1 hydrofluoric acid (HF), ethanol, and H_2O (v/v/v) while being gently stirred for 1-2 hrs. Less than 10 mL of one of the following solvents, pentane, octane, or toluene, was gently poured into the Teflon beaker. Once the stir bar was stopped, the aqueous layer was allowed to settle. Plastic pipettes were used to extract the organic layer, containing the etched hydride terminated silicon nanoparticle into a Schlenk flask. The HF remaining in the Teflon flask was neutralized with $CaCl_2$. The Schlenk flask was placed under vacuum, removing the organic solvent. With a positive flow of Ar (g) the solvent was replaced with a known volume of distilled or degassed solvent. The Schlenk flask was sonicated to ensure the particles were dispersed throughout the solvent.

Aging analysis and quantum yield determination. Equal volumes of the hydride-terminated silicon nanoparticle in pentane, octane, or toluene were collected into two cuvettes. Solvent used did not affect results. The background absorption spectrum of each cuvette had been measured with the solvent and saved. Cuvette #1 contained a sample, which was kept unsealed, exposing it to air throughout the remaining experimental procedures. During the experiment, any evaporation observed was

replenished with neat solvent from the bottle for the exposed samples. Cuvette #2 was evacuated under vacuum then purged with Ar (g) three times through a septum sealed with copper wire to maintain inert conditions. The solvent line was also marked on cuvette #2, and the solvent level was maintained with degassed solvent. Immediately following hydride-terminated silicon nanoparticle preparation, the sample absorption, excitation, and emission spectra were measured. Relative quantum yield (Φ) values were determined by using the following equation:

$$\Phi_x = \Phi_r \{A_r(\lambda_r)/A_x(\lambda_x)\} \{I(\lambda_r)/I(\lambda_x)\} \{n_x^2/n_r^2\} \{D_x/D_r\} \quad (1)$$

Where, $I(\lambda)$ is the relative intensity of the exciting light at wavelength λ, n is the average refractive index of the solution to the luminescence, D is the integrated area under the emission spectrum, and $A(\lambda)$ is the absorbance / cm of the solution at the exciting wavelength λ[19]. Subscripts x and r refer to the unknown and the reference solutions, respectively. The absorbance was used in the relative quantum yield calculations.

Spectroscopy. All absorption spectra were obtained with a Hewlett Packard 8452 UV-Vis Diode Array Spectrophotometer. Fluorescence measurements of solutions were obtained on a Photon Technology International MP1 System. A bandpass slit width of 4 nm was maintained for fluorescence measurements. Measurements were taken every ½ hour for 1.5 hours, and then were extended based on the observations. Rhodamine 6G was diluted with methanol to match the absorption intensity with the nanoparticle samples at 220 nm. The absorption, excitation, and emission spectra were measured for Rhodamine 6G at the same time intervals as the sample.

For the absorption measurements, an empty cuvette was used as a blank. It was then filled with the appropriate solvent, a spectrum was taken and it was then subtracted

from the nanoparticle spectrum throughout the experiment. An aliquot of the synthesized nanoparticles was removed and quantitatively transferred to a previously blanked cuvette. The sample was filled to a mark with the desired solvent in order to subtract the measured blank from subsequent UV/Vis measurements.

4.3 Results and Discussion

Aging analysis. We attempted to determine the stability of the nanoparticles after synthesis. We compared two samples; one was exposed to air while the second sample was kept sealed under N_2 or Ar.

Figure 4.1 shows the normalized absorption spectrum of the sealed SiH sample measured over a 211 hour period. One peak at 190 nm and two shoulders at 220 nm and 270 nm were observed for the sealed sample. The 190 nm peak decreased in absorbance at longer aging times. No major changes, in the absorption intensities of the sealed or exposed samples, were observed for either of the main peaks at 220 or 270 nm during the duration of the experiment. Similar results were observed for the exposed sample (Fig. 4.2). A slight offset is observed in Figure 4.2. A drop in absorbance for wavelengths greater than 225 nm occurred after the 0 hr measurement. This may be a result of improper mixture of the sample solution. Since we are working with small particles that do not dissolve in solution, they may settle if not properly mixed prior to absorbance readings.

These peaks in the absorption spectra of the sealed and exposed SiH samples were used to determine the optimum excitation wavelengths for probing their emission bands. Both 220 and 270 nm were used to excite the sealed samples while only 270 nm was used to excite the air-exposed sample, due to a lack of signal obtained when exciting at 220 nm.

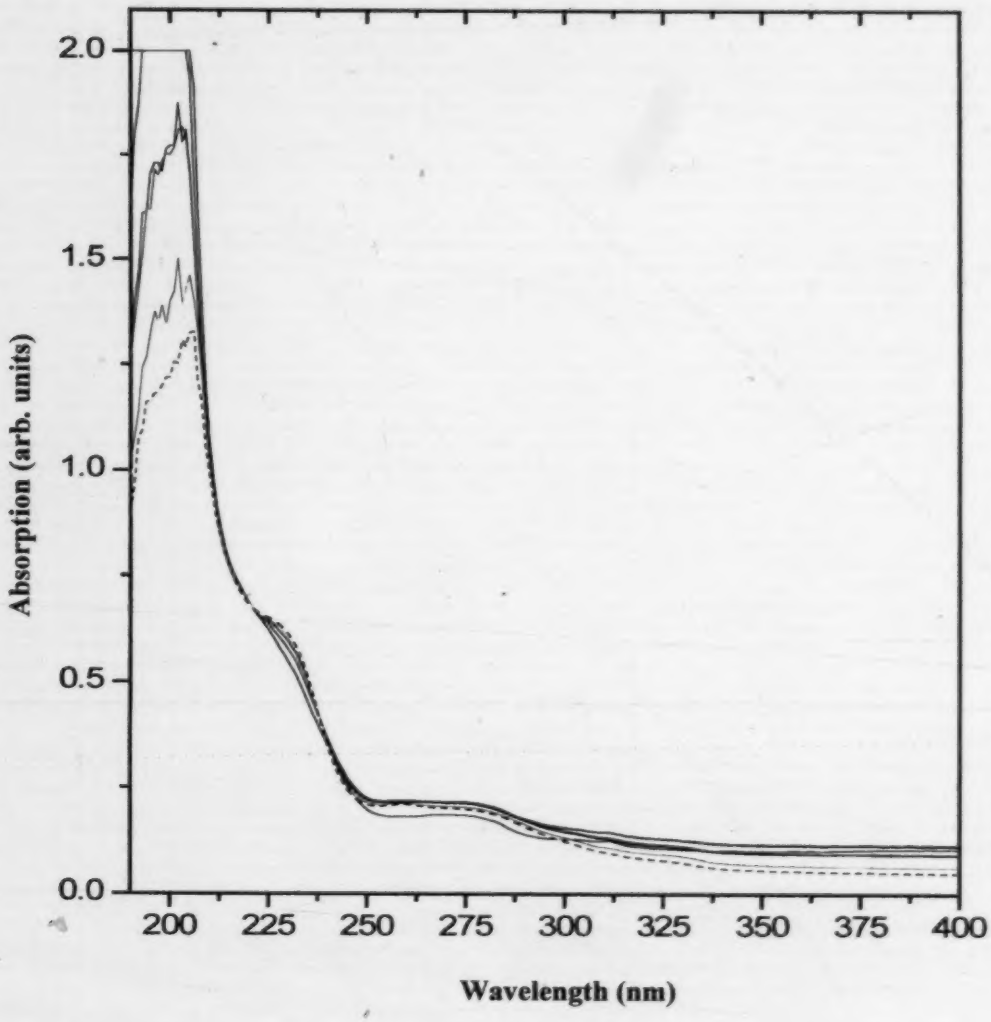

Figure 4.1 – Normalized UV-Vis spectrum of the sealed SiH in toluene. Absorption measurements were obtained at the following times: 0 hr (black), 24 hrs (red), 48 hrs (green), 72 hrs (blue), 94 hrs (cyan), 165 hrs (magenta), 190 hrs (yellow), 211 hrs (dashed).

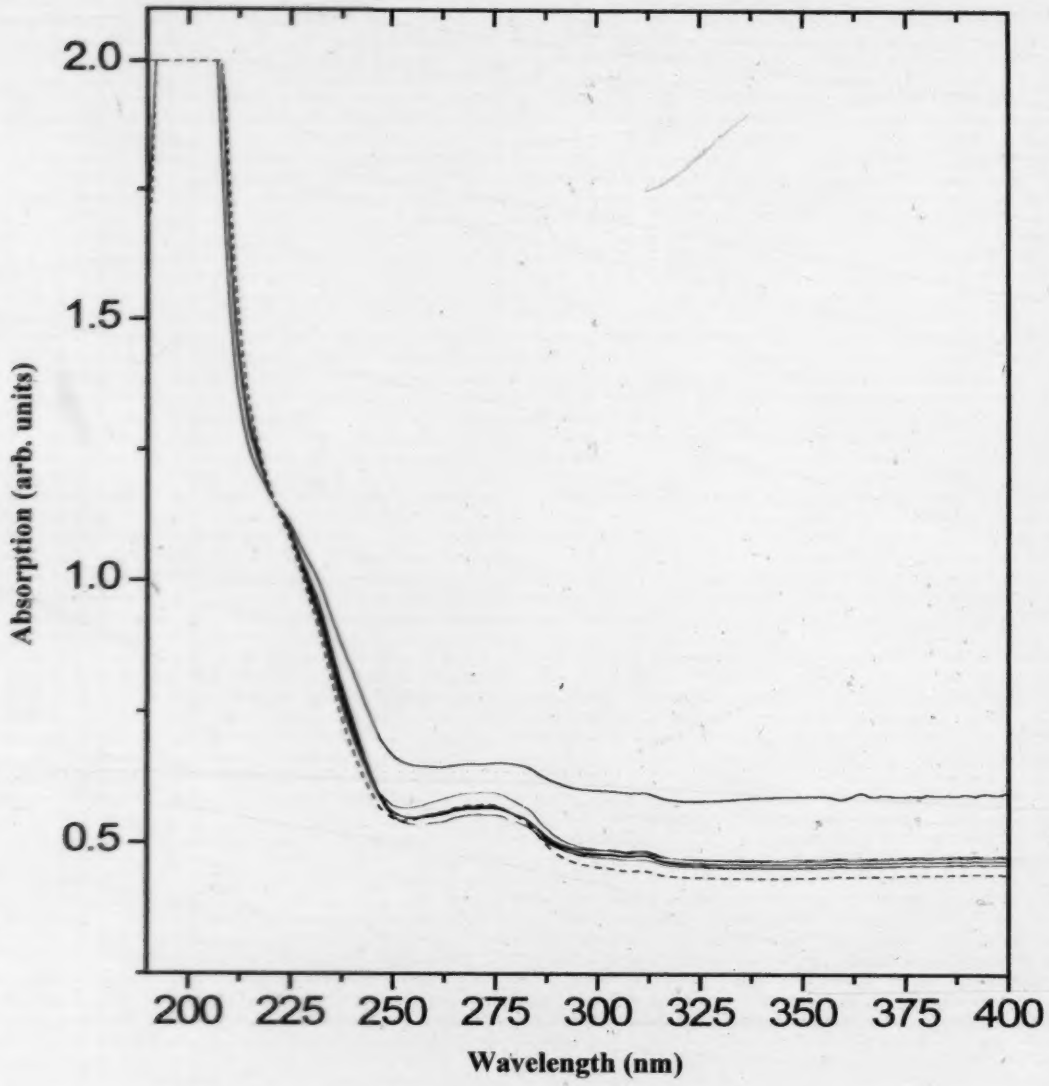

Figure 4.2 – As in Figure 4.1, but for the exposed SiH sample.

Both sealed and exposed SiH absorption spectra displayed a maximum absorption peak at 190 nm. Attempts were made to excite the samples with this wavelength, however this resulted in no emission. This peak may be a result of solvent absorption[20].

Figures 4.3A and B show the emission spectra for the sealed SiH samples. When the Si nanoparticle sample was excited at 270 nm (Figure 4.3A) two emission bands were observed, one from 300 – 400 nm and the second from 550 – 700 nm. The short UV emission band (Figure 4.3A (a)) showed a maximum intensity of 4.5×10^5 counts/sec at 48 hours after synthesis. The intensity for subsequent measurements decreases to the lowest emission intensity 2.75×10^5 counts/sec, observed at the final time period 312 hours while maintaining the same peak shape and maximum emission wavelength. Figure 4.3A (b) also shows a general decreasing trend with a maximum emission intensity of 1.7×10^4 at 48 hours to the lowest emission intensity of 1.2×10^4 at 312 hours after synthesis. Figure 4.3 B (a and b) show the emission from the sealed SiH sample when excited at 220 nm. The maximum intensity is approximately 10-fold lower than Figure 4.3A (a) at 4.0×10^4 counts/sec. The maximum emission intensity for Figure 4.3 B (a and b) is observed for the 0 hour measurement and decreases until the final measurement at 312 hours after synthesis. Monitoring the fluorescence emission over time allowed the stability of the nanoparticle emission to be investigated. The sealed SiH sample displayed a general decreasing trend, which we interpret as a result of the changing surface on the nanoparticle. The gradual oxidation of the hydride terminated sites on the nanoparticle surface, producing SiO_2 terminating sites on the surface may result in decreased fluorescence.

Conversely, the exposed SiH emission spectra in Figure 4.4 A (a and b) show increasing intensity for both the UV and near IR emission bands. The zero hour emission intensity was 6.0×10^4 counts/sec for the UV band from 290 - 450 nm, while the near IR band from 500 - 775 nm zero hour intensity was 4.0×10^3 counts/sec for the exposed SiH

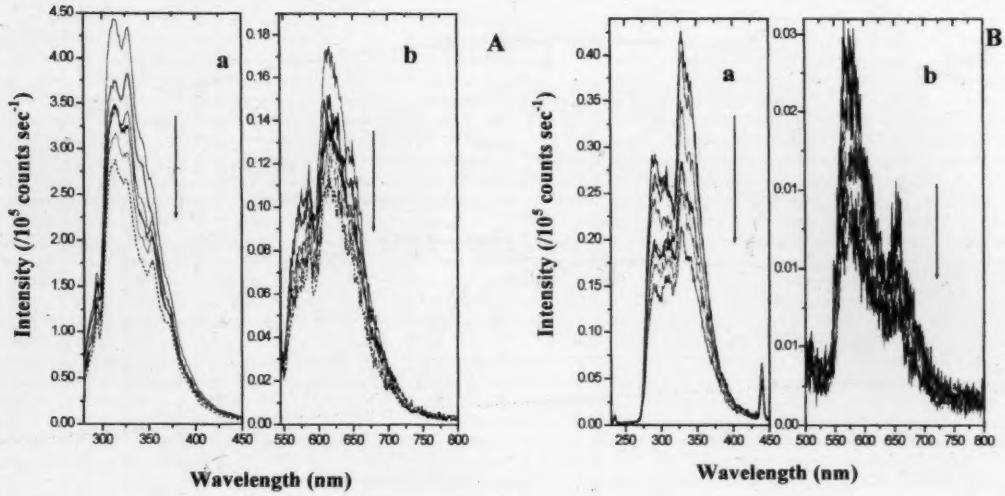

Figure 4.3 – Fluorescence emission spectra of the sealed SiH in pentane excited at 270 nm (A) and at 220 nm (B). The time after synthesis are 0 (black), 24 (red), 48 (green), 72 (blue), 96 (cyan), 120 (magenta), 144 (yellow), 168 (orange), and 312 hours (dashed) after synthesis. (a) is the main emission band and (b) represents the near- IR band.

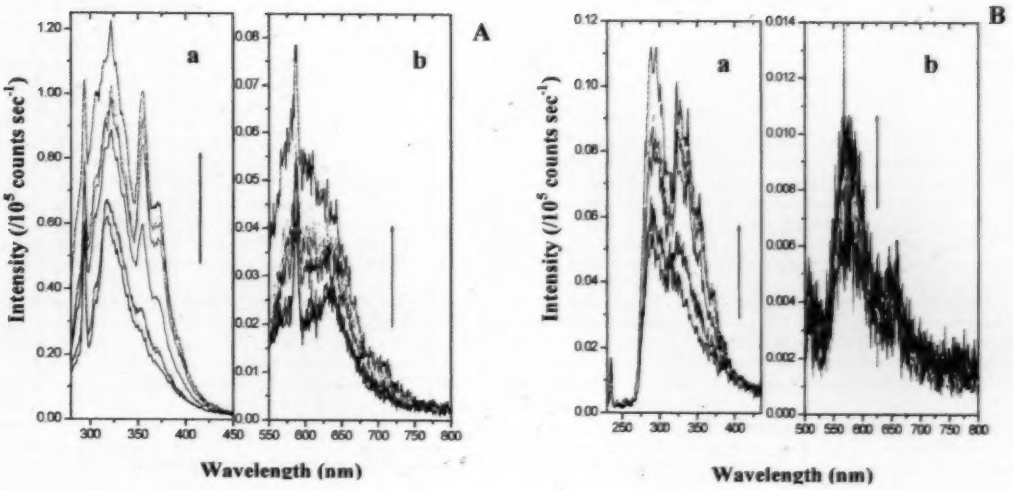

Figure 4.4 – As in Figure 4.3, but for the exposed SiH sample excited at 270nm (A) and at 220 nm (B).

sample when excited at 270 nm. The UV and near IR bands both reach their maximum intensity, 1.2 x 10^5 and 8 x 10^3 counts/sec respectively, after 312 hours. The emission spectra for the exposed SiH sample were measured with an excitation wavelength of 220 nm in Figure 4.4B. The emission for the two bands (UV and near IR) followed the same trend as when excited with 270 nm light, increasing in intensity with increasing time after synthesis. These emission bands were also similar in wavelength range as in Figure 4.4A. However, the intensities were lower when excited with 220 nm light, beginning with a zero hour emission of 4.0 x 10^3 counts/sec for the UV band and increasing only to 1.1 x 10^4 counts/sec after 312 hours. The near IR emission band intensity did not deviate significantly from an average intensity of 1.4 x 10^3 counts/second with aging time. The exposed SiH sample displayed an increasing emission intensity trend with increasing time. This result is opposite to what we observed for the sealed sample. The exact cause of this is not understood, but it has been postulated that this trend will continue until an equilibrium is reached, resulting in a similar sealed and exposed emission intensity.

Figures 4.5A and B and 4.6 show the normalized emission spectra for the sealed and exposed SiH samples respectively. Both of these samples were finely ground using a mechanical grinder prior to extraction. The emission bands span fewer wavelengths. The sealed sample emits from 300 to 400 nm and 600 to 700 nm, while the exposed sample emits from 300 to 375 nm and 600 to 725 nm. The emission intensities for the sealed and exposed samples both decrease over time, however the initial intensities were higher than for the previous samples in pentane. The quantum yield calculated for the normalized sealed SiH sample excited with 220 nm wavelength at the zero hour was 11.89 % and after 231 hours was 9.07 %.

The range of wavelengths over which the emission bands were observed was shown to decrease when the mechanical grinder was used. The hand-ground samples emit over

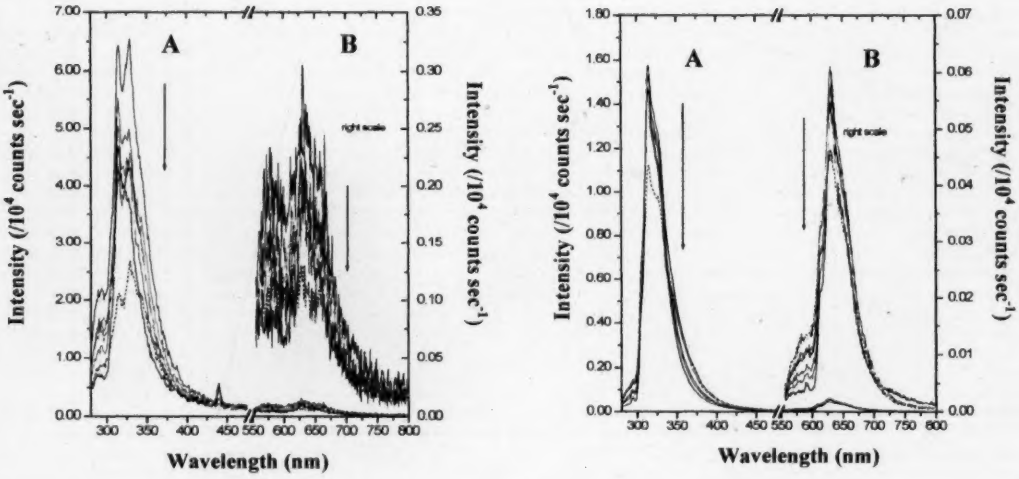

Figure 4.5 – Normalized fluorescence emission spectrum of the sealed SiH in toluene excited at 220 nm (A) and at 270 nm (B). Samples were ground up in a Schlenk flask containing glass beads on a mechanical grinder. Samples emission spectra were obtained at the following time periods: 0 hrs (black), 24 hrs (red), 48 hrs (green), 72 hrs (blue), 94 hrs (cyan), 165 hrs (magenta), 190 hrs (yellow), and 231 hrs (dashed).

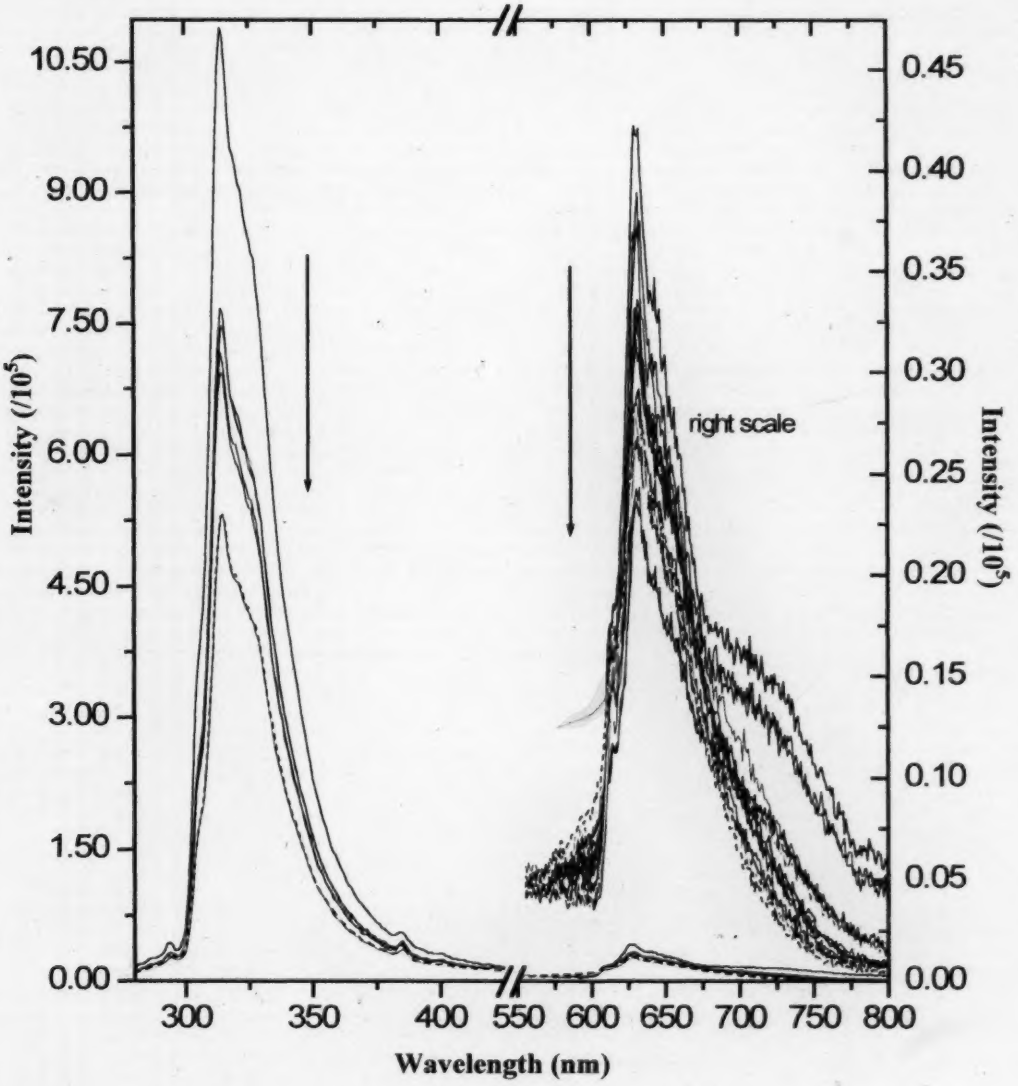

Figure 4.6 – As in Figure 4.5, but for the exposed SiH sample excited at 270 nm.

approximately 125 nm, while the mechanically ground samples emitted over an average wavelength of 75 nm. The smaller wavelength range may be a result of a much more mono-dispersed nanoparticle size in this sample, since emission wavelength is significantly guided by the size of the particles[12]. Thus, a smaller deviation in particle sizes leads to a more defined emission range. Though the emission intensity for the exposed SiH sample was lower than for the sealed SiH sample, both may be proceeding toward a surface equilibrium over time. This decreasing trend in emission intensity may be a result of surface oxidation as mentioned previously. The quantum yields calculated for both the exposed and sealed SiH samples at zero hour and at the 231 hour (Table 4.1) displayed the range of values possible depending on the parameters in the experiment. The sealed sample quantum yields were found to decrease slightly with increasing time, more specifically, over a period of 10 days, thus showing the high stability of these particles. It was also determined that samples which were maintained in the sealed environment were able to produce greater emission at both the UV and near IR wavelength ranges. The exposed sample quantum yields reduced by approximately half over the 10 day period, showing that under atmospheric conditions the emission is not as stable as the sealed samples.

4.4 Conclusions

We have quantified the optical properties of silicon nanoparticles synthesized from hydrogen silsesquioxane. These particles possessed two emission bands, one in the UV region and one in the near IR region. The UV emission for both a sealed and an exposed sample were maintained at significantly higher quantum yields over various time periods. The nanoparticles demonstrated their stability, making them ideal candidates for future

Table 4.1 – Calculated Quantum Yields of SiH samples

	Sealed SiH Excitation 220 nm	Sealed SiH Excitation 270 nm	Exposed SiH Excitation 270 nm
UV region (0 hours)	11.89 %	22.11 %	4.18 %
UV region (231 hours)	9.07 %	23.77 %	2.19 %
Near IR region (0 hours)	1.09 %	1.31 %	0.48 %
Near IR region (231 hours)	0.9 %	1.44 %	0.24 %

investigation on their bioconjugation with biological molecules for their use as molecular probes.

4.5 References

[1] Jing, Z., Baldwin, R. K., Pettigrew, K. A., Kauzlarich, S. M. *Nano Letters*, **2004**, 1181-1186.

[2] Trindade, T. *Chemical Materials*, **2001**, 3843-3858.

[3] Baldwin, R. K., Pettigrew, K. A., Garno, J. C., Power, P. P., Liu, G., Kauzlarich, S. *American Chemical Society Journals.* **2002**, 1150-1151.

[4] Maxwell, D. J., Taylor, J. R., Nie, S. *American Chemical Society Journals.* **2002**, 9606-9612.

[5] Dubertret, B., Calame, M., Libchaber, A. J. *Nature*, **2001**, 365-370.

[6] Veinot, J. G. C. *Chem. Commun.* **2006**, 4160-4168.

[7] Gerion, D., Fanqing, C., Kannan, B., Fu, A., Parak, W. J., Chen, D. J., Majumdar, A., Alivisatos, A. P. *Analytical Chemistry*, **2003**, 4766-4722.

[8] Bruchez, M. Jr., Moronne, M., Gin, P., Weiss, S., Alivisatos, A. P. *Science*, **1998**, 2013-2016.

[9] Chan, W. C. W., Maxwell, D. J., Gao, X., Bailey, R. E., Han M., Nie, S. *Current Opinion in Biotechnology*, **2002**, 40-46.

[10] Mitchell G. P., Mirkin, C. A., Letsinger, R. L. *American Chemical Society Journals*, **1999**, 8122-8123.

[11] Mattoussi, H., Mauro, J. M., Goldman, E. R., Anderson, G. P., Sundar, V. C., Mikulec, F. V., Bawendi, M. G. *American Chemical Society Journals*, **2000**, 121412- 12150.

[12] Cai, W., Hsu, A. R., Li, Z., Chen, X. *Nanoscale Research Letters*, **2007**, 265-281.

[13] Liu, Q., Kauzlarich, S. M. *Materials Science and Engineering*, **2002**, 72-75.

[14] Van Buuren, T., Dinh, L. N., Chase, L. L., Siekhaus, W. J., Terminello, L. J. *Physical Review Letters*, **1998**, 3803-3806.

[15] English, D. S., Pell, L. E., Yu, Z., Barbara, P. F., Korgel, B. A. *Nano Letters*, **2002**, 681-685.

[16] Bley, R. A., Kauzlarch, S. M., Davis, J. E., Lee, H. W. H. *Chemical Materials*, **1996**, 1881-1888.

[17] Iacona, F., Franzo, G., Spinella, C. *Journal of Applied Physics*, **2000**, 1295-1303.

[18] Hessel, C. M., Henderson, E. J., Veinot, J. G. C. *Chemical Materials*, **2006**, 6139-6146.

[19] Demas, J. N.; Crosby, G.A. *Physical Chemistry* **1971**, 75, 991-1024.

[20] Upstone, S. L. *Encyclopedia of Analytical Chemistry*; Editor, Meyers, R. A.; John Wiley and Sons Ltd., Chichester, WS, 2000, p1704.

5 Conclusions and Future Work

5.1 Reducing Error and Detecting DNA Photodamage on Microarray Slides

The reduction of error incurred in microarray experiments required the investigation of different parameters involved in the experimental procedures. We found that the dFAM short ssDNA could be used as an internal standard in microarray experiments. The use of the internal standard aided in lowering data percent errors obtained when the ratio of the Cy5 probe / FAM fluorescence intensity was used instead of the Cy5 probe fluorescence intensity alone. Optimization of concentrations used for microarray experiments were determined as 50 μM for the target sequences and 35 μM for the probe sequences. Analyzing results obtained from microarray experiments accurately and efficiently is crucial for producing reliable results. Here, we have determined, that for our current purposes, Spot Finder is a sufficient tool for the data analysis of microarray experiments.

As with all experiments, defining the controls required is of the utmost importance. Here, we demonstrated that the controls required for microarray experiments included elimination of ambient light, the reduction of ozone when drying the slides, and removing reflective surfaces during UV irradiations. With the appropriate controls in place, we were able to detect the production of UV-induced DNA damage, using fluorescently-labeled hairpin probes. From the results obtained, we fit the fluorescence intensity data to first-order exponential decay curves and determined the rate constants for DNA photodamage production to be 51.59113 ± 2.14881 min (R^2 = 0.95881) for ATTA, 47.78764 ± 3.5573 min (R^2 = 0.83409) for AAAA, and 53.52365 ± 1.26358 min (R^2 = 0.96956) for GTTG DNA sequence.

5.2 Silicon Nanoparticle

The determination of the spectral properties of silicon particles provides a better understanding of their possible applications. The stability of silicon nanoparticle's absorption and photoluminescence emission was determined for two experimental conditions, sealed and exposed to the atmosphere, for a period of 14 days. The nanoparticles were observed to emit in both the near IR and UV spectral regions. The average observed emission from the sealed samples displayed larger quantum yield for the UV region (17%) and near IR region (1.27%) compared to the exposed SiH samples with quantum yields of 4.18% and 0.48%, respectively. Only slight decreases in quantum yield values were observed after a period of 14 days for both samples.

5.3 Future Work

The results obtained in this research have led to a better understanding of the intricate nature of microarray experiments. The results presented here also suggest future work, which may correct additional challenges in microarray techniques. The use of a new fluorophore, which does not possess an overlap between the emission band of one fluorophore and the excitation of the other, could be attempted in order to reduce any effects of cross-talk between fluorophores. An alternative pair of fluorophores that could be used are cascade blue, which absorbs at 405 nm and emits at 440 nm, coupled with Cy5.5, which absorbs at 685 nm and emits at 705 nm.

The determination of the effects of UVC light on the AAAA target sequence could be further investigated first in solution, initially with molecular beacon detection of damage. A more photostable fluorophore could be of great use for the detection of DNA

damage in the microarray system in order to prevent photobleaching of the fluorophore during long irradiations. And lastly, functionalization of the nanoparticles with a short linker group that could bind to the glass slide directly could be used to replace the current dFAM internal standard. In doing so, any reactions which may occur between the fluorophore and the target DNA would be eliminated since the nanoparticles are bioinert.

6 Appendix

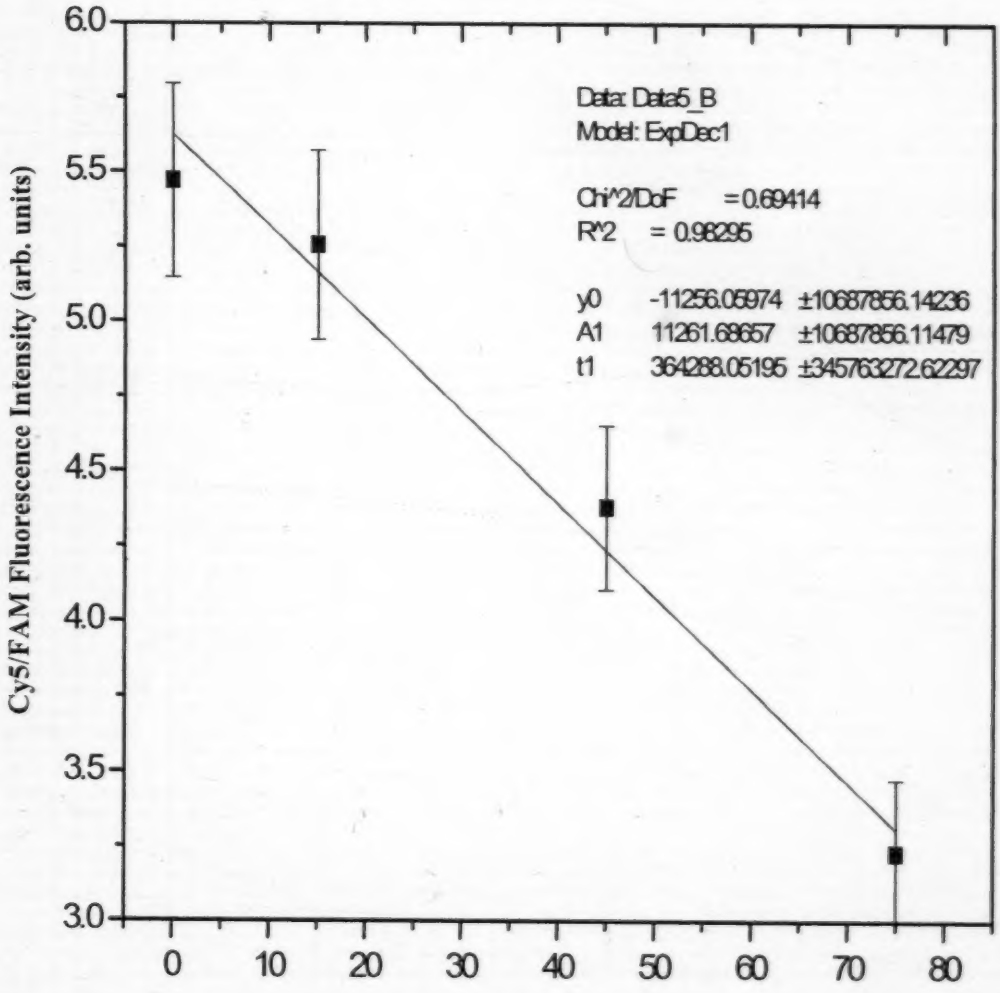

Figure 6.1 – Median Cy5/FAM fluorescence intensities for the ATTA target sequence for the experimental slide, as in Figure 3.27, but fit to a first-order exponential decay curve.

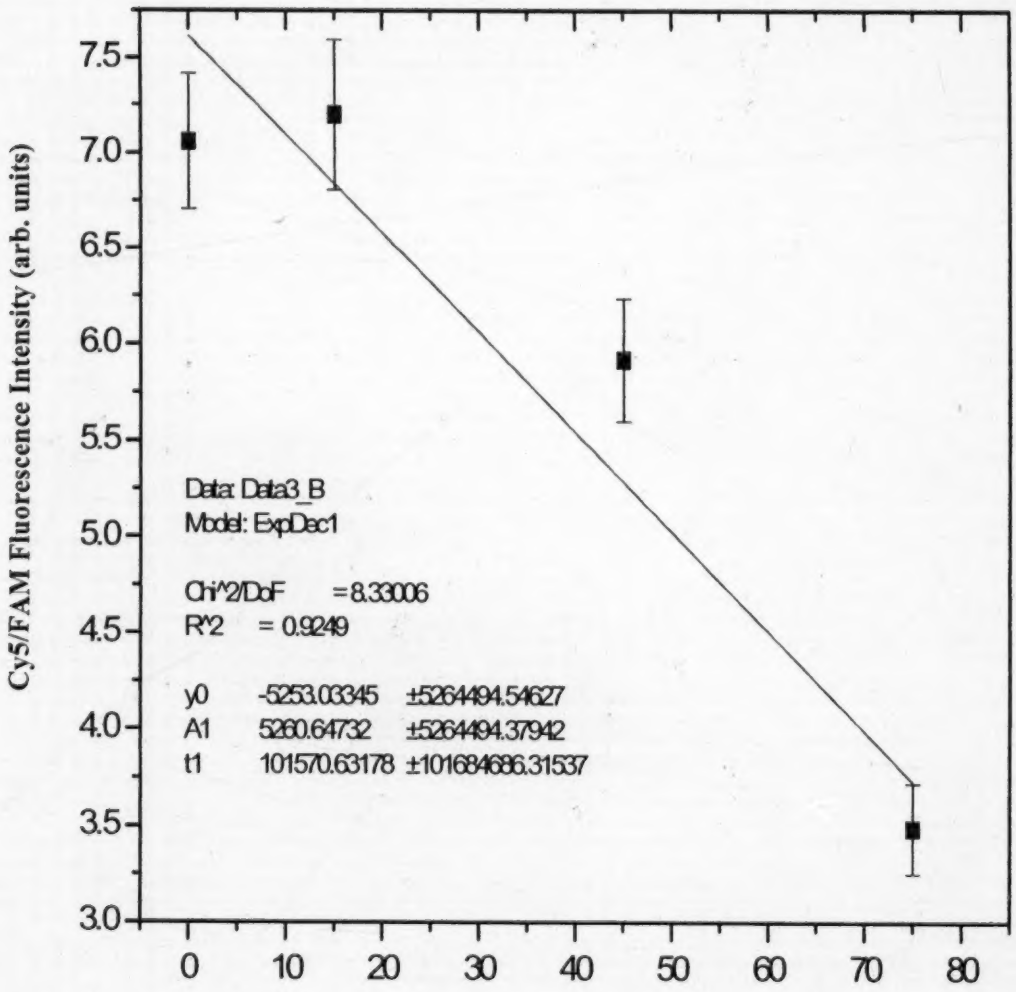

Figure 6.2 – Median Cy5/FAM fluorescence intensities for the AAAA target sequence for the experimental slide, as in Figure 3.27, but fit to a first-order exponential decay curve.

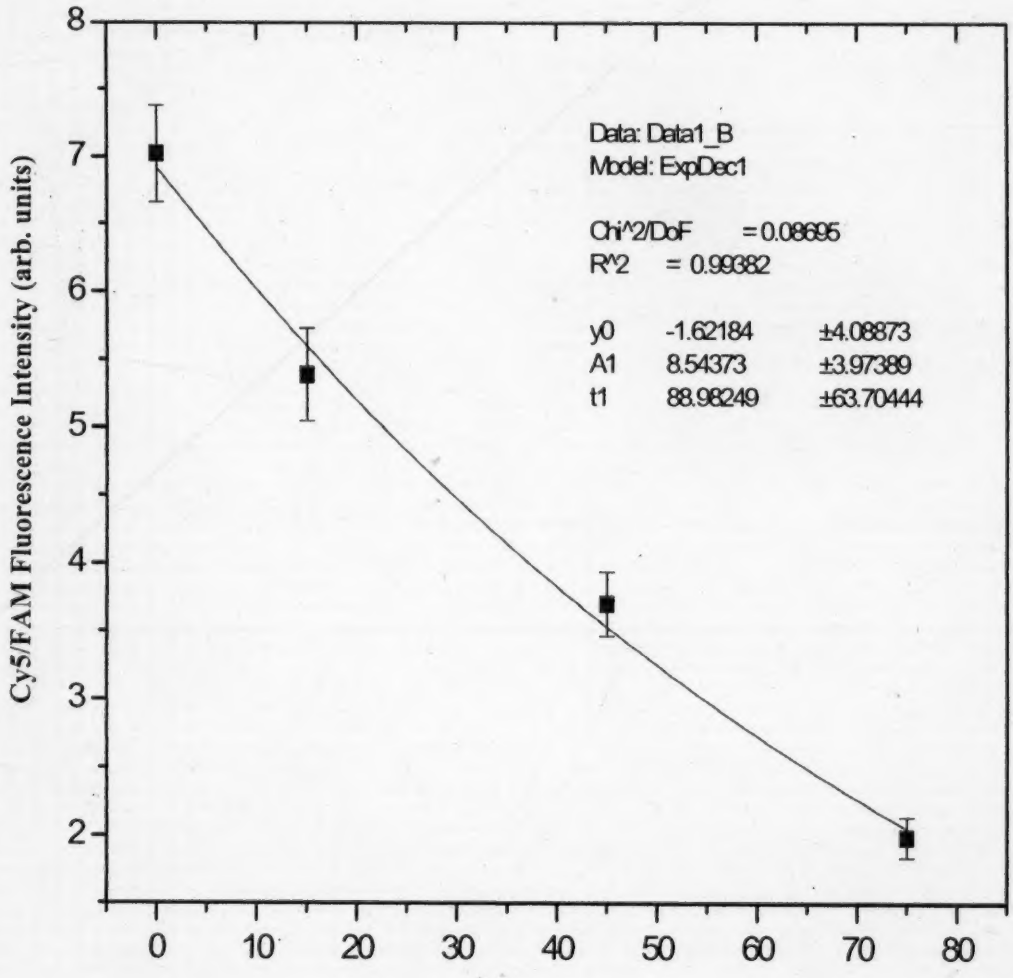

Figure 6.3 – Median Cy5/FAM fluorescence intensities for the GTTG target sequence for the experimental slide, as in Figure 3.27, but fit to a first-order exponential decay curve.

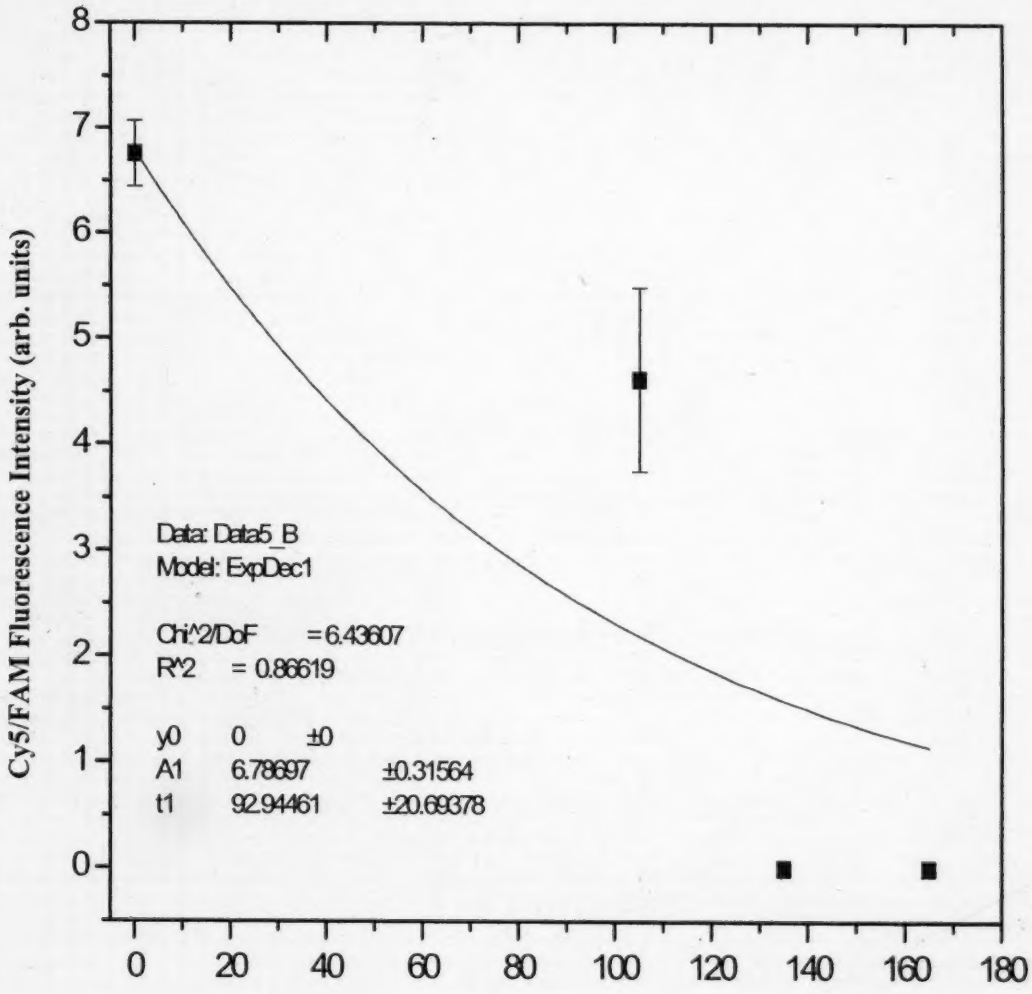

Figure 6.4 – Median Cy5/FAM fluorescence intensities for the ATTA target sequence for the experimental slide, as in Figure 3.27, but fit to a first-order exponential decay curve and with irradiation time 0-165.

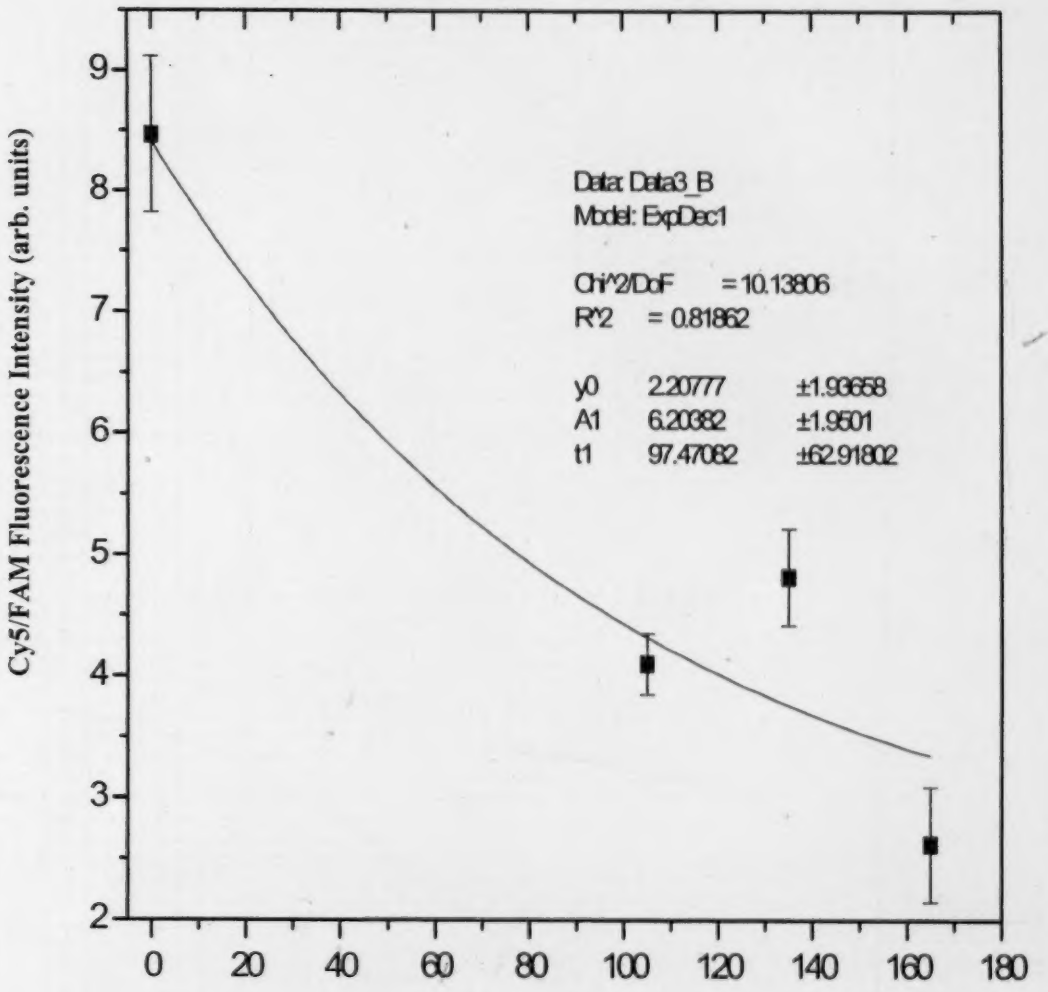

Figure 6.5 – Median Cy5/FAM fluorescence intensities for the AAAA target sequence for the experimental slide, as in Figure 3.27, but fit to a first-order exponential decay curve and with irradiation time 0-165.

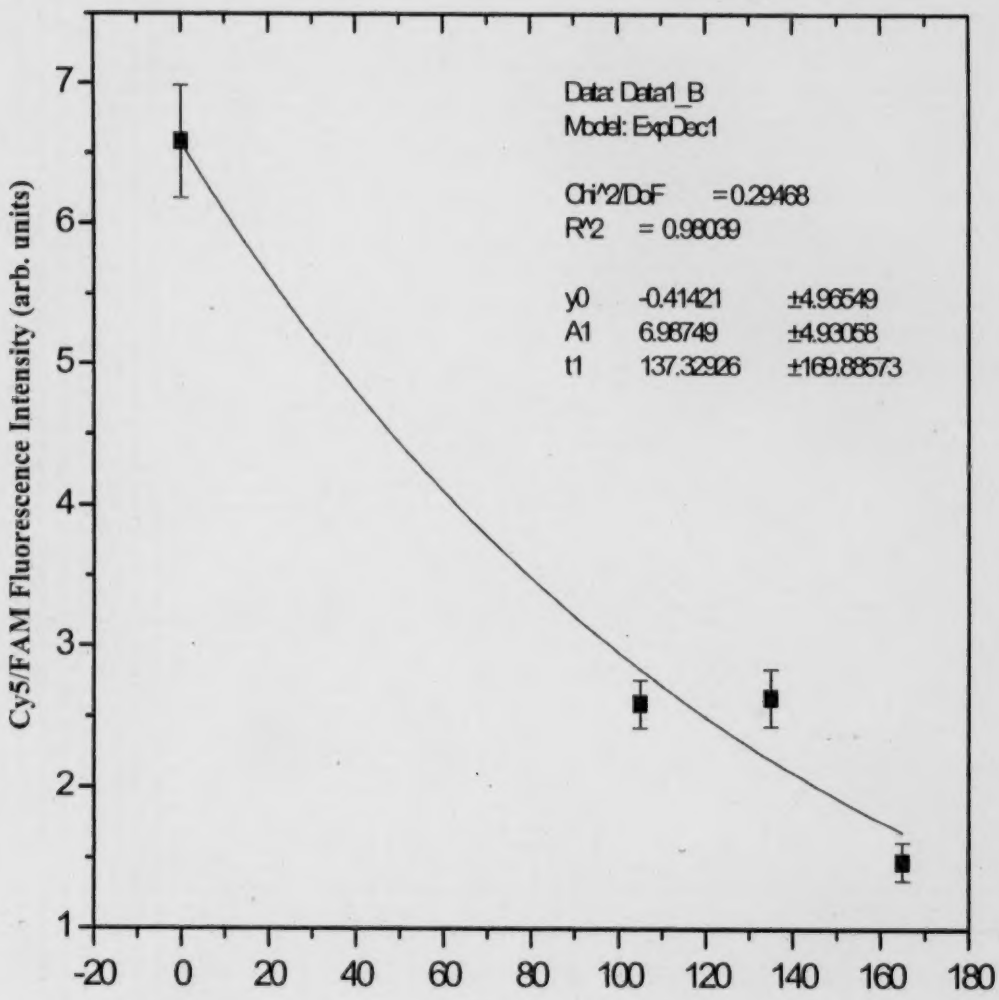

Figure 6.6 - Median Cy5/FAM fluorescence intensities for the GTTG target sequence for the experimental slide, as in Figure 3.27, but fit to a first-order exponential decay curve and with irradiation time 0-165.

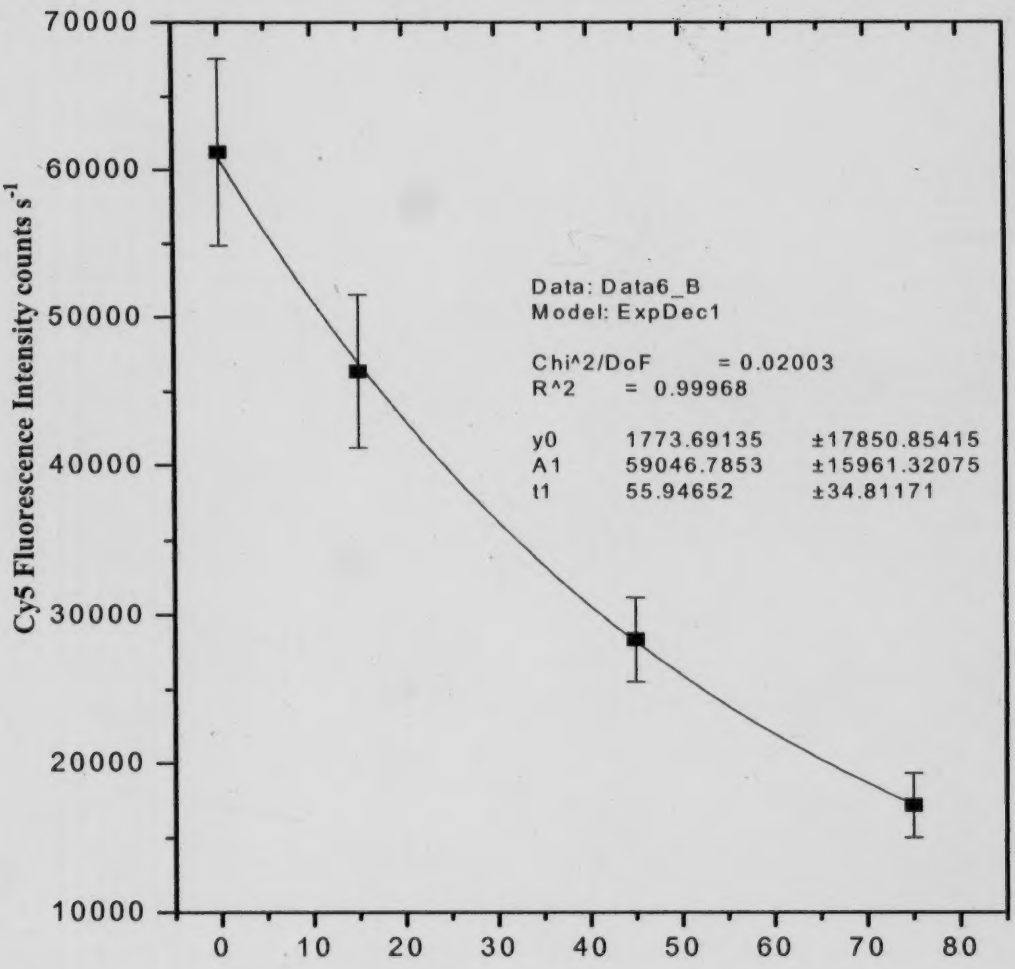

Figure 6.7 - Median Cy5 fluorescence intensities for the ATTA target sequence for the experimental slide, as in Figure 3.27, but fit to a first-order exponential decay curve.

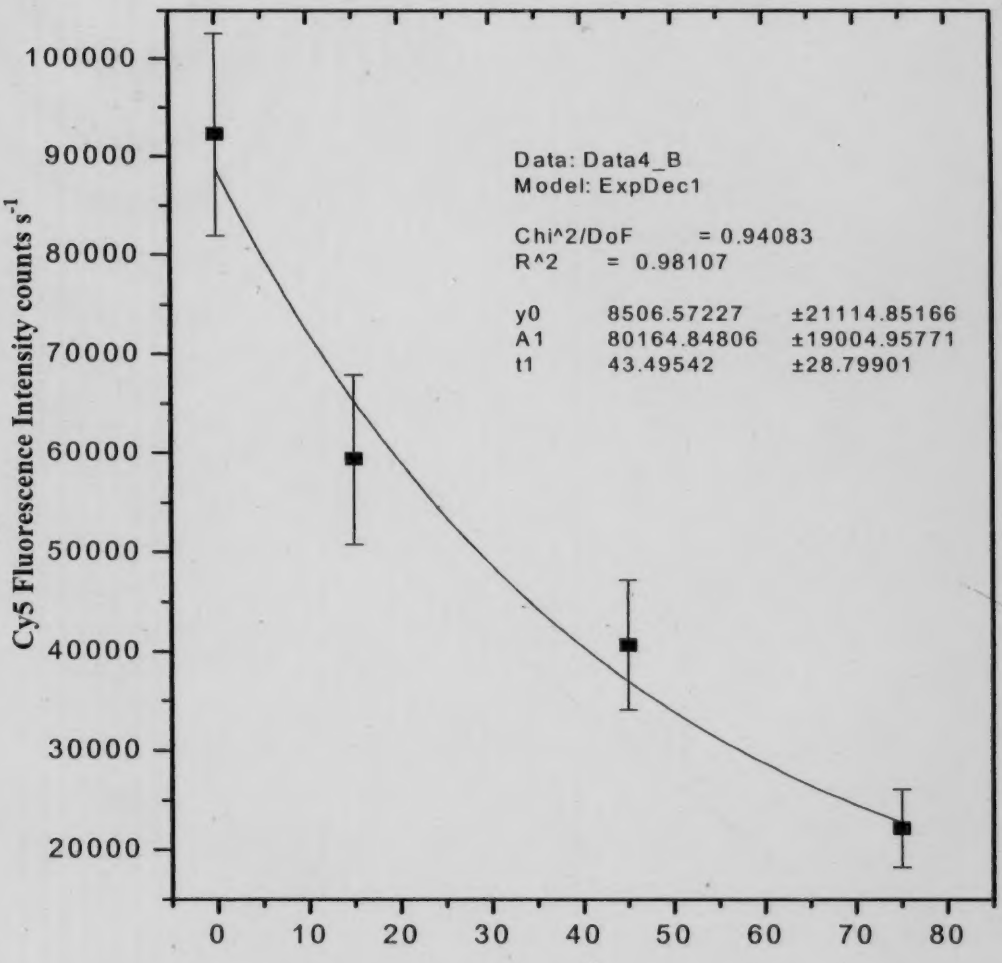

Figure 6.8 - Median Cy5 fluorescence intensities for the AAAA target sequence for the experimental slide, as in Figure 3.27, but fit to a first-order exponential decay curve.

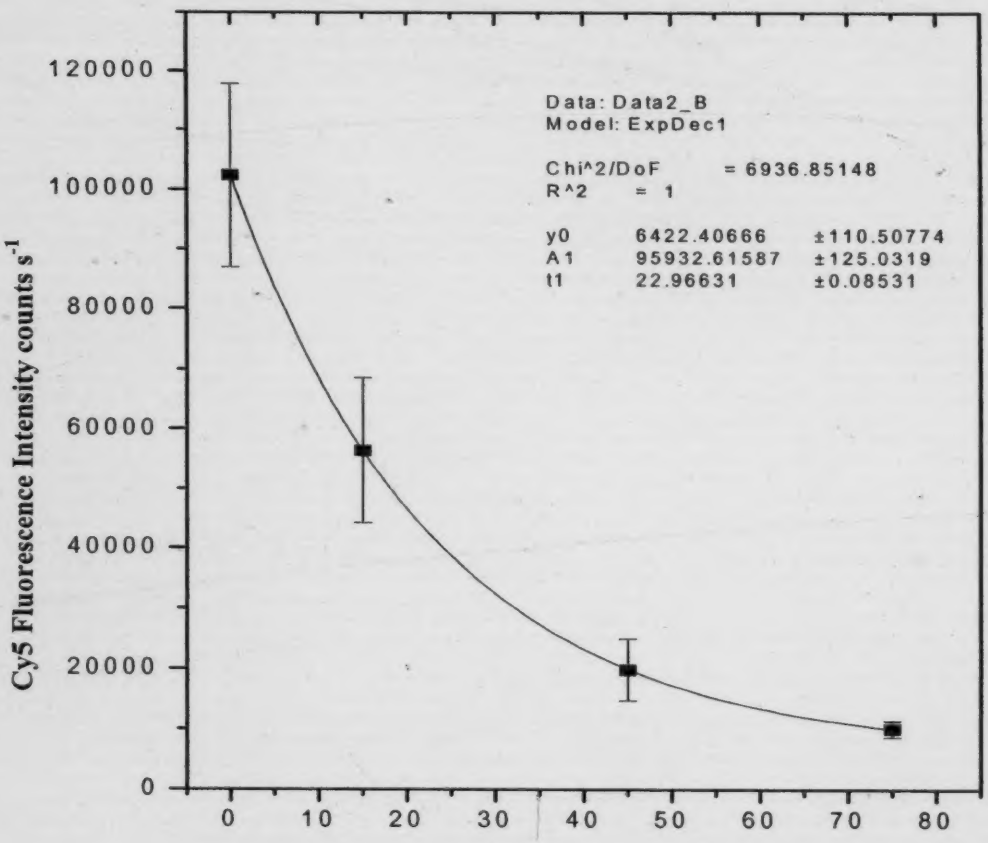

Figure 6.9 - Median Cy5 fluorescence intensities for the GTTG target sequence for the experimental slide, as in Figure 3.27, but fit to a first-order exponential decay curve.

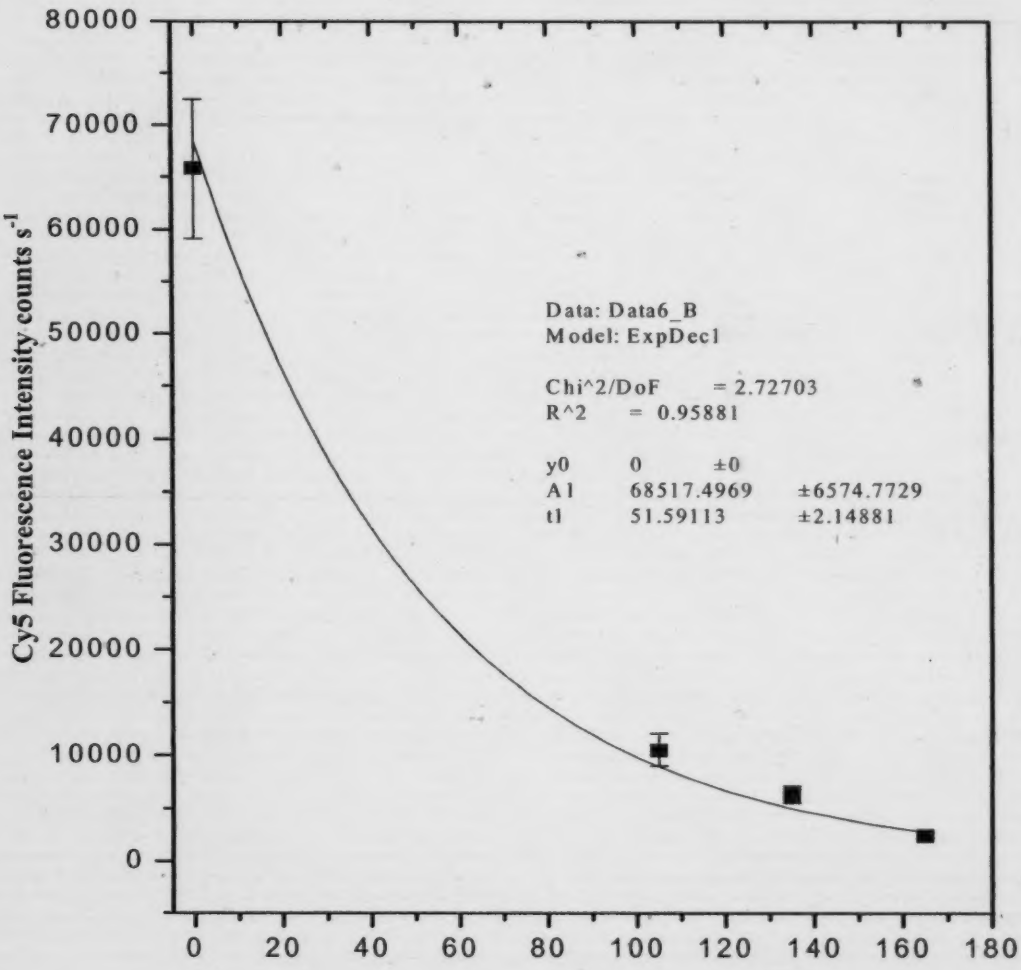

Figure 6.10 - Median Cy5 fluorescence intensities for the ATTA target sequence for the experimental slide, as in Figure 3.27, but fit to a first-order exponential decay curve and irradiation times 0-165 min.

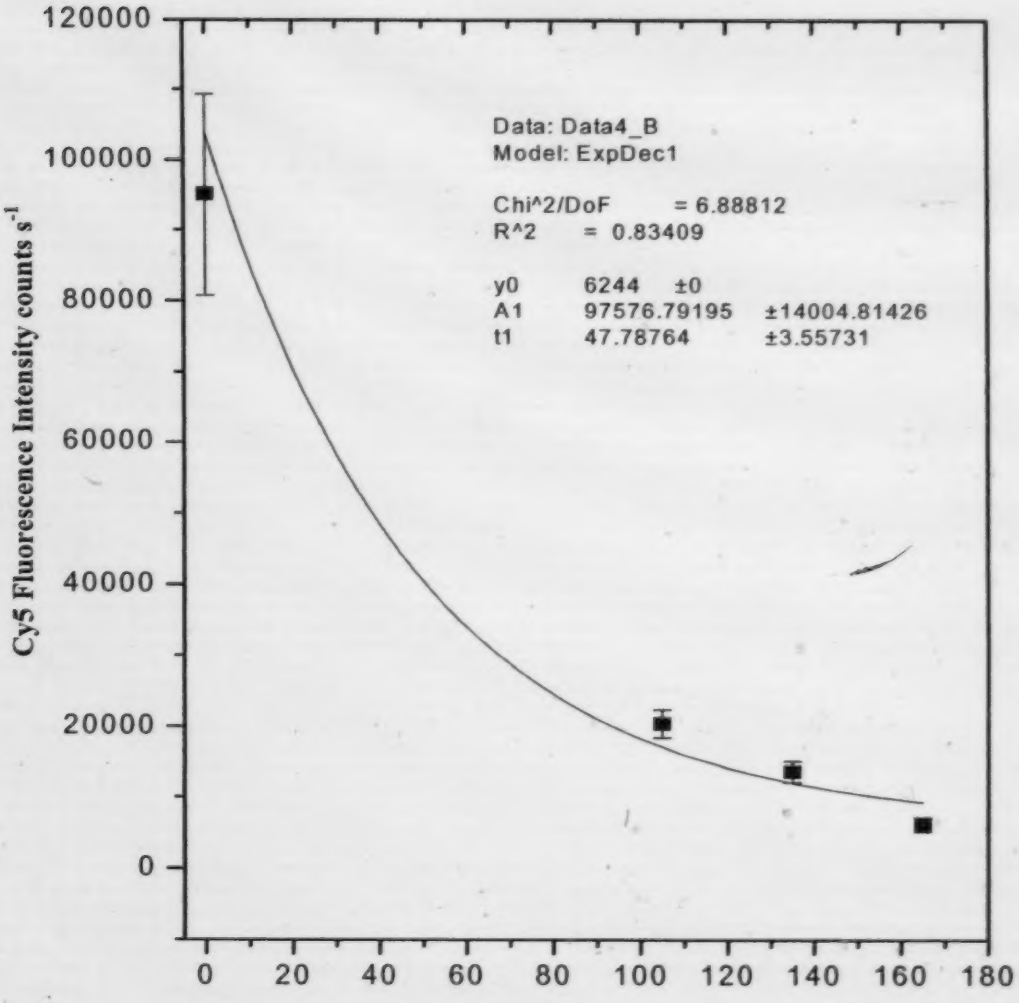

Figure 6.11 – Median Cy5 fluorescence intensities for the AAAA target sequence for the experimental slide, as in Figure 3.27, but fit to a first-order exponential decay curve and with irradiation time 0-165.

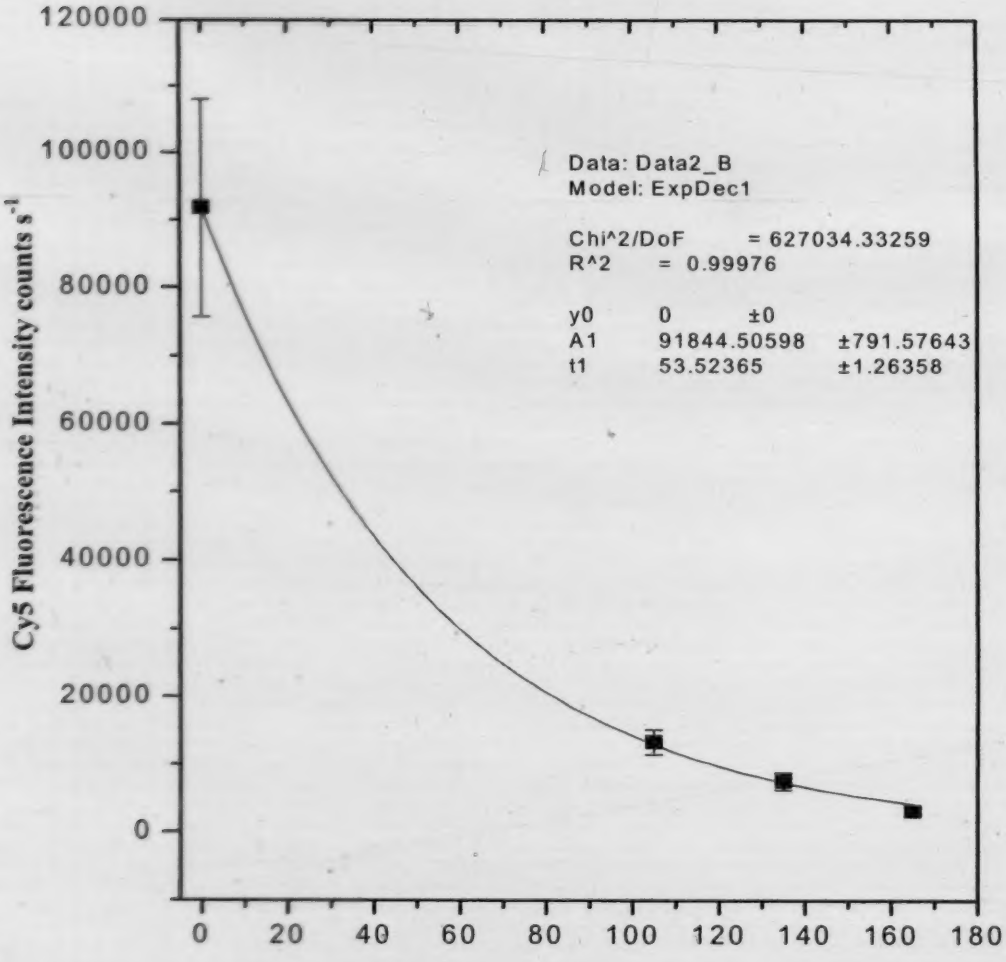

Figure 6.12 – Median Cy5 fluorescence intensities for the GTTG target sequence for the experimental slide, as in Figure 3.27, but fit to a first-order exponential decay curve and with irradiation time 0-165.